Experimental and theoretical determination of nonlinear pressure fields in biological fluids

Verma, Prashant K.

Award date:
1995

Awarding institution:
University of Bath

EXPERIMENTAL AND THEORETICAL DETERMINATION OF NONLINEAR PRESSURE FIELDS IN BIOLOGICAL FLUIDS.

Submitted by Prashant K. Verma

for the degree of Ph.D.
of the University of Bath.

1995

ProQuest LLC
789 East Eisenhower Parkway
P.O. Box 1346
Ann Arbor, MI 48106-1346

EXPERIMENTAL AND THEORETICAL DETERMINATION OF NONLINEAR PRESSURE FIELDS IN BIOLOGICAL FLUIDS.

Submitted by Prashant K. Verma

for the degree of Ph.D.
of the University of Bath.

1995

To ami and papa

ABSTRACT

This thesis is concerned with extending the use of numerical models to the prediction of nonlinear ultrasonic fields in biological fluids and forms part of a longer term programme to predict nonlinear propagation of medical ultrasound *in vivo*.

The numerical model used in this work (Aanonsen *et at* 1984) takes into account the diffraction, attenuation and nonlinear propagation of sound from a circular single element source. Predictions, using the model, require knowledge of source and medium parameters. In particular the source characteristics and the frequency dependence of attenuation are needed.

This thesis describes the design of an experimental facility that is capable of measuring both the frequency dependence of attenuation and nonlinear pressure distributions (for high drive levels) on the same sample of biological fluid. The main feature of the flexible experimental rig is its variable length fluid chamber.

Broadband measurements (5 MHz to 20 MHz) of the frequency dependence of attenuation in three biological fluids, amniotic fluid, urine and 4.5% Human Albumin solution, are presented. This data, in conjunction with measurements of the sound source, is used to predict pressure distributions in the above fluids.

Measurements of the nonlinear pressure distribution, made using a 2.25 MHz single element transducer coupled to a PMMA lens with a focal gain of 12 are also presented. The transducer was driven with a pulse of 8 cycles at pressures ranging from 0.007 MPa to 0.244 MPa. The received signal was detected with a broadband 0.5 mm diameter bilaminar Pvdf membrane hydrophone, so enabling the axial nonlinear pressure distribution to be measured.

A comparison between the experimental and theoretical pressure distributions for the first five harmonics is presented. In general the agreement is very good and indicates how more complex and 'real' *in vivo* situations can be modelled.

TABLE OF CONTENTS

LIST OF KEY SYMBOLS

a	-Transducer (source) radius
A	-ratio of diffraction to nonlinearity
b	-Hydrophone (receiver) radius
b_{max}	-maximum hydrophone radius
(B/A)	-parameter of medium nonlinearity
C	-capacitance of hydrophone
C_l	-capacitance of load
c	-velocity of sound
c_m	-velocity of sound in medium
c_p	-velocity of sound in perspex
c_n, d_n	-coefficients representing the resolved vector components of the pressure amplitude of the n^{th} harmonic
D	-focal length
f	-frequency of sound
$F(z)$	-diffraction term
G	-focusing gain of source
I	-Intensity
I_l	-Intensity of a plane wave propagating under linear conditions
I_{nl}	-Intensity of a plane wave propagation under nonlinear conditions
$(I_l)_o$	-Intensity of linear plane wave propagation at source
$(I_{nl})_o$	-Intensity of nonlinear plane wave propagation at source
J_n	-bessel function of order n
k	-wavenumber $(2\pi/\lambda)$
l_2	-thickness of mylar
l_d	-plane wave shock distance
m	-index for frequency dependence of attenuation
M_l	-loaded end of cable sensitivity of hydrophone
M_c	-open end of cable sensitivity of hydrophone
n	-harmonic number
S	-sensitivity of PVdF film
p_n	-amplitude of n^{th} harmonic
P	-excess pressure
P_o	-source pressure
$\widetilde{P}$	-normalised pressure
$P_2(z)$	-pressure amplitude of second harmonic at a distance z.
P'	-acoustic power
r	-distance between point of observation and a point on the surface of the source
R_o	-Rayleigh distance $(ka^2/2)$
R_1, R_2	-radii of curvature of a lens
s	-normalised axial distance
$T_m(f)$	-frequency dependent transmission loss
t	-time

u	-particle velocity
u_o	-source particle velocity
v	-radius of circular disc
w	-angular frequency ($2\pi f$)
z	-axial distance
z_o	-axial position of the last maximum
Z	-ratio of acoustic impedance in water to PVdF film
Z_1	-acoustic impedance of water
Z_2	-acoustic impedance of mylar
α	-amplitude attenuation coefficient (dB cm^{-1})
α_o	-amplitude attenuation coefficient at 1 MHz (dB $cm^{-1}MHz^{-m}$)
α_1	-attenuation coefficient of fundamantal
α_2	-attenuation coefficient of second harmonic
α_l	-attenuation coefficient due to linear propagation (Nepers/distance)
α_{nl}	-additional attenuation coefficient due to nonlinear propagation (Nepers/distance)
ρ	-instantaneous density
ρ_o	-equilibrium density
β	-nonlinearity parameter
ε	-acoustic Mach number
Γ	-Goldberg number (represents ratio of nonlinearity to attenuation)
λ	-wavelength of sound
ξ	-particle displacement (also radial co-ordinate in Chapter 3)
Φ	-scalar potential
ϕ_n	-phase of n^{th} harmonic
σ	-palne wave shock parameter
τ	-retarded time
$\nabla_\perp$	-two dimensional Laplace operator

1.0 INTRODUCTION

1.1 Background

The last twenty-five years have seen the widespread use of ultrasound in medicine. This is, in part, due to technological advances in transmission and detection at ultrasonic frequencies and in part due to the non-invasive and non-ionising nature of the radiation. The non-ionising aspect of ultrasound has in particular been attractive and has allowed clinical information to be obtained in areas such as obstetric scanning where other imaging techniques are not viable.

Allied to this there has subsequently been a growth in research into the fundamental physics behind the propagation of ultrasound and the biological consequences associated with its passage through living systems. This project is a continuation of this work and in particular is concerned with the nonlinear propagation of ultrasound beams in biological fluids. This section, with sections 1.2 and 1.3, therefore gives a brief overview of areas of uses of ultrasound in medicine, the possible biological effects of ultrasound and the nature of the nonlinear propagation that results from medical ultrasonic transducers.

At present the uses of ultrasound in medicine can be broadly classed into the following areas:

(i) Diagnostic imaging, including pulsed Doppler techniques;

(ii) Physiotherapy;

(iii) Surgery (including hyperthermia).

Pulse-echo imaging is by far the most common use of medical ultrasound. Its applications and mode of operation are varied, the most common being in obstetric scanning. Here unique and valuable diagnostic information concerning the foetus is obtainable. For example information on placental location, foetal maturity and foetal abnormalities are all available. Foetal maturity can be assessed by measurements of skull and abdomen size and foetal abnormalities such as spinal defects can be imaged. In addition to this, obstetric imaging allows the clinical procedure of amniocentesis to be carried out with increased safety.

Other areas of pulse-echo imaging include ophthalmology, cardiology and general body imaging. In ophthalmology abnormal anatomical features in the eye can be investigated. In cardiology and general body imaging the usefulness of pulse-echo techniques includes the ability to obtain real-time images that can convey movement information and also allow very flexible interrogation of a region of interest.

An increasingly useful technique in diagnostic ultrasound is the use of Doppler techniques for quantitative measurements of movement and flow. Foetal heart rate can be monitored and blood flow through normal and stenotic vessels can be measured.

In physiotherapy and surgery ultrasound plays a therapeutic rather than diagnostic role. Ultrasound physiotherapy is thought to provide help in accelerated soft tissue

healing, pain relief and improved joint mobility. Ultrasonic surgery is used, for example, in lithotripsy where renal calculi are destroyed. More recently surgical applications are finding use in cancer therapy (hyperthermia) either by direct destruction of cancerous cells or as an enhancing agent for chemotheraputic drugs.

The wide variety of uses of ultrasound in medicine has led to the use of different modes of operation depending on the application. In pulse-echo imaging short pulses in the region of 2 MHz to 10 MHz are employed to give good spatial resolution. The peak pressures at the transducer reach values up to 1 MPa with focusing gains of 3 to 8. In lithotripsy use is made of short high pressure pulses (with focusing to produce peak positive pressures of 50 MPa) in the hundreds of kilohertz frequency range. For physiotherapy long tonebursts or continuous waves are most commonly used with low intensities (3 W cm^{-2} spatial average temporal average) and frequencies of 1 MHz to 3 MHz. In surgery high intensities (200 W cm^{-2}) and highly focused pulses, lasting up to ten seconds, in the low megahertz frequency range are used to obtain spot sizes of approximately $2mm^2$ in the focal region.

Ultrasound physiotherapy and surgery rely on biological changes occurring in the interrogated region. In surgery the damage is usually caused by thermal effects (the direct conversion of deposited energy to heat) but in physiotherapy there is no thorough understanding of the mechanisms of action. In particular the effect of non-thermal mechanisms (for example cavitation) is poorly understood.

Although there are no reported references of biological effects associated with ultrasonic imaging *in vivo* the subject is by no means closed, mainly due to the lack of understanding of ultrasonic effects. In particular, the case of obstetric scanning has received attention recently due to the particular geometry associated with the scan (in which the sound beam passes through a substantial fluid path before impinging on the foetus) and the lack of data on the effects of ultrasound on the human foetus. Indeed, the available data shows that proliferating tissues are more susceptible to damage than non-proliferating tissue (Dickinson & Shah, 1972). Given that there may be biological effects associated with ultrasonic insonification a more detailed description of the possible effects is given below.

1.2 Biological effects of ultrasound

The effects of the passage of ultrasound through the human body can be classed into those that produce thermal effects and those that produce non-thermal effects. Thermal effects result in heating of the interrogated region, non-thermal effects include cavitation (bubble growth, oscillation and collapse) and streaming (bulk fluid movement).

1.2.1 Thermal effects

Heating of biological tissues arises due to the absorption of acoustic energy as the ultrasound wave passes through the body. The conversion of this acoustic energy into heat is the result of absorption, caused by relaxation and viscous processes.

Both processes result in absorption of energy by causing the medium and the propagating wave to go out of phase with each other so preventing all the energy transferred to the medium returning to the wave. For example, Hynynen (1987) measured *in vivo* temperature rises of the order of 2°C in dog's thigh using hyperthermia beams. The exact form of the absorption depends on the medium of propagation. For example, in distilled water the absorption is purely viscous and therefore depends on the square of the frequency of propagation in the megahertz range. In biological media it is generally reported that the frequency dependence of absorption lies somewhere between one and two, the exact dependence being governed by factors such as the protein content of the medium. Pauly & Schwan (1971) measured the frequency dependence of absorption in homogenised liver to be a little greater than one. They attributed this behaviour to the multiple relaxation processes that occur from the protein structures in liver. The superposition of these relaxation's, over the low megahertz frequency range, produces a smooth frequency dependence which is non-square law.

The production of heating effects has consequently gained increased importance in recent years. The World Federation of Ultrasound in Medicine and Biology (WFUMB, 1991) published a report on 'issues and recommendations regarding thermal mechanisms for biological effects'. Since measurement of temperature rises *in vivo* is not at present possible, the report takes a computational approach and gives recommendations for permissible temperature rises. The computational models are based on the bio-heat equation (NRCP, 1983) which models the situation in terms of a thermal source function and a cooling function. The report states that accurate

knowledge of the parameters that constitute these two terms is required in order to obtain realistic and meaningful results.

The thermal source function depends on the absorption coefficient in the medium of interest and the square of the pressure (proportional to intensity) at the point of interest. The absorption coefficient varies considerably for different tissue types and different specimens. Determining the pressure at the point of interest is also not a trivial problem due to the complex nature of the ultrasonic field from medical transducers.

The cooling function depends on factors such as blood temperature and blood flow and poses even more problems in modelling accurately. For the case of obstetric scanning (in second and third trimester) local deposition of heat is likely to occur in the foetal bone where there is little blood flow. Here the modelling is simplified as the cooling function can be set to zero.

In general the report provides useful guidelines as to the important parameters that need consideration and establishes the importance of further work in this area. For the particular case of foetal scanning the report recommends, based on experiments in other species and results from theoretical models, that temperature rises of less than 1.5°C are deemed to be safe. The report does however point out that the accuracy of the models used is an important consideration when assessing the usefulness of the predictions. For example a typical accuracy of $\pm$ 0.5°C could encompass an overall temperature rise between 1°C and 2°C, the former being deemed safe whereas the latter potentially harmful.

1.2.2 Non-thermal effects

There exists a wide variety of non-thermal mechanisms associated with ultrasound, but only cavitation and streaming will be considered here. Cavitation is a complex phenomenon, and has many definitions in the literature. Broadly speaking, it can be termed as the formation and activity of simple or complex bubble systems in an acoustic field. There are generally two types of cavitation, stable and transient. With stable cavitation a bubble simply oscillates about an equilibrium radius in response to the pressure field generated by an ultrasonic wave. Transient cavities tend to oscillate nonlinearly; they expand to several times their mean radius and then collapse. This collapse can produce high temperatures and pressures which may be significant in terms of safety considerations. The actual role that cavitation plays in terms of biological effects is unclear due to the difficulty in performing and interpreting measurements *in vivo*. *In vitro,* membrane permeability and DNA degradation have been observed.

Acoustic streaming is referred to as bulk fluid movement. It is essentially a nonlinear phenomenon of wave propagation. In a linear system acoustic variables (pressure, density, displacement) have time average values of zero. When second order terms are introduced in the equations of motion and state the fluid element experiences forces which result in bulk fluid movement. The verification of streaming in water, from medical transducers, has been demonstrated with great clarity by Starritt (1990), but the occurrence and the effects, *in vivo,* of these forces on tissue structures is not so clear.

1.3 Propagation of ultrasound

Although there are a number of modes of operation for ultrasonic transducers (described in section 1.1) the range of frequencies and pressures employed in medical applications results in nonlinear propagation being significant. Nonlinear acoustic propagation has been the subject of investigation since the time of Earnshaw (1860). However, the realisation that nonlinear propagation could be important for medical ultrasonic systems was first reported by Muir & Carstensen (1980).

1.3.1 Linear propagation

The wave equation that describes the propagation of sound in a medium can be obtained by combining the equations of continuity, motion and state. The equation of continuity is a statement of the conservation of mass, the equation of motion concerns the conservation of momentum, and the equation of state is an expression that relates the response of a medium to thermal and mechanical stress. The combination of these equations results in relationships between the pressure in a medium, the density of a medium and the local particle velocity in the medium during the passage of an acoustic disturbance. If the acoustic disturbance produces small changes in the pressure, density and particle velocity (compared to the equilibrium value of these quantities) then the equations of propagation can be simplified by considering only first order approximations. Under such conditions the wave equation for particle displacement in one dimensional form (i.e. a plane wave) reduces to:

$$\left(\frac{\delta^2\xi}{\delta t^2}\right) = c^2\left(\frac{\delta^2\xi}{\delta z^2}\right) \qquad 1.1$$

where ξ is the particle displacement, c is the infinitesimal sound velocity, t is time and z is a distance co-ordinate. Solutions to this equation can be obtained for the particle displacement, particle velocity and pressure displacement. For example, for a harmonic source the excess pressure (P) can be expressed as:

$$P = P_o \sin(\omega t - kz) \qquad 1.2$$

where P_o is the source pressure ω and k are the angular frequency and wavenumber respectively.

Equation 1.2 illustrates that an initially sinusoidal disturbance will propagate linearly with no change in frequency of propagation. In addition it shows that the velocity of the acoustic disturbance, c, is constant during propagation.

The above equations describe propagation in a non-dissipative medium. Stokes (1845) was in fact the first to consider absorption of energy into the medium via viscous processes. Taking into account viscosity leads to a modified equation of motion (the Stokes-Navier equation) and yields the following expression for the pressure of a plane wave:

$$P = P_o \sin(\omega t - kz)e^{-\alpha z} \qquad 1.3$$

where α is the amplitude absorption coefficient. More importantly the analysis based on Stokes' work (Beyer 1974) also revealed that for purely viscous processes the attenuation of the wave was proportional to the frequency of propagation squared.

As stated in section 1.2.1 the absorption of energy in biological media is influenced by viscous and relaxational processes. Relaxational processes result in the conversion of translational modes of energy propagation (i.e. the sound wave) into vibrational, rotational and chemical modes and there is consequently a departure from the squared law frequency dependence of attenuation.

1.3.2 Nonlinear propagation

For the frequencies and pressures employed in medical ultrasound the initial acoustic disturbance cannot be assumed to be small. This requires retention of second order quadratic terms in the equations of motion and state. The result is that wave propagation is affected by nonlinearity in the medium and nonlinearity in wave propagation. The two types of nonlinearity are usually referred to as medium and convective nonlinearity.

Medium nonlinearity arises from the equation of state for a medium. This relates the total pressure P and the instantaneous density ρ by:

$$P = P_o + \left(\frac{\delta P}{\delta \rho}\right)_{\rho_o} (\rho - \rho_o) + \left(\frac{1}{2}\right)\left(\frac{\delta^2 P}{\delta \rho^2}\right)_{\rho_o} (\rho - \rho_o)^2 + \ldots, \qquad 1.4$$

where P_o and ρ_o are the equilibrium pressures and densities of the medium and only terms up to 2nd order have been retained. For a large acoustic disturbance the second term on the right-hand side cannot be ignored and results in the sound velocity being non-constant. The relationship between the sound velocity and pressure is given by

$$P = c^2\left(\rho + \frac{B}{2A}\left(\frac{\rho^2}{\rho_0}\right)\right), \qquad 1.5$$

where c is the sound velocity, B and A are the 2nd and 1st terms in equation 1.4.

The medium nonlinearity is expressed by the parameter (B/A) and is basically the ratio of the second order term to the first order term. The physical reason for medium nonlinearity lies in the fact that during the compression half cycle of a wave the medium is compressed. This causes an increase in its stiffness and therefore an increase in the sound velocity during this part of the cycle. Using a similar argument one can see that during the decompression half cycle the sound velocity decreases.

Convective nonlinearity arises from the equation of motion. Under linear propagation conditions the particle velocity u is much smaller than the sound velocity c and its effects can be ignored. It is usual to express this mathematically as:

$$\varepsilon = \left(\frac{u}{c}\right), \qquad 1.6$$

where ε is known as the acoustic Mach number. When $\varepsilon << 1$ we have linear propagation. Under conditions of nonlinear propagation the local sound velocity is dependent on the propagation velocity relative to the medium and the velocity of the medium relative to a fixed observer. In effect because the wave itself induces local motion in the medium the wave is convected by the fluid particles it sets into motion. For longitudinal waves the consequence is that during the compressional half cycle the particle velocity adds onto the sound velocity whereas during the decompressional half cycle it subtracts from the sound velocity.

Both types of nonlinearity combine and cause the compressional half cycle of the wave to travel at a velocity $c+\beta u$ and the decompressional half cycle to travel at a velocity $c-\beta u$. Here β is the nonlinearity parameter and is related to medium and convective nonlinearity by:

$$\beta = \left(\frac{B}{2A} + 1\right). \qquad 1.7$$

Consequently the peaks travel faster than the troughs resulting in them 'catching up' with the troughs. For a plane wave the effects that nonlinearity produces are cumulative and after propagation over a sufficient distance in a lossless medium, an initially sinusoidal wave will distort so that it resembles a sawtooth as illustrated in Figure 1.1.

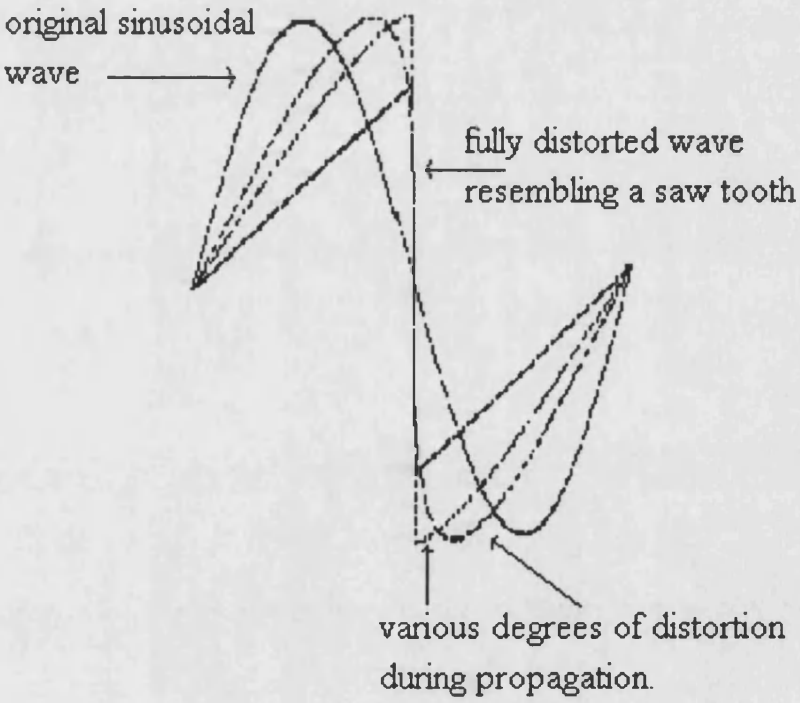

Figure 1.1 Sketch illustrating progressive waveform distortion of an initially sinusoidal wave during propagation. The resultant waveform is fully distorted and forms a shock front.

The extent of distortion of a plane wave is often characterised by a shock parameter σ. For plane waves the shock parameter is defined as:

$$\sigma = \beta \varepsilon k z. \qquad 1.8$$

If $\sigma << 1$ then nonlinear effects are small and can be neglected. When $\sigma = 1$ the wave has distorted to such an extent that a vertical discontinuity forms at the zero crossing of the pressure waveform. At this stage the fundamental has lost 1 dB of energy. If $\sigma = 3$ a sawtooth shock forms. A large vertical discontinuity appears due to the peaks moving forward by ($\pi/2$) radians and the troughs lagging by the same phase.

The distortion of the wave shape in the time domain is equivalent to the generation and propagation of harmonics in the frequency domain. The generation of harmonic frequencies represents a loss of energy from the fundamental frequency of propagation. In a lossless medium the formation of a sawtooth shock, i.e. $\sigma = 3$, results in the generation of a large number of harmonic frequencies, with the amplitude of each harmonic (n) being inversely proportional to its harmonic number. In the absence of dissipation the distance at which an initially sinusoidal, plane wave disturbance forms a mature shock can be expressed in terms of the discontinuity distance l_d, which is given by:

$$l_d = \left(\frac{\rho_o c^3}{\omega P_o \left(1 + \left(\frac{B}{2A}\right)\right)} \right) . \qquad 1.9$$

As can be seen the effect of nonlinear distortion increases as the source frequency, source pressure and nonlinearity parameter increase. By way of example, an

unfocused transducer operating at 1 MHz with a source pressure of 1 MPa into water forms a mature shock at approximately 150 mm.

In an attenuating medium the extent of shock formation is dependent on the attenuation coefficient at the fundamental frequency of propagation and the frequency dependence of attenuation for the higher harmonics.

1.3.3 Consequences of nonlinear propagation

There are various consequences associated with nonlinear propagation of the ultrasound beam, which include:

(i) Enhanced heating;

(ii) Enhanced streaming;

(iii) Calibration;

(iv) Image quality.

(i) Harmonic frequencies, produced as a result of nonlinear distortion, are absorbed at a faster rate and result in a higher effective attenuation coefficient in the medium of propagation. This increase in the attenuation coefficient obviously has consequences when considering the safety aspects of medical ultrasound. The World Federation of Ultrasond in Medicine and Biology (1991) consider the effects of nonlinear propagation by estimating the shock parameter (degree of nonlinear distortion for a plane wave) and the resulting harmonic content of the distorted wave. Although

appreciation of nonlinear effects is an important step towards making realistic estimates of temperature rises the above approach is to some extent very simplified as the processes of nonlinear generation and attenuation, from a finite source, have a complex interaction.

Measurements on the enhancement in heating due to nonlinear propagation have been made by Bacon & Carstensen (1990) in tissue mimicking gels. They observed a threefold increase in the temperature rise compared to the linear case. The large temperature rises measured by Hynynen (1987), *in vivo,* are also attributable to nonlinear effects.

(ii) Although streaming is a separate nonlinear phenomenon, enhanced attenuation due to nonlinear distortion of the waveform is also thought to play a role resulting in enhanced streaming. Starritt *et al* (1990) argue that the enhanced streaming observed in water is likely to be due to enhanced attenuation arising from the increased absorption of nonlinearly generated harmonics.

(iii) Biomedical hazards caused by ultrasound exposure are important and need consideration, however the accurate calibration of medical systems is also of paramount importance in quality control, exposure control and defect detection. Unless the output field and source parameters are known, any studies of ultrasonic effects are of limited value.

In order to calibrate the ultrasonic field a medium of propagation is required. This is normally water, the reasons being that it is available in large quantities and its physical and chemical properties are well documented. Water does, however, have its disadvantages. It is not necessarily a good tissue-mimicking material. In particular the frequency dependence of attenuation in tissue (Duck, 1990) is reported to be quite different from water, so the field *in vivo* has to be inferred (via a de-rating procedure) from water based measurements.

Standardisation on the type of measurement made also needs to be considered. Normally the parameters measured are in four categories:

(a) output power;

(b) pressure and intensity;

(c) beam shape;

(d) transducer characteristics;

Under linear conditions determination of the ultrasonic field is not a great problem, as long as the calibrated receiving hydrophone does not have a resonance at the source frequency and its active area is small enough. However under nonlinear conditions the problems are accentuated. Waveform distortion causes the generation of harmonics which result in loss of energy from the fundamental. Simply measuring the amplitude of the fundamental will therefore not characterise the field. This is especially true in water where due to the low attenuation coefficient harmonic generation is rich. Accurate measurement of the pressure in the field requires use of calibrated wide bandwidth hydrophones. In addition waveform distortion and

diffraction effects result in the peak positive pressure and the peak negative pressure being unequal. The importance of each in terms of biological effects is unclear.

(iv) Nonlinear propagation of the sound beam could be used advantageously to improve image quality in two ways. Firstly measurement of the degree of distortion after passage through a medium may in itself be used as an extra parameter by which to classify the medium. Apfel (1983), Everbach (1989) and other workers have considered this approach, however the interpretation of the results requires good knowledge of the nonlinearity parameter of the medium and the acoustic characteristics of the ultrasonic field. A more promising use of nonlinear effects is to use the harmonics generated in the imaging procedure. This is advantageous as these harmonics are more tightly focused than the fundamental and so could improve the lateral resolution of images considerably.

1.4 Aims of the project

The discussion above has attempted to give a brief overview of the uses of ultrasound in medicine, its biological effects and in particular the problems posed by the nonlinear propagation of the sound wave.

The biological effects of ultrasound cannot directly be determined due to the ethical and practical difficulty in performing experiments *in vivo*. An alternative approach is to try to numerically model the ultrasonic fields that may occur *in vivo*. When considering the nonlinear effects in the acoustic field of medical ultrasound

transducers one also needs to take into account the diffraction of the sound beam due to a finite sized source (this is discussed further in Chapter 2). This requires that models that attempt to predict the ultrasonic field need to take account of the physics of nonlinearity, diffraction and attenuation.

Previous work at the University of Bath (Baker *et al* 1987,1988,1989) has demonstrated that excellent agreement can be obtained between experiment and theory for nonlinear ultrasonic fields in water. The aim of the present work was to extend this work to measurements made in real biological media. As a starting point it was decided to consider physically simple media such as biological fluids, where ultrasonic scattering does not play a role.

The general scheme of the project can be described with reference to Figure 1.2. The overall goal of the project is to compare experimentally measured nonlinear pressure distributions with those predicted theoretically.

In order to theoretically model the pressure distributions a finite difference model (Aanonsen *et al* 1984) based on the KZK equation (Kuznetsov 1971) was used. This model propagates the sound beam from a circular source taking into account the effects of attenuation, diffraction and nonlinear propagation and is described in more detail in Chapter 3.

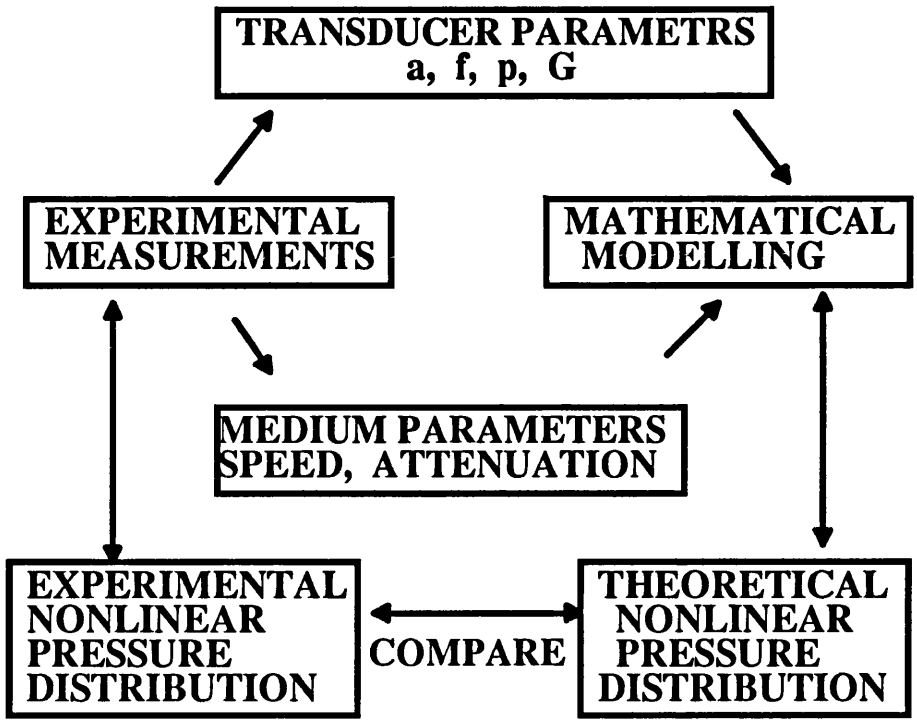

Figure 1.2. A schematic representation of the direction of the work presented in the thesis.

The theoretical model requires a number of input parameters that relate to the source and the medium of propagation. The source parameters relate to the transducer radius a, source pressure P_o, frequency f and gain G of the source. These are relatively easy to obtain experimentally. The medium parameters include the sound velocity c, the frequency dependence of attenuation $\alpha = \alpha_o f^m$ and the nonlinearity parameter β. In contrast, these parameters, and in particular the frequency dependence of attenuation may not be well known for biological fluids. It was, therefore, essential that as many of these parameters were measured at the same time as the nonlinear measurements. The data would also provide a useful addition to the available data on biological fluids. The fluids used in this work were amniotic fluid, urine, 4.5% Human Albumin solution and 20% Human Albumin solution.

1.6 Thesis content

The remainder of this thesis is composed of the following sections. Chapters 2 and 4 give a brief review of the literature on acoustics and measurement of acoustic parameters in biological media. Chapter 3 introduces the model used in the simulations and describes some initial experiments in water that demonstrate the importance of enhanced attenuation. Chapter 5 describes the design of an experimental rig for making the measurements described in section 1.5. Chapters 6 and 7 illustrate the results of the frequency dependent attenuation, sound velocity and axial nonlinear pressure distribution for the biological fluids mentioned above. Chapter 8 discusses the results and their implications. In addition Appendix A is concerned with the measurement of the medium nonlinearity parameter B/A.

2.0 REVIEW OF LITERATURE ON ACOUSTICS

Medical ultrasonic systems vary widely in their method of producing ultrasonic fields. In general the methods employed to transmit, receive and focus the sound beam are complex. For example the array in a typical B-mode scanner for imaging may have sixty or more elements each of which transmits individually with focusing achieved by electronic time delays between transmitting elements. In addition the elements themselves are not generally circular; rectangular, annular or square geometries are often used. Although a number of designs exist one can gain an understanding of the propagation of the sound beam from these complex geometries by considering a much simpler arrangement. The one most commonly cited in the literature is that of a plane piston radiator located in an infinite rigid baffle with focusing incorporated by introducing a phase variation across the source. This chapter reviews the relevant literature on linear and nonlinear propagation with an emphasis on the acoustic fields produced by a circular piston sources.

2.1 Infinitesimal acoustics

2.1.1 Plane Piston

Figure 2.1 illustrates the geometry that is often used to represent the physical situation of radiation from a plane piston located in an infinite rigid baffle.

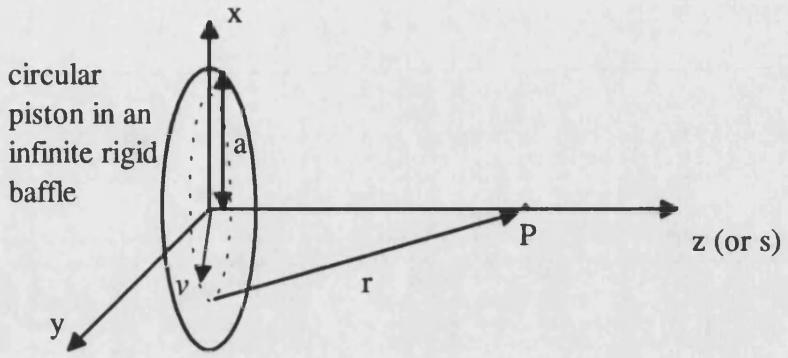

Figure 2.1 Schematic of the geometry associated with a circular piston source.

The piston source has a radius *a* and is located at the origin of the Cartesian co-ordinate system with *v* being the radius of a concentric ring. The *z*-axis is normal to the transducer face. It is also common to express the axial distance in terms of a dimensionless co-ordinate *s* which is given by:

$$s = \left(\frac{z\lambda}{a^2}\right), \qquad 2.1$$

where *z* is the axial distance, λ is the wavelength of sound and *a* is the piston radius. The advantage of this nomenclature is that the variables determining the structure of the ultrasonic field (the source radius and wavelength of sound) are normalised.

Initial studies of the pressure field from a baffled piston source were made by Rayleigh. The pressure field was expressed as the integrated effect of point sources over the piston face. This is referred to as the Rayleigh integral (a special case of Helmholtz integral equation) in the literature and is in effect a statement of Huygens principle of linear superposition. The integral is expressed below in terms of Φ, where Φrepresents a scalar potential:

$$\Phi = -u_o e^{i\omega t} \int_o^a \left(\frac{e^{-ikr}}{r}\right) v\delta v. \qquad 2.2$$

Here u_o is the source particle velocity, r is the distance between the point of observation and a point on the surface of the source and the integration is performed over concentric shells of thickness δv. The expression under the integral represents the sound field produced by a secondary point source. Although the form of this expression is simple its solution in general is not easily attainable due to the difficulty in expressing the variable r into an integral form.

An exception to this lies in the on axis field. Due to symmetry, equation 2.2 reduces to one which can be integrated simply and results in the following relationship for the on axis pressure distribution:

$$P = 2P_o \sin^2\left(\left(\frac{\pi}{\lambda}\right)\left[(a^2 + z^2)^{\frac{1}{2}} - z\right]\right). \qquad 2.3$$

Figure 2.2a and 2.2b plot the characteristic on-axis diffraction pattern produced by a plane piston radiator in terms of the actual axial distance and the normalised axial distance respectively. The result in Figure 2.2a is for a circular 38 mm diameter transducer operating at 2.25 MHz into a lossless medium. The main features are:

(i) The rapid oscillations in average pressure which increase in occurrence as one approaches the source;

(ii) The variation in average pressure from 0 to $2P_o$;

(iii) The presence of two regions in the axial field.

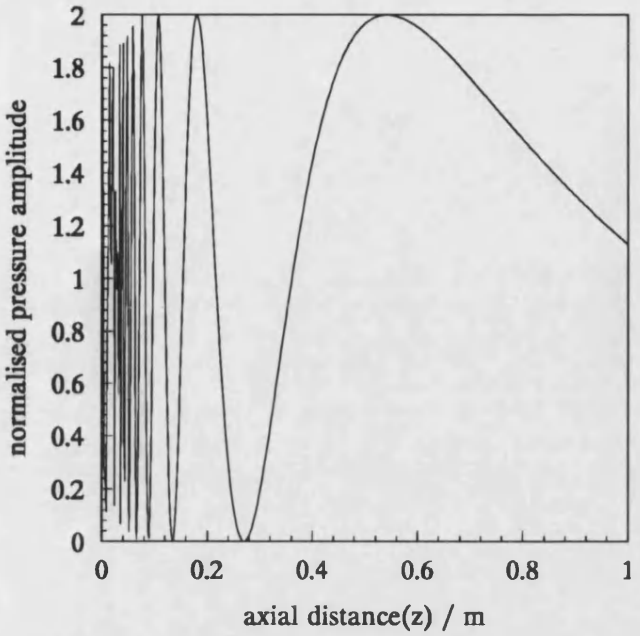

Figure 2.2a On-axis diffraction pattern for a plane piston with respect to the axial distance in metres.

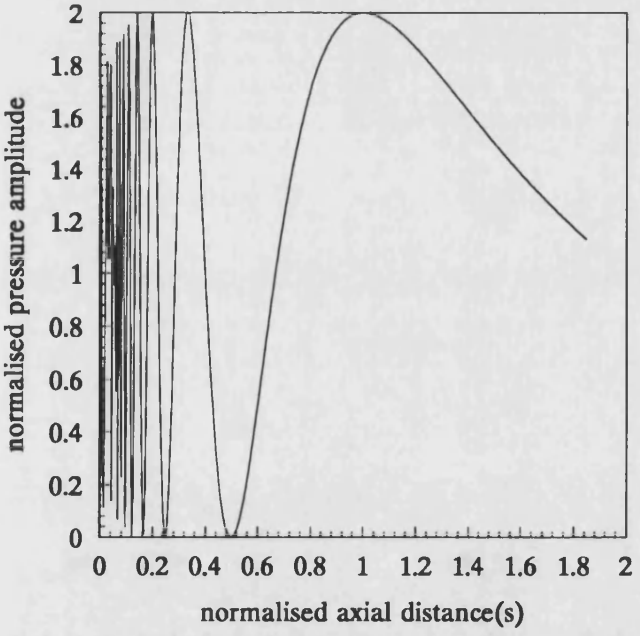

Figure 2.2b On-axis diffraction pattern for a plane piston with respect to the normalised axial distance.

The two regions are commonly referred to as the near field (Fresnel diffractive zone) and the far field (Fraunhofer diffractive zone). The transition between the two

regions is sometimes defined at the normalised distance s =1, the position of the last axial maximum. In the near-field rapid changes in phase, due to the contribution from concentric rings on the piston face, dominate the expression for the axial variation in pressure. For example, when all the components are in phase the resultant pressure is twice the source pressure. In the far-field the spherical spreading component from the secondary sources dominates resulting in a much slower variation in axial pressure (due to a slower phase variation) beyond the last axial maximum.

More general solutions to the Rayleigh integral, which include off-axis variations in the pressure, fall into two categories, i.e. those that consider the far-field and those that consider the near-field.

Historically the far-field distribution has been treated extensively. In this case the observation point r (i.e. the point at which the pressure is to be determined) is such that, mathematically $r>>a$. This allows the integral to be simplified, by approximations, so yielding a closed form solution. The main features of the pressure field obtained are in the directivity of the pressure distribution. Off-axis maxima and minima are revealed (side lobes) which vary in accordance with Bessel functions of zero order. In addition it is found that as the ratio of wavelength to piston radius is decreased so the number of side lobes increases.

Closed form solutions to the Rayleigh integral in the near-field, without approximations, are generally not attainable. Zemanek (1970) obtained numerical

results (3-dimensional plots) from the Rayleigh integral for the near-field behaviour of a circular piston source. The method did not require any approximations in the integral equation, but merely considered the piston source as a double summation of discrete secondary sources. His results were valid for a wide range of piston sources ($\frac{a}{\lambda}$ from 1 to 20) and indicated, with great clarity, the complex near-field behaviour caused by interference. He also demonstrated that a regular beam pattern (in the far-field) forms much closer to the source than previously thought and that the minimum beam width (-3 dB falloff in intensity) is approximately one quarter of the transducer radius.

Tjotta & Tjotta (1980) produced an analytical expression for the sound pressure when $kr>>1$ based on a parabolic equation. Using the parabolic approximation, only waves with small offset angle with respect to the propagation axis are considered. The expression was shown to be similar to the first order expansion of the Helmholtz equation. They reproduced the numerical results of Zemanek (1970) and verified that near the source the sound beam could be considered as plane and collimated whereas in the far field it had a Bessel function directivity. They included in their analysis the effects of absorption. Depending on the 'strength' of absorption the rapid near field oscillations in pressure between 0 and $2P_o$ were diminished in magnitude and in general caused a blurring of interference effects. Including dissipitative effects also revealed insights into how close to the piston source the parabolic approximation was valid. For example in the absence of absorption equations based on the parabolic approximation break down and do not yield the correct pressure of P_o at the piston face.

Recently Hutchins *et al* (1986) developed a single integral equation to describe the whole pressure field from circular sources with variable amplitude and phase distributions across the face of the piston. They also performed a detailed set of experiments measuring the pressure distribution to a spatial resolution of $\frac{\lambda}{5}$. In order to achieve this resolution ultrasonic frequencies were not employed, however, the $\frac{a}{\lambda}$ ratio was still in the region of 5. They obtained good agreement between experiment and theory. In particular some asymmetric measured fields were accurately modelled using non-uniform source excitations.

2.1.2 Focused piston

In addition to plane piston excitation a considerable amount of work has been performed on focused sources. Initial work was done by O'Neil (1949). He expressed the sound field in terms of a double integral:

$$P(z,\xi) = \frac{jkP_o}{2\pi}\int\int_s \frac{e^{-jkr}}{r} dS, \qquad 2.4$$

where, ξ is the radial co-ordinate. From equation 2.4 expressions for the axial pressure distribution, pressure at the focus and pressure across the focal plane were derived.

A useful insight into the field of a focusing source is given by Lucas & Muir (1982). They approach this problem by solving the Helmholtz equation in terms of the complex velocity potential. Instead of considering a physically concave source they make the assumption that an identical result can be obtained by treating the problem as radiation from a phase modulated plane source. A parabolic approximation is

again applied yielding a single integral equation for the pressure field. The solution to this equation gives the pressure distribution on-axis and in the focal plane. Figure 2.3 illustrates the axial pressure distribution for a 38 mm diameter circular source operating at 2.25 MHz with a focal length of 140 mm.

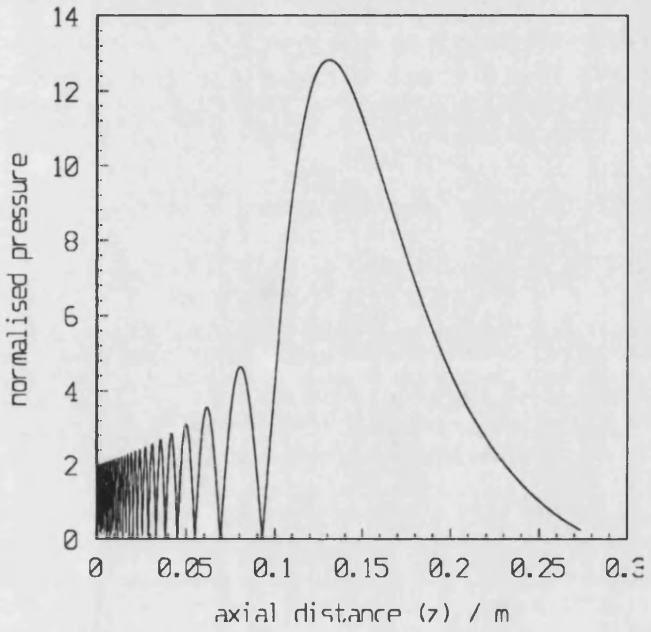

Figure 2.3 Axial variation of the pressure field for a 2.25 MHz, 19 mm radius transducer with a focal length of 140 mm.

They show that the maximum pressure, on-axis, is achieved just before the focal plane on the transducer side. The axial distance to the position of maximum pressure is given by:

$$\left(\frac{z_o}{D}\right) = 1 - 12\left(\frac{D}{R_o}\right)^2 + O\left[\left(\frac{D}{R_o}\right)\right]^4, \qquad 2.5$$

where z_o is the position of the maximum pressure, D is the radius of curvature of the wavefront and R_o is the Rayleigh distance ($ka^2/2$). Their results demonstrate that decreasing the ratio of the radius of curvature to the Rayleigh distance causes the position of the maximum pressure and focal plane to converge towards the same axial point. As can be seen in Figure 2.3 the two positions are close together due to the relatively high focusing gain. In addition the pressure at the focus is given by:

$$P(0,D) = -i\left(\frac{R_o}{D}\right)P_o e^{(ikD)}. \qquad 2.6$$

Using this expression a definition for the focusing gain of the source can be obtained as the ratio of the pressure at the focal point to that at the source. This results in the gain being expressed as:

$$G = \left|\left(\frac{P(0,D)}{P_o}\right)\right| = \frac{R_o}{D}. \qquad 2.7$$

The near-field phase behaviour can be interpreted in terms of the central spherical component and the edge wave emanating from the rim of the transducer. On-axis the edge wave components are all in phase and add to form a significant edge contribution which adds vectorially to the spherical component. This produces periodic oscillations which result in on-axis maxima and minima. When the observation point is off-axis the components from the edge waves do not add coherently, so the phase is determined predominantly by the spherical component.

The results are also compared with those of O'Neil (1949) and found to be in excellent agreement for sources with small radii of curvature and high *ka* value. The main disagreement between the results is close to the source, at distances within 30% of the focal distance. The discrepancy arises due to the break down of the parabolic approximation close to the source in a similar way to that reported by Tjotta & Tjotta (1980) for the plane piston case.

Other researchers have also demonstrated good agreement between experiment and theory for focused sources. For example Madsen *et al* (1981) made measurements for a low gain transducer (G of approximately 4) that agreed well with an exact solution derived by them. As with Lucus & Muir (1982) the solution requires only a single integral to compute the pressure distribution.

2.1.3 Diffraction correction

The literature quoted above refers to the pressure field distributions that would be obtained with an infinitesimally small receiver. In reality however any measurements will always use a finite size receiver. The effect of this is to give a signal output proportional to the average pressure amplitude over the receiver. This is referred to as a diffraction correction (or diffraction loss) and has received significant theoretical study in the literature.

Huntington *et al* (1948) were one of the first to investigate the averaged pressure field over a finite sized receiver that was coaxial to and the same size as the source.

They numerically integrated an expression derived by Lommel (1886). Lommel's expression originates from work done on the diffraction of light from a circular hole in an opaque screen (a situation that is analogous to the acoustic problem) and is composed of trigonometric functions and series expansions of cylindrical Bessel functions. Huntington *et al* (1948) expressed the integral in terms of the dimensionless parameter *s*. The results showed the Lommel diffraction integral to be a monotonically decreasing function of *s*.

Seki *et al* (1956), while measuring the attenuation in materials, observed that the usual exponential fall off in the detected signal amplitude with distance was not strictly correct. The non-exponential pattern was due to the presence of peaks in the amplitude of the detected signal. For confirmation the Lommel diffraction correction integral was evaluated numerically illustrating the presence of the peaks. They stated that the earlier computations of Huntington *et al* (1948) were not evaluated at close enough intervals and so skipped the observed peaks. Other researchers, Williams (1951) and Bass (1958) have obtained exact integral expressions. Both derive expressions from work done by King (1934) for radiation from an ideal piston radiator. Williams result has been calculated and verified experimentally by Seki *et al* (1956).

The work cited above was for an equal size transmitter and receiver. The more general case of unequal size apertures has been studied by Beissner (1981). He transformed a quadruple integral (based on Rayleigh's integral equation) into a single integral expression (based on elementary functions) using geometrical considerations

and a change of variables. The resulting integral was evaluated numerically, and Figure 2.4 illustrates some results for the axial field from a 39 mm diameter, 2.25 MHz transducer with various receiver sizes, *b*, plotted against the normalised axial distance *s*.

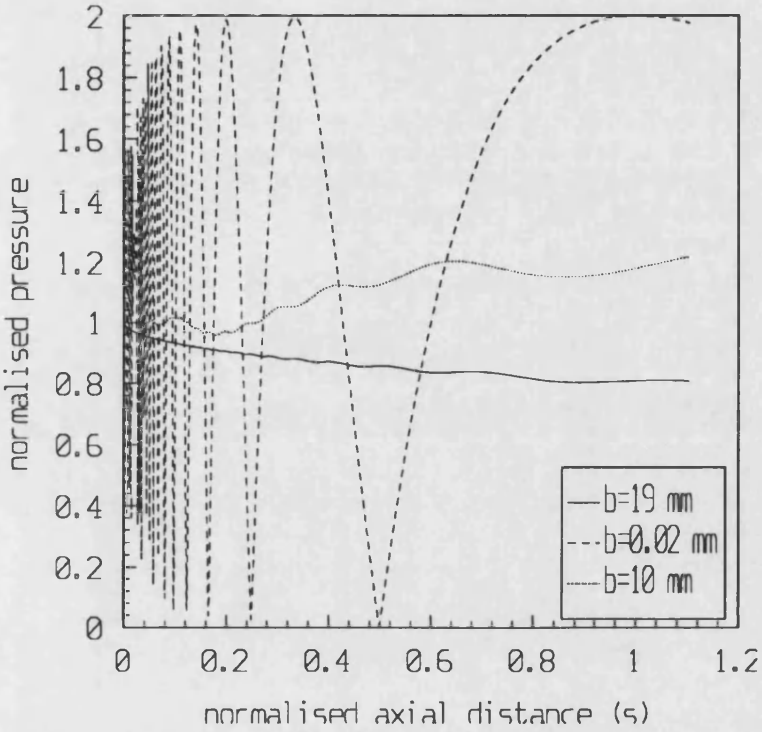

Figure 2.4 Illustration of the diffraction loss for a 19 mm radius 2.25 MHz transducer with receiver radii of 0.02 mm, 10 mm and 19 mm.

Figure 2.4 shows that as the receiver size is increased the minima and maxima appear at different locations in the axial field, but in general the axial variation in pressure is reduced.

Another source of diffraction correction (or diffraction loss) occurs when sound propagation is through media of different velocities. This is often the case with

experiments where the attenuation properties of a medium are being investigated, and is discussed in Chapter 5 section 5.4.4.

2.2 Finite amplitude acoustics

2.2.1 Plane wave propagation

Equation 1.1 gave an approximate wave equation for particle displacement, for conditions of linear propagation. A more accurate expression for the particle displacement in a liquid is that given below:

$$\left(1+\frac{\delta\xi}{\delta z}\right)^{\frac{B}{A}+2}\left(\frac{\delta^2\xi}{\delta t^2}\right)=c^2\left(\frac{\delta^2\xi}{\delta z^2}\right) \qquad 2.8$$

where ξ represents the particle displacement and B/A represents the medium nonlinearity. Earnshaw (1860) solved equation 2.8 implicitly to yield the following relationship for the particle velocity:

$$u(z,t)=u_o\sin\left[\omega t-\frac{\omega z}{c_o}\left(1+\frac{Bu}{2Ac_o}\right)^{-\frac{2A}{B}-1}\right]. \qquad 2.9$$

The expression demonstrated that points of high particle velocity move faster than those of low velocity, resulting in progressive waveform distortion, as illustrated in Figure 1.1, and the formation of a discontinuity distance as given by equation 1.7 and illustrated in Figure 1.1.

A number of workers have obtained solutions that are based on power series expansions of the excess pressure or particle velocity, expressed as a Fourier series. Fay (1931) obtained an analytical solution for highly shocked waves taking into account attenuation. Fubini (1935) considered the case of weak shocks in lossless media and expressed the particle velocity as an infinite summation of the harmonic components of the distorted waveform. The expression derived by Fubini (1935) is:

$$\left(\frac{u}{u_o}\right) = \Sigma_{n=1}^{\infty} B_n \sin n(\omega t - kz), \qquad 2.10$$

where

$$B_n = \left(\frac{2l_d}{nz}\right) J_n\left(\frac{nz}{l_d}\right). \qquad 2.11$$

The expression illustrated that for low levels of nonlinearities (i.e. small u and small z) the second harmonic varied as the source particle velocity squared, the third harmonic varied as the source particle velocity cubed etc.

A large amount of work in the area of finite amplitude acoustics has been done by Blackstock (1962, 1964, 1966). He realised that the solutions of Fay and Fubini applied to different regions of propagation and was able to combine the two solutions to produce expressions for the pressure of the harmonic components of finite amplitude plane waves during propagation under both weak and strong shock. In addition Blackstock (1962) also initiated the analysis of finite amplitude wave by considering solutions to Burgers equation. The attractiveness of this approach was

that Burgers equations could take into account both dissipative and dissipationless processes.

Because of problems in obtaining full analytical solutions to Burger's equation, many workers attempted numerical solutions. Fox and Wallace (1954) used a method analogous to nonlinear distortion in electrical circuit analysis. This was computationally time consuming due to the need to apply a large number of Fourier transforms. Trivett and Van-Buren (1981) applied an efficient algorithm, carried out entirely in the frequency domain, to solve Burger's equation for plane, spherical or cylindrical waves. The solution took on the form of a trial Fourier series of linear waves, the coefficients of the series relating to the amplitude of the harmonic components. The above methods considered only one dimensional waves, with diffraction effects not included, and so were not capable of predicting the near-field of finite size sources.

2.2.2 Piston sources

In order to take diffraction into account two approaches are possible. Ingenito and Williams (1971) used a perturbation method to obtain the second harmonic variation in the near-field of finite size sources, finding good agreement between experiment and theory. Although this method is numerically simple it has some disadvantages. Since it uses a perturbation approach only low levels of nonlinearity can be considered and information at higher harmonics is not available. In addition diffraction of the second harmonic is also excluded.

Lucas & Muir (1983) considered finite amplitude propagation from focused sources. Although their approach was a perturbation one and so valid for weak shocks, Humphrey *et al* (1986) have provided experimental confirmation for the predicted second harmonic levels.

An alternative is to start with the nonlinear parabolic equation of wave propagation in two dimensions. This equation is an approximation to the nonlinear wave equation and is relatively easy to implement numerically. In view of this Zabolotskaya & Khovkhlov (1969) (also Tjotta & Tjotta 1981) derived a parabolic equation for nonlinear waves. In 1971 Kusnetsov extended it to include absorption. This particular approach is discussed further in Chapter 3.

Recent work has concentrated on measuring and predicting the finite amplitude field of piston sources (in many cases at ultrasonic frequencies) and these will be mentioned briefly. Aanonsen *et al* (1984) and Hamilton *et al* (1985) used the parabolic approximation with a frequency domain solution for continuous waves and axially symmetric fields. Hart and Hamilton (1988) also produced an efficient frequency domain solution to solve coupled parabolic differential equations. Their method was very good for focused fields and agreed with available experimental data. In particular they illustrated the presence of higher harmonic sidelobes which earlier models had not accounted for. Baker *et al* (1987,1988,1989) using the solution described by Aanonsen *et al* (1984), for the KZK equation, produced a comprehensive set of theoretical and experimental results for plane, focused and pulsed fields in water with emphasis on medical systems. Their results showed good

agreement, for the amplitude and phase of the first five harmonics, between experiment and theory. Discrepancies were caused by both experimental and theoretical limitations. Experimentally limitations occurred due to the accuracy with which measurements could be made for the higher harmonics especially due to the effects of hydrophone calibration, hydrophone averaging, hydrophone alignment and source pressure determination. Theoretical limitations resulted from the use of the parabolic approximation (especially for results close to the piston face) and a trade off between numerical accuracy and computational time.

The most recent model of nonlinear propagation, that takes into account attenuation and diffraction is that by Christopher & Parker (1991). This model does not rely on the parabolic approximation. The diffractive field, from a baffled piston source, is computed by considering the angular spectrum of the harmonic field at a particular plane. The harmonic field at a plane is in effect decomposed into a sum of plane waves travelling in different directions (i.e. at different angles) by applying a two dimensional Fourier transform to the field. The harmonic field at any other plane can then be calculated by summing these spatial Fourier components, in the new plane. Although this approach to diffractive field propagation is not new, Christopher & Parker (1991) have developed a computationally efficient algorithm for sources that resemble those encountered in medical ultrasound imaging. The model is similar to that of Aanonsen in that non-linearity is accounted for in the frequency domain. The predictions of the model agree well with the predictions and experiments of Baker *et al* (1988).

3.0 THE NUMERICAL MODEL

The theoretical simulation of the pressure fields produced by medical ultrasonic transducers requires models to take into account the processes of attenuation, diffraction and nonlinear propagation. In chapter two reference was made to the approach taken by Kuznetsov *et al* (1971). The numerical implementation of Kuznetsov's equations by Aanonsen *et al* (1984) forms the basis of the model used in this work. The first part of this chapter gives a brief overview of the numerical model. The later part will demonstrate one of the uses of the model in the calculation of the enhancement of attenuation resulting from nonlinear propagation.

3.1 Introduction

The model used for the simulations discussed in this report is based on the equation of propagation (the so called KZK equation) for finite amplitude waves in a viscous heat conducting fluid derived by Kuznetsov (1971). In its general form the KZK equation can be expressed in terms of a scalar potential Φ:-

$$\frac{\delta^2\Phi}{\delta t^2} - c^2\nabla^2\Phi = \frac{\delta}{\delta t}\left(2\alpha ck^2\nabla^2\Phi + (\nabla\Phi)^2 + \frac{B}{2Ac^2}\left(\frac{\delta\Phi}{\delta t}\right)^2\right). \qquad 3.1$$

The right hand side of the equation consists of three terms, the first represents absorption, the second convective nonlinearity and the third medium nonlinearity.

The left hand side of the equation corresponds to the wave equation for a lossless linear medium.

Kuznetsov also demonstrated that equation 3.1 could be simplified by using the parabolic approximation i.e. when most of the energy in the beam is confined to the axial direction, as is the case for the geometry's used from medical ultrasonic transducers. Mathematically this is normally fulfilled when $ka >> 1$, where k is the wavenumber and a is the aperture radius. Physically the approximation implies that at the frequency of operation the aperture is many wavelengths across. The simplified equation is normally expressed in dimensionless form as:

$$\frac{\delta^2 \tilde{P}}{\delta\sigma\delta\tau} = \alpha R_o \frac{\delta^3 \tilde{P}}{\delta\tau^3} + \frac{1}{4}\nabla_\perp^2 \tilde{P} + \frac{R_o}{2l_d}\frac{\delta^2\left(\tilde{P}\right)^2}{\delta\tau^2}, \qquad 3.2$$

where $\tilde{P}$ is the pressure normalised to the source pressure.

τ is a retarded time that takes into account the phase behaviour for a plane progressive wave.

σ is an axial distance normalised by the Rayleigh distance.

$\nabla_\perp^2$ is the two dimensional Laplace operator applied to the dimensionless vector ξ.

The parameters αR_o and R_o/l_d indicate the importance of absorption and nonlinearity respectively.

There is no general analytical solution to equation 3.2. However Aanonsen *et al* (1984) considered a numerical approach. They started by obtaining a trial Fourier

series solution for the harmonics in terms of their amplitudes and phases with respect to axial and radial co-ordinates. The trial solution can be expressed in terms of the normalised pressure as:

$$\tilde{P} = \Sigma_{n=1}^{\infty}(c_n \cos n\tau + d_n \sin n\tau). \qquad 3.3$$

Substituting this solution into equation 3.2 results in a set of coupled differential equations for the coefficients c_n and d_n which are in effect the resolved vector components of the pressure amplitude of the n^{th} harmonic. The differential equations are given below in equations 3.4 and 3.5, where n represents the harmonic number:

$$\frac{\delta c_n}{\delta \sigma} = -\alpha r_o n^2 c_n - \frac{1}{4n}\nabla_{\perp}^2 d_n +$$

$$\frac{r_o n}{2l_d}\left[\frac{1}{2}\Sigma_{i=1}^{n-1}(c_{n-i}d_i + d_{n-i}c_i) + \Sigma_{i=n+1}^{\infty}(d_i c_{i-n} - c_i d_{i-n})\right]; \qquad 3.4$$

$$\frac{\delta d_n}{\delta \sigma} = -\alpha r_o n^2 d_n + \frac{1}{4n}\nabla_{\perp}^2 c_n +$$

$$\frac{r_o n}{2l_d}\left[\frac{1}{2}\Sigma_{i=1}^{n-1}(d_{n-i}d_i - c_{n-i}c_i) - \Sigma_{i=n+1}^{\infty}(c_i c_{i-n} + d_i d_{i-n})\right]. \qquad 3.5$$

These indicate how the coefficients c_n and d_n change with the normalised axial distance σ. The right hand side of the above equations are composed of three terms, the first term relates to absorption, the second term to diffraction and the third to the nonlinear interaction between the harmonics. Taking either equation we can gain a qualitative understanding of the processes occurring during the propagation along the normalised axial co-ordinate.

As can be seen the absorption term depends on the harmonic number squared and is simply the classical viscous attenuation of sound in water. The forms of equations 3.4 and 3.5 allow this term to be generalised into an arbitrary absorption form (Korpel, 1980).

The diffractive term depends on the reciprocal of the harmonic number. This implies that diffraction becomes less important for the higher harmonics. In effect for the higher harmonics *ka* becomes larger and more wavelengths fit across the aperture resulting in their propagation tending towards that of a plane wave.

The nonlinear term is directly proportional to the harmonic number and inversely proportional to the plane wave shock distance. This results in nonlinearity becoming more important as the harmonic number, nonlinearity parameter and source pressure are increased. One can also see how the contribution from any particular harmonic is determined, for example the third harmonic results from interactions of the 1st and 2nd, 1st and 4th, 2nd and 5th etc.

3.2 Numerical implementation and associated errors

The above differential equations can be solved by numerical methods; these solutions are based on that of Aanonsen *et al* (1984) who used a stepwise integration scheme using a backward finite difference formula. In order to obtain the numerical solution some approximations were made. These are grouped into three classes and discussed below.

3.2.1 Region of integration

Firstly, the infinite series of harmonics that represents the wavefield has to be truncated. Truncation causes the flow of energy to stop at the highest harmonic retained in the calculation, so artificially increasing its energy. Because energy also flows from the higher to the lower harmonics this truncation can also effect the energy in the lower harmonics and leads to inaccurate results. Provided a sufficient number of harmonics are retained the resultant error is negligible.

As in the case of truncation of the infinite harmonic series, there also needs to be a finite region of integration in the radial plane. In order to numerically implement the solution the radial boundary has to be at a sufficient distance so that ultrasonic energy does not reflect energy back from it. This reflection is easily identified due to the presence of an oscillatory behaviour, resulting from the interference between the direct and reflected wave, in the on-axis pressure distribution.

3.2.2 Axial and radial step sizes.

The stepwise integration method used by Aanonsen calculates the coefficients (c_n and d_n) along the next radial plane by a direct iteration method. This imposes strict limitations on the values of the axial and radial step sizes. For the iteration to converge the step sizes must be chosen such that $\left(\frac{\Delta\sigma}{\Delta\xi^2}\right) < 0.5$.

Since the solution is a numerical one there are errors associated with the chosen axial and radial step sizes. If the spatial variation of the pressure field is faster than either these step sizes then there will be some averaging in the predicted results. In particular the radial step size can be important in calculating the position of the rapid near field oscillations. The position of these maxima and minima depend on the square of the aperture radius. In the numerical implementation the aperture pressure distribution is represented by amplitude and phase variations across it. Given that the exact aperture radius can only be represented by using a finite radial step size it follows that the step size chosen will determine how well the aperture is modelled. Using small step sizes does not necessarily produce higher accuracy; machine rounding error can become an important factor as the number of calculations performed increases.

3.2.3 Mathematical approximations

The numerical method implemented for the calculation relies on the reduction of fully implicit equations for c and d to partially implicit ones. This simplification in effect assumes that the variations in c and d due to the nonlinear term are small in comparison to the variations produced by the diffractive term. The result is that only nonlinearity from the previous calculation step is considered, so decreasing computer run-time significantly. Aanonsen indicated that for his conditions this was a valid approximation. The other simplification in the model is the parabolic approximation which has been mentioned previously.

The simulated pressure and phase distributions, obtained from Aanonsen's model have been verified experimentally for ultrasonic measurements in water (Baker *et al*, 1987,1988,1989). The next section will demonstrate some of the other calculations that can be performed with the model, in particular the determination of the enhancement of attenuation due to nonlinear propagation.

3.3 Enhanced attenuation

In the introductory chapter reference was made to measurements of enhanced streaming, resulting from nonlinear propagation, made by Starritt (1990). The explanation offered for the enhanced streaming was the extra absorption of energy resulting from the higher attenuation of nonlinearly generated harmonics. In order to quantify this enhanced attenuation, the numerical model has been used to simulate the experimental conditions used by Starritt. The remainder of this chapter will describe the method employed to determine the enhanced attenuation theoretically. A comparison will then be made between the measurements made by Starritt and the predictions of the model; this will illustrate the parameters required to simulate experimentally determined pressure distributions. In addition measurements and predictions for a 5 MHz focused single element transducer operating in water will be presented. These results will demonstrate the potential of using numerical models to accurately predict derived parameters such as enhanced attenuation.

3.3.1 Determination of enhanced attenuation.

Determination of the enhanced attenuation, due to nonlinear propagation, requires a knowledge of the intensity in the sound beam. In general detectors of acoustic radiation measure pressure not intensity. However a quantity that is closely related to intensity is the pressure squared integral and is discussed below.

3.3.1.1. Pressure squared integral (PSI).

Intensity is defined as:

$$I = P.v, \qquad 3.6$$

where P and v are the acoustic pressure and particle velocity respectively. Note that both the intensity and particle velocity are vector quantities.

For an infinite plane progressive wave the pressure and particle velocity are always in phase so the intensity becomes proportional to P^2. In the near-field of a piston source the particle velocity has both axial and radial components and it cannot immediately be assumed that it and the pressure are in phase. However for most piston sources the radius of the source is much larger than the wavelength of the sound and quasi-plane wave propagation can be assumed, allowing the intensity to be approximated to pressure squared. The validity of this has been studied by Mair *et al* (1987). They calculated the intensity using the formal definition (given by equation 3.6) and compared it with the pressure squared assumption. Their results suggest that the approximation is valid, on-axis, when the axial distance from the

source is greater than a few piston radii. In the very near field however the results can differ by as much as 50%. They also presented results for focused sources, but only for piston sizes of a few wavelengths across. The results seem to indicate that there is some difference between intensity and the pressure squared approximation, but the effect is reduced for larger pistons.

For a plane wave the time average intensity is expressed as:

$$I = \frac{1}{\tau \rho_o c} \int_o^\tau P^2(t) dt, \qquad 3.7$$

where τ is the period of the wave and $P(t)$ is the complex acoustic pressure. The complex acoustic pressure for a distorted sine wave can itself be expressed as:

$$P(t) = \Sigma_n p_n e^{i(n\omega t + \phi_n)}. \qquad 3.8$$

Here the summation is simply the Fourier series representation of the waveform in terms of Fourier components, where p_n represents the amplitude of the n^{th} harmonic and ϕ_n its phase.

Because $P(t)$ is complex, $P^2(t)$ is obtained by multiplying it by its complex conjugate $P^*(t)$. This then gives

$$P^2(t) = \Sigma_n \Sigma_m p_n p_m e^{i\omega m t} e^{-i\omega n t}, \qquad 3.9$$

where m is used to distinguish $P(t)$ from its complex conjugate. The intensity can now be expressed as,

$$I = \frac{1}{\tau \rho_o c} \Sigma_n \Sigma_m p_n p_m \int_o^\tau e^{i\omega(m-n)t} dt. \qquad 3.10$$

If $m \neq n$ then the integrand goes to zero because a complex function and its conjugate are orthogonal. If $m=n$ then the integrand goes to 1, and we have,

$$I = \frac{1}{\tau \rho_o c} \Sigma_n p_n^2 \tau. \qquad 3.11$$

So by summing the squares of the harmonic pressures in the wave the intensity, on-axis, can be inferred. The summation described in equation 3.11 is known as the pressure squared integral and was incorporated into the numerical model. Given that the intensity in an ultrasonic beam can be determined, by considering the pressure squared integral, the enhancement of attenuation due to nonlinear propagation can be calculated using the following argument.

The attenuation of a plane progressive wave is defined as:

$$I_l = (I_l)_o e^{-2\alpha_l z}, \qquad 3.12$$

where I_l is the intensity at a distance z, α_l is the attenuation coefficient (expressed in Nepers per unit distance) and $(I_l)_o$ is the intensity at the source. The subscript l denotes a wave propagating under linear conditions. A similar expression can be obtained for a wave propagating under nonlinear conditions:

$$I_{nl} = (I_{nl})_o e^{-2(\alpha_l + \alpha_{nl})z}, \qquad 3.13$$

where the subscript nl denotes a contribution from nonlinear propagation, and α_{nl} represents the contribution from the additional attenuation coefficient due to nonlinear propagation effects.

Normalising both equations (3.12 and 3.13) by their respective source intensities and rearranging one obtains the following equation:

$$\left(\frac{-1}{2z}\right)\ln\left(\frac{\frac{I_{nl}}{(I_{nl})_o}}{\frac{I_l}{\left(\frac{I_l}{I_{lo}}\right)}}\right) = \alpha_{nl} \qquad 3.14$$

From equation 3.14 one can see that the additional attenuation due to nonlinear propagation can be determined by knowledge of the intensity in the nonlinear and linear ultrasonic field. This procedure is attractive because by considering the ratio of axial variation of energy in the two beams, one can cancel out variations in the energy due to the diffractive effects of a finite sized source. It should be noted that in the results presented below the intensity has been replaced by the pressure squared integral (PSI).

3.3.1.2 Starritt's measurements of PSI

Starritt (1990) measured enhanced streaming from medical ultrasound transducers. In order to investigate the source of the high streaming velocities measurements of the PSI in the ultrasonic beam were also measured. These measurements were made with a 19 mm diameter single element circular transducer with moderate gain operating at a centre frequency of 3.5 MHz. It was driven with a short tone burst at a pressure of 0.03 MPa and at 0.39 MPa. These two source pressure conditions determined the linear and nonlinear ultrasonic beams.

The detection system used was the Ultrasound Beam Calibrator (BECA, Preston 1988) which consisted of a detector, amplifier and digitiser, with subsequent analysis of the recorded waveforms being performed by commercial software. The detector used was a 21 element PVdF bilaminar membrane hydrophone, each element having an active diameter of 0.5 mm. Part of the attractiveness of the whole acquisition system was that each element could be accessed simultaneously so facilitating alignment of the ultrasonic beam and that the amplifier stage was designed such that the hydrophone sensitivity was flat from 1 MHz to 15 MHz. In addition the software allowed the determination of the PSI of the waveform. The results of these measurements will be presented in the next section.

3.3.1.3 Modelling the ultrasonic field.

The numerical implementation of the KZK equation requires certain input parameters that relate to the source and the medium of propagation. This information is fed into the model via four parameters, Γ, A, G, m which are described below.

(a) Γ, the Goldberg constant, represents the ratio of nonlinearity to attenuation and is expressed as:

$$\Gamma = \frac{\beta \varepsilon k}{\alpha}, \qquad 3.15$$

where β is the parameter of nonlinearity and ε is the acoustic Mach number. The nonlinearity parameter, β is given by equation 1.7.

For water at room temperature β is equal to 3.5. The acoustic Mach number ε is the ratio of particle velocity to sound velocity and can be expressed as:

$$\varepsilon = \left(\frac{p_o}{\rho_o c_o^2}\right). \qquad 3.16$$

For water the density is 1000 kg m^{-3} and the sound velocity is 1486 ms^{-1}, at room temperature.

α is the attenuation of the fundamental frequency component and is expressed as:

$$\alpha = \alpha_o f^m, \qquad 3.17$$

where α_o is the attenuation coefficient at 1 MHz and m is the frequency dependence of attenuation. For water the attenuation coefficient is 0.025 Np m^{-1} MHz^{-2} at room temperature.

(b) A represents the ratio of diffraction to nonlinearity and is given by

$$A = \left(\frac{2R_o}{\beta\varepsilon k}\right). \qquad 3.18$$

The denominator is the plane wave shock distance. R_o is the Rayleigh distance and is expressed as

$$R_o = \left(\frac{ka^2}{2}\right), \qquad 3.19$$

where a is the source radius (9.5 mm for these simulations). The Rayleigh distance describes the diffractive field of the transducer.

(c) The third parameter is G, the focusing gain of the source and is expressed as:

$$G = \frac{R_o}{D}, \qquad 3.20$$

where D is the focal length. With most medical ultrasonic transducers the focusing is achieved by having a curved transducer surface as opposed to a plane surface with a detachable lens and in general only nominal values are given for the focal length or the gain. The value quoted by Starritt was 4.0.

(d) The fourth term is the frequency dependence of attenuation index m. The original numerical implementation of the model took the valye of m to be 2.0, so simulating attenuation in water. In order to accomodate a non-squared law frequency dependence of attenuation, as is often observed in biological fluids (see Chapters 4 and 6), the model was altered to allow the frequency dependence of attenuation index to be input as a variable.

The values quoted above were input into the model to yield pressure distributions for the two source pressure conditions. These were compared with measurements made by Starritt (1990) in order to check that the input parameters represented the transducer accurately. It was, however, found that there were two major differences between the experimental and theoretical results.

Firstly the axial positions of the minima and maxima did not agree with those observed experimentally. For example the last axial minima occurred at 69 mm theoretically whereas it was at 52.5 mm experimentally. Secondly, pressure values at the last axial maxima did not agree.

The most likely cause for the discrepancy between experiment and theory was in the values chosen for the transducer radius and the focusing gain. Using Starritt's value

for the last axial minima, an 'independent' value for G was calculated using the standard relationship between the axial positions of minima, z_{min} , in the diffractive field and focal length (see for example Lucas & Muir 1982):

$$\frac{1}{f_s} = \left(\frac{1}{z_{\min}} + \frac{2\pi n}{R_o} \right). \qquad 3.21$$

For the last axial minimum the value of n in equation 3.21 is one. Substituting for z_{min} in equation 3.21 gave a value for the focal length which was in turn used in equation 3.20 to give a value of 6.5 for the focusing gain. The model was rerun and found to produce a much better match between experiment and theory. The axial variation of the first three harmonics for the two source pressure conditions (0.39 MPa and 0.03 MPa) are illustrated in figures 3.1 and 3.2.

There are two features worth noting from the theoretical results. Firstly one can confirm that with the high drive case, condition 'A' (0.39 MPa), there is a large degree of nonlinear distortion in and beyond the focal region. For example in the region of the focus the second harmonic is approximately 6.0 dB below the value of the fundamental implying the formation of a mature shock wave. On the other hand the second harmonic level for condition 'B' (0.03 MPa) is approximately 20 dB down from the fundamental in the region of the focus, implying more linear propagation. Secondly it is interesting to note that the harmonics illustrated (for condition 'A') in figure 3.1 peak slightly later than the fundamental. This will be referred to subsequently.

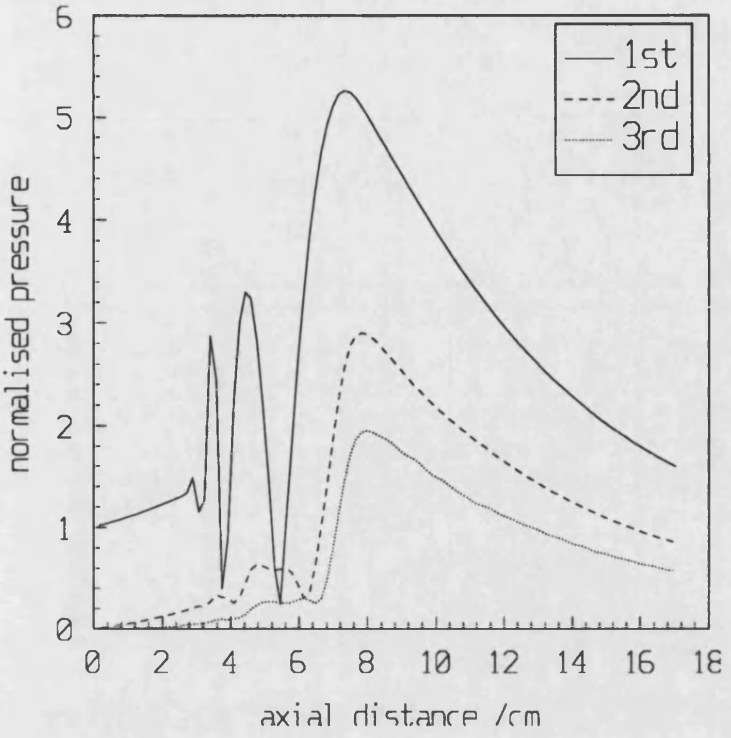

Figure 3.1. The axial variation of the normalised pressure for the first three harmonics for condition 'A' (0.39 MPa). Theory.

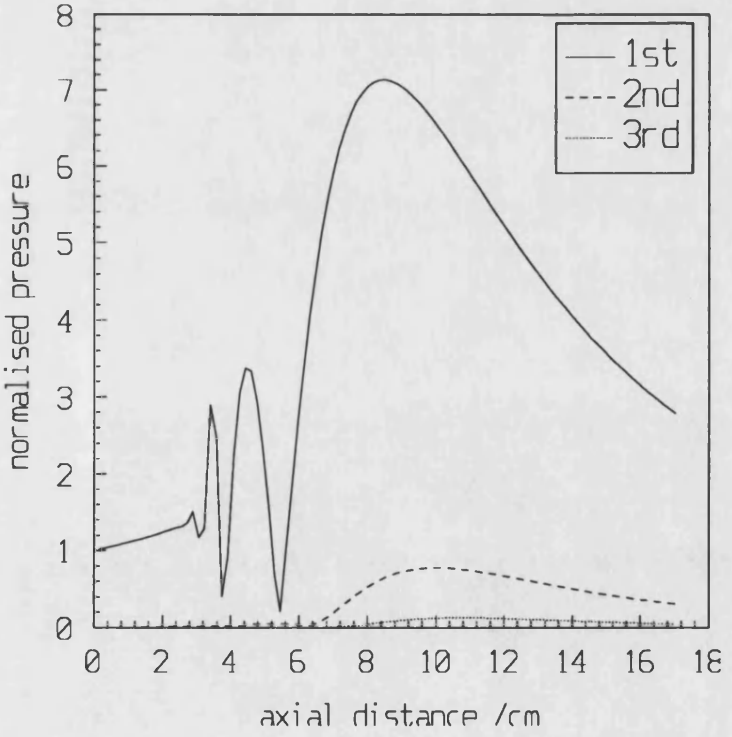

Figure 3.2. The axial variation of the normalised pressure of the first three harmonics for condition 'B' (0.03 MPa). Theory.

Figure 3.3 illustrates the axial variation of the PSI for the two source pressure conditions. Both results are normalised to the PSI at the source. As can be seen the PSI in the nonlinear beam ('A'), after the last axial minimum, is less than that in the linear beam. Given the arguments presented above concerning the relation between the PSI and the intensity in the beam it seems plausible to conclude that there is relatively less energy present in the nonlinear beam. This is presumably due to the enhancement of attenuation resulting from the higher attenuation of nonlinearly generated harmonics.

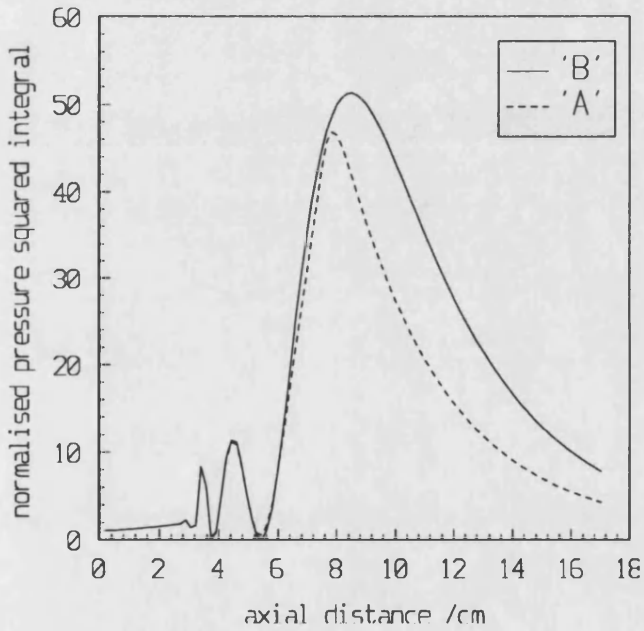

Figure 3.3. Axial variation of the normalised PSI for conditions 'A' and 'B'. Theory.

The enhancement of attenuation, due to nonlinear propagation, can be calculated by plotting the ratio of PSI for condition 'A' with respect to the PSI with condition 'B'. Figures 3.4 and 3.5 illustrate the axial variation of the PSI ratio. The first result is obtained from theoretical simulations whereas the second result is taken from the experiments performed by Starritt (1990). It should be noted that the experimental

results are not normalised to the source PSI as this was not done originally. Both the results illustrate a similar variation in the PSI ratio, however the theoretical result in figure 3.4 will be used to comment on the behaviour of the variation in the PSI ratio.

From figure 3.4 it can be seen that there are three regions in which different behaviour can be identified. These are from the source to approximately 6 cm, from 6 cm to 10 cm and from 10 cm to 17 cm.

The first region represents the very near-field (pre-focal region) of the ultrasonic beam where the PSI ratio is predominantly unity. Here nonlinearity has not had time to build up (in part due to the rapid oscillations of the fundamental) so almost all the energy is confined to the fundamental for both drive cases. Within this region there are however a few points where the PSI ratio rises sharply. These points correspond to a minima in the field of the fundamental. For condition 'A' a small amount of second harmonic is present resulting in a finite non zero value for the PSI. The result is that the PSI ratio rises to a large value.

In the second region the PSI falls below unity, implying that more energy has been lost from the nonlinear beam ('A'). The physical reason for this is as follows. In the region of the focus, energy is transferred to the harmonics. The attenuation of the harmonics is proportional to frequency squared and therefore energy is lost from the wave at a faster rate than would be expected from an undistorted wave.

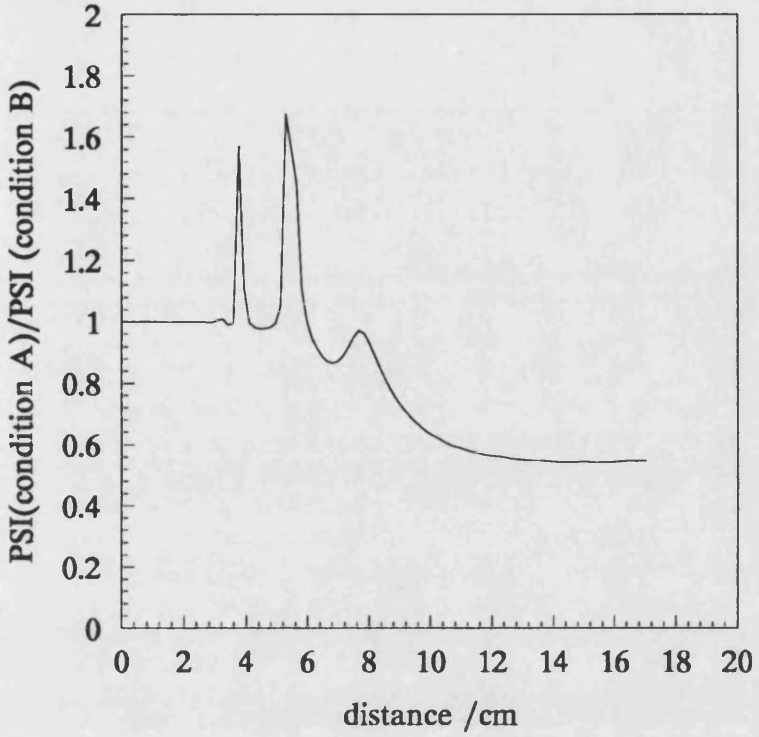

Figure 3.4. Theory. Axial variation of the pressure squared integral ratio of condition 'A' (nonlinear beam) to condition 'B' (linear beam). The result is normalised to the pressure squared integral at the source.

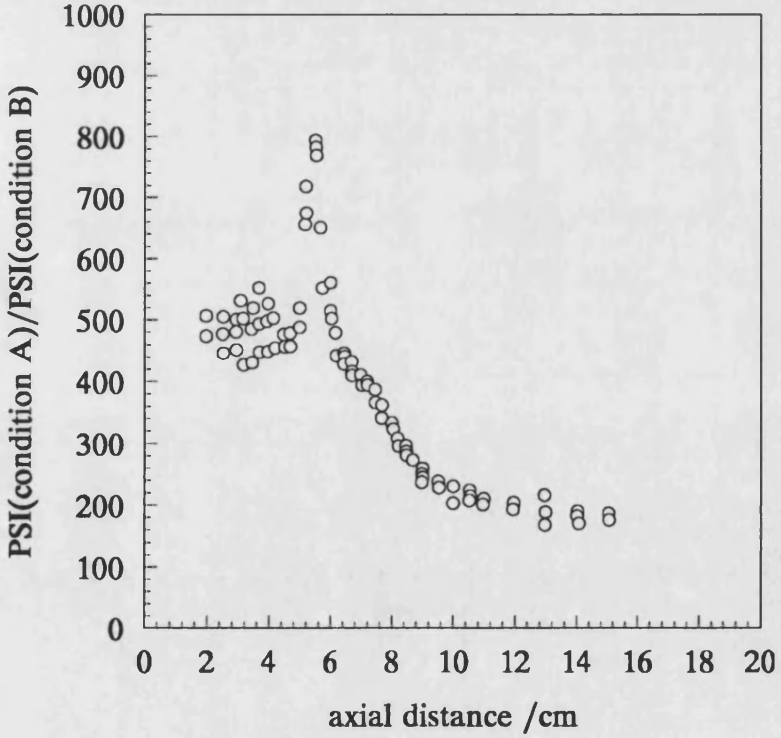

Figure 3.5. Experiment. Axial variation of the pressure squared integral ratio of condition 'A' (nonlinear beam) to condition 'B' (linear beam). The experimental result are taken from Starritt (1990) and are not normalised.

The second region also contains a peak in the region of 8 cm from the source. The peak implies that energy in the nonlinear beam is again building up so reducing the enhanced loss of energy for a short distance. An explanation for this behaviour can be found with reference to figure 3.1. Here it can be seen that a significant proportion of energy is present in the harmonics, generated by nonlinear propagation, which are not as strongly diffracted as the fundamental and so focus beyond the maximum of the fundamental.

The third region represents the post focal region. In this region the rate of energy loss due to nonlinear effects decreases, as the fundamental has lost a significant proportion of its amplitude as a result of nonlinear effects, and the PSI ratio reaches a plateau.

The enhanced attenuation in the post focal region (8cm to 10 cm) can be calculated, using the arguments used to obtain equation 3.14, from the gradient of figures 3.4 and 3.5. The theoretical results yield a value of 0.96 dB cm^{-1} (α_{nl} in equation 3.14) for the additional attenuation coefficient. For a linear wave the attenuation at 3.5 MHz is 0.027 dB cm^{-1}. This corresponds to an enhancement of energy loss by a factor of 36. The experimental results indicate a value of 1.1 dB cm^{-1} for the enhanced attenuation. The experimental and theoretical results show reasonably good agreement. Furthermore the enhanced attenuation indicates that on-axis 97% of the total attenuation is due to generation and attenuation of harmonics. The theoretical results also illustrate that after sufficient propagation the nonlinear wave has lost 45% of its intensity on-axis while the experimental results indicate a higher loss, in the region of 60%.

3.3.1.4 PSI and enhanced attenuation measurements with a 5 MHz transducer

Additional measurements of the enhanced attenuation from a 5 MHz single element circular transducer were also made. The radius of the transducer was 6.5 mm and its focusing gain was again determined by locating the last axial minimum. Using this method the gain was calculated to be approximately 4.5.

The arrangement used to detect and capture the acoustic waveform was similar to that used by Starritt in that the BECA detection and amplification system were used. However after the amplification stage the signals were captured and stored on a Lecroy 9310 storage oscilloscope (described in chapter 5). This allowed the subsequent analysis of the waveforms to be made independently. For example the PSI over one cycle rather than the whole waveform was determined. It was thought that this would provide more accurate results as measurements over the whole waveform assume that each cycle is distorted by the same amount. A comparison of the results for the cycle and pulse PSI's are not presented here (the PSI results over one cycle are presented) , however it was found that both methods gave similar results.

Measurements of the axial PSI were made for four source pressure levels, 0.565 MPa, 0.428 MPa, 0.35 MPa and 0.02 MPa representing fields with different degrees of distortion. Measurements of the source pressure were made with a 0.5 mm diameter PVdF bilaminar membrane hydrophone and with a power balance.

The ratio of square root of the PSI for the three highest drive levels with respect to the lowest drive level are illustrated in figure 3.6. Plotting the logarithm of the square root of the PSI ratio is equivalent to plotting the PSI provided one removes the factor of a half from equation 3.14. Once again there is reasonably good agreement between experiment and theory. The enhanced attenuation in the region just beyond the focus (60 mm to 70 mm) was calculated for the three drive levels in a similar manner to before and the results are tabulated in figure 3.7. As can be seen the enhancement in attenuation for the highest drive level case is approximately 30.

Although the agreement between experiment and theory for both transducers is reasonable there are some possible sources of discrepancy that can be identified. These are related to the hydrophone used in the experimental arrangement and are listed below:

(i) The finite bandwidth of the hydrophone (1 MHz to 25 MHz) will result in energy present in the higher harmonics (i.e. above 25 MHz) not being detected. Consequently it will appear that there is less energy in the nonlinear beams. When calculating the enhanced attenuation this error will tend to produce overestimates for the values of attenuation.

(ii) The finite hydrophone size will result in spatial averaging of the PSI distribution. The problem will become increasingly significant for nonlinear beams where there is appreciable energy in the higher harmonics (which are concentrated near the axis) and also as one increases the fundamental frequency of operation. The effect of

hydrophone averaging was incorporated into the model and it was found that for the 3.5 MHz transducer the PSI was reduced by about 10% for nonlinear beams with a 0.5 mm diameter hydrophone. Again this apparent reduction in PSI for nonlinear beams tends to increase the calculated value of enhanced attenuation.

From the experimental and theoretical results presented it seems plausible that enhanced streaming may result from enhanced attenuation in the focal and post-focal region of medical transducers. In addition to this the enhancement by a factor of approximately 30 in the attenuation of water due to nonlinear generation and attenuation makes the total attenuation comparable with that of some soft tissue.

These results also show the potential of the numerical model for obtaining derived parameters, such as PSI and enhanced attenuation, in nonlinear fields. In addition the results also demonstrate that an accurate knowledge of transducer parameters (such as radius and gain) is required in order to obtain good agreement between experimental and theoretical results.

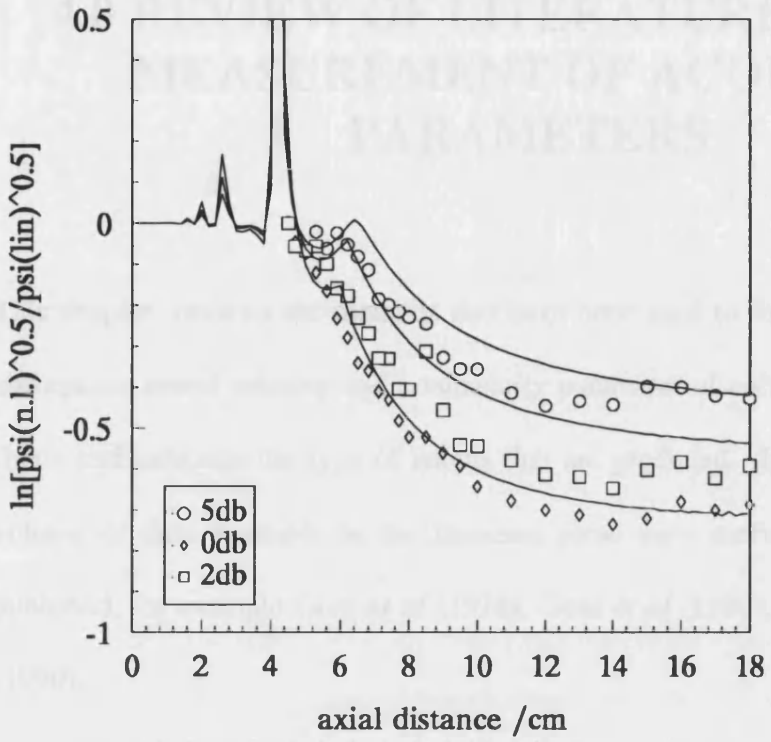

Figure 3.6. Axial variation of the ratio of the square root of the pressure squared integral for three source pressures, 0.565 MPa,0.43 MPa, 0.35 MPa (0dB,2dB and 5dB) with respect to a source pressure of 0.02 MPa for a 5 MHz focused transducer. Solid lines correspond to theoretical predictions.

Source pressure /MPa	Theory. Enhanced attenuation $dBcm^{-1}$.	Experiment. Enhanced attenuation. $dB\ cm^{-1}$ (+/-) 1 S.E.	Enhancement factor.
0.565	1.67	1.3 +/- 0.1	31
0.428	1.34	1.25 +/- 0.08	24
0.35	1.0	1.1 +/- 0.14	19

Figure 3.7. Tabulated values for the measured and predicted enhanced attenuation from the 5 MHz transducer in water.

4.0 REVIEW OF LITERATURE ON THE MEASUREMENT OF ACOUSTIC PARAMETERS

This chapter reviews the methods that have been used to measure the attenuation, absorption, sound velocity and nonlinearity parameter of soft tissues and biological fluids and indicates the type of results that are produced. In addition to the large volume of data available in the literature some very useful reviews have been published, for example Goss *et al* (1978), Goss *et al* (1980), Hill (1986) and Duck (1990).

Before discussing the literature it is worth noting that some of the earlier work does not distinguish between measurement of attenuation and absorption. For inhomogeneous media, such as soft tissue, absorption is the conversion of ultrasonic energy into heat whereas attenuation includes losses due to scattering. For homogeneous media (e.g. water and biological fluids) the two quantities are identical. Further to this attenuation measurements are generally made in a diffractive sound field and so require an understanding of the spatial variation of the sound pressure field. Early work on estimating the attenuation in a medium sometimes ignored this aspect. Diffraction loss leads to an error in attenuation measurements, but can be minimised experimentally or corrected for theoretically.

4.1 Methods of measurement

4.1.1 Attenuation

There are a number of ways of classifying the method of measurement. An initial classification can made by considering narrowband and broadband techniques (see for example Bamber (in: Hill, 1986 Chapter 4).

In narrowband techniques the transmitted signal is assumed to be of sufficient duration (defined by the number of cycles) such that it can be assumed to be at a single frequency. Within this classification there exist fixed-path and variable-path methods. With variable path methods the change in the amplitude of the received signal as a function of the range of the receiver yields an absolute value for the attenuation coefficient. However the method needs to take account of diffraction loss and can require significant corrections to the data in the low megahertz frequency range. Pellam & Galt (1946) used this technique at 15 MHz with a long toneburst to obtain attenuation results with an accuracy of 5%. If high frequencies are employed then diffraction errors can be neglected. Eggars *et a*l (1981) devised an ultrasonic absorption cell for measurements with very small fluid volumes (millilitres) for the frequency range 15 MHz to 150 MHz. They suggest that if the errors in electronic calibration, transducer alignment and distance measurements are minimised then an accuracy of +/- 0.5 % is possible. The major limitation of this method is that it is not suitable for solid tissues.

Fixed path measurements include the substitution (Schwan & Carstensen 1952) and insertion (Kremkau 1981) methods. In both cases diffraction corrections are often neglected and transducer alignment is not so crucial. Whether the assumptions on diffraction corrections and alignment are correct depend to some extent on the geometry of the experiment. Thick samples with sound velocities significantly different from the reference medium (for example greater than 10%) will alter the ultrasonic field leading to a contribution in signal change from diffractive effects. With the substitution method the distance between the source and receiver is fixed but the path length in the sample and reference medium is altered. Because a reference medium is used the attenuation coefficient is relative. Normally relatively large sample volumes are required (one to four litres) and again the sample generally needs to be a fluid. Pauly and Schwan (1971) did measure the attenuation coefficient of liver with this method, by mincing the tissue and assuming that this had no effect on the propagation of sound through it. With the insertion method again a reference medium is used but this time the attenuation coefficient is determined from the signal received with and without the sample. The method is well suited to solid samples however errors result due to reflections at the specimen faces and non-parallel cutting of the sample slabs. The accuracy is therefore in the region of +/-10%.

Finally there are also narrowband techniques that employ continuous wave methods and make use of resonances. One of these is the ultrasonic interferometer. Here the variation in strength of a resonance with path length or frequency can be used to measure the attenuation coefficient. Diffraction corrections and side-wall reflections cause errors and a test liquid is required for calibration. However the method can be

useful if only small volumes of the sample is available. Eggars & Funck (1973) measured the attenuation coefficient in aqueous solutions of 1 ml volume over a frequency range of 0.5 MHz to 50 MHz.

Broadband techniques have recently become popular due to the advances in signal processing. They have the advantage that the attenuation coefficient can be measured over a wide frequency range using a single pair of transducers. The normal procedure is to use the insertion method. The transmitted pulse is very short (one or two cycles) and on reception is Fourier transformed to give the spectrum of the pulse. The change in amplitude at each frequency component when the sample is inserted is used to calculate the attenuation coefficient as a function of frequency. Papadakis *et al* (1973) used broadband techniques in pulse-echo mode. In order to eliminate errors due to transducer reverberation a buffer rod was used to obtain a train of echoes from the specimen. Their analysis also considered diffraction correction procedures using standard curves.

Some of the differences between broadband and narrowband techniques have been mentioned above. Another important difference is the receiver used. With narrowband methods a phase sensitive or phase insensitive receiver can be used. When dealing with inhomogeneous media the former will introduce phase cancellation errors. Marcus & Carstensen (1975) investigated errors in attenuation measurements resulting from phase cancellation for muscle tissue (with a fat inclusion). They showed that using a phase sensitive receiver resulted in the attenuation being overestimated by approximately four times. The explanation

offered was based on distortion of the phase front due to inhomogeneities. With broadband measurements, because of spectral processing, phase sensitive detectors are required to store all the r.f. information. Although phase cancellation can be recognised through signal processing and dealt with by averaging and curve fitting, these processes will themselves degrade the original information.

The subject of phase cancellation has been dealt with by Bamber (1979). He showed that the effect was due to either variations in the path length or sound velocity within a medium. He derived an expression that depended on the above two and the relative area of the receiver in each inhomogeneity. His results illustrated that the effect was a significant problem which increased with sound frequency. Parker (1983) also looked at the problem over the frequency range 1-6 MHz in liver tissue. The results acknowledge the problem of phase cancellation but do suggest that careful experimental procedure (e.g. small receivers, alignment and multiple measurements) can reduce the error. For fluids phase cancellation is not a problem as the medium can be thought of as homogeneous.

4.1.2 Absorption.

Probably the most widely used technique is the use of a thermocouple to measure temperature rises. The rate of rise of temperature (for approximately one second) is linear and can be attributed to absorption. The gradient of the linear slope gives the absorption coefficient provided density, specific heat and intensity are known. The technique has been used by Fry & Fry (1954). The method has three limitations.

Firstly it assumes that the propagation is of a plane wave nature and secondly it requires that the thermocouple is small in comparison to the wavelength of sound. Because of this there is a high frequency limit to its applicability, of approximately 7 MHz. Thirdly a knowledge of viscous heating, due to motion of the thermocouple wires in the ultrasonic field is also required. Fry & Fry (1954) however demonstrated that the temperature rise with time can be separated into regions representing viscous heating and those from absorption. In addition they demonstrated that, within experimental error, thermocouple methods and radiation pressure methods give similar results. Dunn (1962) and Dunn & Breyer (1962) used this technique for measurement of absorption coefficients in tissue (at 1 MHz) and standard oils (in the frequency range 3-100 MHz) and found good agreement with other workers. Frizzell *et al* (1979) made attenuation measurements (using a radiation pressure receiver) and absorption measurements (using a thermocouple method) *in vitro* and *in vivo* over the frequency range 0.5-10 MHz. Their main findings were that the presence of gas bubbles can effect attenuation measurements (due to scattering of the sound wave off the bubble) but that for absorption measurements much better agreement between *in vitro* and *in vivo* measurements could be obtained. In general they suggest storage of tissue at low temperatures to dissolve any bubbles present.

4.1.3 Sound velocity.

Many of the methods employed are similar to the attenuation measurements, so only a brief review will be given. It should be noted that when considering pulse methods a distinction needs to be made between phase and group velocity. In a pulse several

frequencies are present which potentially travel at different velocities (that are medium dependent) and so cause dispersion of the wave. In biological tissues dispersion is small, typically there is a 0.7% variation in velocity over the frequency range 1 MHz to 10 MHz.

By far the most common method is based on pulse transit times and is in essence a time of flight technique. This was first used by Pellam & Galt (1946) for organic liquids with quoted errors of the order of 0.05%. The measurement of travel time can be made using a calibrated timebase on an oscilloscope. Ludwig (1950) employed such a method to give an accuracy of the order of 3%. Most problems with pulse techniques are due to the difficulty in timing the beginning of the pulse due to an absence of a sharp leading edge. With the advancement in electronic gating techniques and signal capture, travel times can be measured to better than 1%.

4.1.4 Nonlinearity parameter.

Measurements of nonlinearity falls into two main categories, thermodynamic methods and finite amplitude methods. The thermodynamic method involves monitoring the changes in sound velocity as a function of changes in hydrostatic pressure (at constant temperature) or changes in temperature (at constant pressure). With additional data on the density, infinitesimal sound velocity, specific heat at constant pressure and coefficient of thermal expansion, for the medium of interest, the value of B/A can be determined. The thermodynamic method (Sehgal *et al* 1984) is accurate (+/- 3% for liquids) due to the precision with which transit times and pressure

changes (10 MPa to 20 MPa) can be detected. However the method is only applicable *in vitro* and often results in irreversible changes occurring to the medium of interest.

The finite amplitude method involves estimating the nonlinearity parameter from waveform distortion, for example, Beyer (1960) measured waveform steepening at a known distance from the source. Alternatively waveform distortion can be measured by observing the growth of harmonics. Alder *et al* (1962) showed that the second harmonic pressure amplitude was given by:

$$P_2(z) = P_1^2(0)\frac{\left(\frac{B}{A}+2\right)\pi f z}{2\rho_o c^3}F(z)\exp\left[-\left(\alpha_1 + \frac{\alpha_2}{2}\right)z\right], \qquad 4.1$$

where z is the distance from the source, $P_2(z)$ is the second harmonic pressure amplitude, $P_1(0)$ is the source pressure amplitude and α_1 and α_2 are the attenuation coefficients of the first and second harmonic. $F(z)$ is a diffraction correction term applied to the source geometry.

This method requires a knowledge of the attenuation coefficients of the fundamental and second harmonic and also of the effect of diffraction correction. The derivation they used assumes the wave amplitude is not too large, that harmonics do not interact and that the medium absorbs energy with a linear frequency dependence. For biological media the assumption of a linear frequency dependence is tenuous. Law *et al* (1985) measured the pressure of the second harmonic as a function of distance from the source, in the near-field. He then extrapolated back to the source and so

avoided measuring the attenuation coefficients and diffraction correction. His method is suitable for liquids, giving an accuracy of about +/- 10%.

4.2 Measured acoustic parameters

There is a large amount of variability in the published values of attenuation (or absorption). There are probably three reasons for this. Firstly, as described above, a large number of experimental methods exist in making such measurements, each of which has its advantages and disadvantages in terms of accuracy and reproducibility.

Secondly, the condition under which measurements are made is thought to be of crucial importance, especially for biological media. Factors such as temperature, tissue composition, tissue pathology, changes due to death, pH, the presence of gas bubbles and acoustic source parameters can all affect the measurement and have generally been poorly documented in the literature. Hence variations in these values between different measurement procedures will undoubtedly cause differences in measurement values. As discussed, Frizzell at al (1979) demonstrated the effect of gas inclusions. Bamber et al (1977) presented results for a number of tissue types over a period of 120 hours after excision. They however suggest that backscatter measurements are more likely to be susceptible to the state of tissue than attenuation measurements (provided gas bubbles are removed). Several workers have described ways to overcome the problem of bubble removal. Parker (1983), for example, pressurised the tissue samples under investigation and gained some success.

In addition nonlinear propagation can also have an effect on the measurements. This type of propagation was only recognised as significant for medical ultrasonic fields after 1980 (Carstensen *et al* 1980, Muir & Carstensen 1980). Measurements made before this time were often performed using high amplitude pulses (in order to obtain a good signal to noise ratio) and so subject to errors. An assessment of the magnitude of the errors resulting from nonlinear distortion of the wave is not trivial as they are dependent on the measurement procedure. For example Carstensen *et al* (1982) demonstrated an overestimation of absorption coefficient and attributed this to the generation of harmonics which were subsequently absorbed at a faster rate than the fundamental. Zeqiri (1992), however, demonstrated that attenuation measurements made by the narrowband insertion technique can underestimate the attenuation coefficient. With this method the experimental attenuation is compared with that of a reference medium, which is normally water. The transfer of energy into harmonics as a result of nonlinear distortion can result in the attenuation of the reference medium being increased. This is especially true if the receiver is narrowband and does not detect the harmonics. Hence the use of the linear attenuation coefficient of water in the calculation of the attenuation of the medium of interest, rather than the true attenuation, can give rise to an underestimate of the attenuation in the medium.

Thirdly, when considering biological media one has to be aware that in such complex dynamic systems there is always bound to be some variability as no two samples can be expected to be the same.

A very brief review of measurements on sound velocity, attenuation and its frequency dependence and the nonlinearity parameter will now be given.

4.2.1 Sound velocity

The velocity of sound in biological media can be broadly classed into four tissue types. These are biological fluid, soft tissue, lung and bone. The velocity in lung is generally less than that in water, for example Dunn (1986) measured values ranging from 600 ms^{-1} to 1100 ms^{-1} in the frequency range 1-5 MHz. The method initially determined the reflection coefficient of the lung and then derived a value for the sound velocity, and attributed the results to the large gas content.

Bone has the highest sound velocity of all the biological media. In addition there is a significant dispersion in bone. Yoon & Katz (1979) measured velocities in dried cortical bone and found the dispersion to be of the order of 15 ms^{-1} over the frequency range 2-10 MHz. In general the velocity is found to be in the region of 3500 ms^{-1}, for example Greenfield *et al* (1981) measured an *in vivo* value of 3311 +/- 307 ms^{-1} in cortical bone using a pulse-echo technique.

The velocity in soft tissue is reported to be similar to water but a few percent higher, the only exception being fat, where it is slightly lower. Errabolu (1988) measured a value of 1427 ms^{-1} in human and animal fat. Kossoff *et al* (1973) made *in vivo* measurements in human breast and found values in the region of 1450 ms^{-1} The method was a comparative one and based on measuring travel times in equivalent

path lengths of breast and water. In addition corrections were applied for various tissue layers in the propagation path. Soft tissues generally exhibit values in the region of 1580 ms^{-1} . For example Rajogopalan *et al* (1979) measured the velocity in a range of human tissue (e.g. liver, muscle and kidney) to between 1550 ms^{-1} and 1580 ms^{-1} . The results were presented over a 20° C to 40° C temperature range illustrating an increase of the order of a few percent. Law *et al* (1985) measured a value of 1566 ms^{-1} in skeletal muscle.

The dependence of sound velocity in soft tissue is attributed to the protein and water content. Dunn (1976) and O'Brien (1977) demonstrated that an increase in protein content correlates directly to an increase in sound velocity, this is particularly true for the case of collagen. Kremkau *et al* (1981) found the velocity in brain white matter to be greater than that in brain grey matter by about 6 ms^{-1} and offered an explanation based on the water content of the two tissue types. Other structural factors also play a role in the sound velocity; in particular there is thought to be some directional dependence due to the anisotropic nature of muscle although this has not been consistently shown. Ludwig (1950) found that measurements made along and perpendicular to the fibres made little difference to the sound velocity; however Mols & Breddels (1982) reported higher sound speeds for measurements along the fibres.

Also apparent from the literature is that in biological fluids the velocity of sound is slightly lower than that in soft tissues. For example Povall *et al* (1984) measured a value of 1534 +/- 3 ms^{-1} in amniotic fluid at physiological temperature at 2 MHz using a time of flight technique. In addition they also report that the state of the fluid

prior to the measurement (frozen or refrigerated) was not significant to the result. Carstensen & Schwan (1959b) measured a value in the region of 1530 ms^{-1} in albumin solutions, with the velocity increasing with the protein concentration in the solution. There is thought to be little frequency dependence (dispersion) of sound velocity in biological fluids, Choi *et al* (1990) illustrated results in Bovine serum albumin over the frequency range 3 MHz to 1 GHz and reported that dispersion over this frequency range was of the order of 2 ms^{-1}.

4.2.2 Attenuation

Here again results can be divided into those that measure lung, biological fluids, soft tissue and bone. Lung and bone will not be considered here except to say that in both the attenuation is much higher than in soft tissue. Generally values in the region of 20 to 30 dB cm^{-1} are reported. For example Fry & Barger (1978) measured the attenuation of human skull bone to be 22 dB cm^{-1} at physiological temperature and Dussik *et al* (1958) reported the attenuation of human lung to be 30 dB cm^{-1}.

For soft tissue and biological fluids the situation is the literature is generally composed of measurements made at a particular frequency and those that encompass a wider frequency range so giving information on the frequency dependence of attenuation. It is common practice to express the attenuation (or absorption) in the form

$$\alpha = \alpha_o f^m, \qquad 4.2$$

where α is the attenuation in dB cm^{-1} , α_o is the attenuation coefficient in dB cm^{-1} MHz^{-m} and f is the frequency in MHz. Most workers report that the values of the attenuation coefficient and m are determined by linearising equation 4.2 with a logarithmic transform to give:

$$\ln \alpha = \ln \alpha_o + m \ln f , \qquad 4.3$$

and then determining the straight line of best fit. Although this 'linear' method seems at first sight to be correct it can introduce a systematic error in the estimation of the attenuation coefficient and its frequency dependence (m). The reason being that transforming the data and applying a straight line fit assumes that all the data points have the same random error. In reality measurements at the higher frequency end of the dataset will generally be more accurate. This may be especially true for materials that intrinsically have a low attenuation which is hard to measure accurately.

For example one can consider the measurements of Zana & Lang (1974) on the attenuation in amniotic fluid. From their data one can apply both nonlinear (equation 4.2) and linear (equation 4.3) fitting procedures to illustrate the effect. The two results produce the following relationships for the frequency dependence of attenuation (α is expressed in dB cm^{-1}):

nonlinear fit: $\alpha = 0.0075 f^{1.58}$
linear fit: $\alpha = 0.014 f^{1.3}$

The curves and the original data are illustrated in figure 4.1. As can be seen the nonlinear fit produces a better representation of the data. It should be pointed out

that Zana & Lang did not apply any functional relationship themselves, however other workers have done so and it may be that their results require re-assessment.

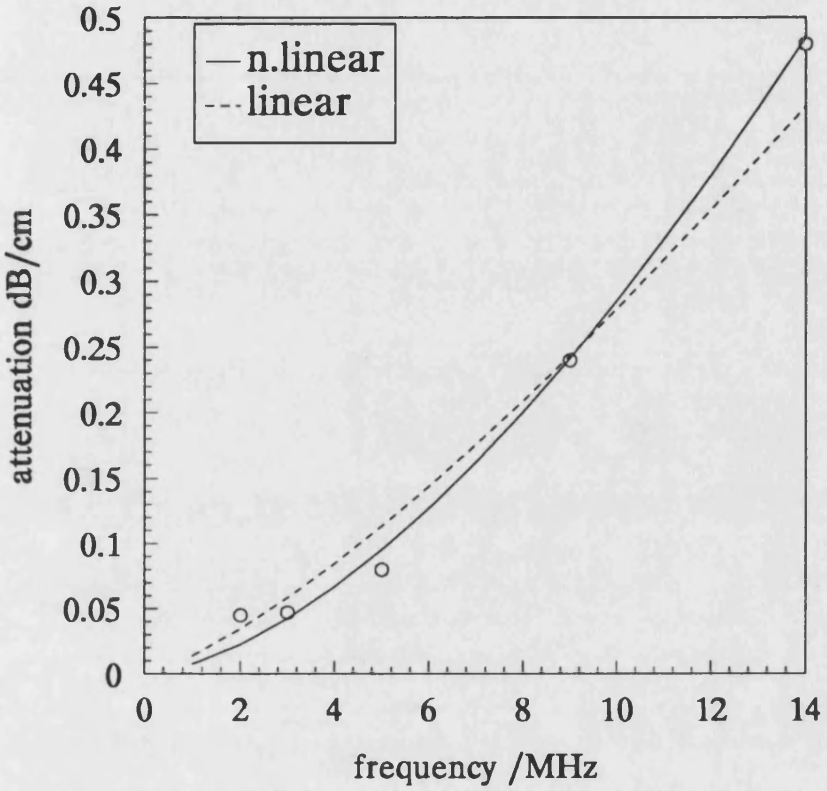

Figure 4.1. Illustration of the influence of curve the fitting procedure employed on the determination of the attenuation coefficient and its frequency dependence. Experimental data from Zana & Lang (1974).

In general there is not much data available for biological fluids. The measurements of Zana & Lang (1974) are the only ones to date reported for amniotic fluid, presumably due to its lack of availability. Narayana *et al* (1984) measured the frequency dependence of attenuation in cyst fluid, pus, bile and human blood using a pulse technique. The centre frequency used was 4.8 MHz giving a frequency

bandwidth from 2.8 to 6.8 MHz. Their results were at room temperature and reported values of:

cyst fluid: attenuation coefficient = 0.05-0.072 $f^{1.27-1.32}$ dB cm-1.
pus: attenuation coefficient = 0.2-0.3 $f^{1.11-1.16}$ dB cm-1.
bile: attenuation coefficient = 0.013-0.031 $f^{1.28-1.34}$ dB cm-1.
blood (human) : attenuation coefficient = 0.12-0.16 $f^{1.19-1.23}$ dB cm-1.

Lang *et al* (1978) measured the frequency dependence of attenuation in cyst fluid and human blood plasma. They obtained the following values:

cyst fluid: attenuation coefficient = 0.076 $f^{1.42}$ dB cm-1.
blood plasma (human) : coefficient = 0.057 $f^{1.41}$ dB cm-1.

over a frequency range of 1.7 to 15 MHz where f is in MHz. Carstensen & Schwan (1959) measured the attenuation in human blood and human blood plasma at 1 MHz, their results are in good agreement with the results of Narayana *et al* (1984) and Lang *et al* (1978) Measurements in other fluids such as amino acid solutions and haemoglobin solutions (Kremkau & Carstensen 1973) generally give results in a similar range.

Overall one can say that, from the few measurements available, the attenuation coefficient in these biological fluids is between 0.001 and 0.1 dB cm^{-1} with a frequency dependence in the range 1.1 to 1.5. Furthermore the exact dependence seems to be linked to the concentration of macromolecules in the solution.

The situation with soft tissue is more complicated because the variability of the attenuation coefficient makes generalisations much harder and also because the distinction between attenuation and absorption is often not made. The variability is in part due to the reasons given previously (on tissue state, tissue type and measurement procedure) and in part due to the scattering contribution to the total attenuation. For example Nassiri & Hill (1986) considered the contribution due to scattering in muscle and blood over the frequency range 4 to 7 MHz. They found that in blood it contributed 0.3 % of the total attenuation but that in muscle it rose to 17%. In addition to this many measurements of the attenuation coefficient quoted in the literature assume a linear frequency dependence (m = 1). On the other hand measurements of the absorption coefficient generally determine the attenuation coefficient and its frequency dependence from the data, here though the normal procedure is to transform equation 4.2. Very useful reviews of the literature are given by Goss *et al* (1979), Hill (1986) and Duck (1990) and in general the attenuation coefficient can vary from 0.1 to 3 dB cm^{-1} with a frequency dependence from 1.0 to 1.5.

(c) Nonlinearity parameter

The value of the nonlinearity parameter has not been measured extensively for biological media. Measurements in biological fluids generally give a value in the region of 6, for example for bile and urine (Sun Yongchen *et al* 1985) and human blood (Gong *et a*l 1989). Soft tissues generally have values in the region of 6 to 9 depending on the protein content. Sehgal *et al* (1986), using the thermodynamic

method, investigated the effect of tissue state on the nonlinearity parameter and found some distinction between normal and malignant tissue. Sun Yongchen et al (1986) also reported similar results using a comparative method with water as the reference medium. The inclusion of fat in soft tissue generally has the effect of increasing the nonlinearity parameter significantly. For example Law *et al* (1985) reported values in the region of 12 when fat was present, while Sehgal *et al* (1984) reported values of 9.6 for human breast fat. This wide range, as a result of tissue composition, makes the nonlinearity parameter an interesting prospect for tissue characterisation. In an attempt to formalise the correlation with tissue composition, Apfel (1983) presents formulae for the nonlinearity parameter which are dependent on the percentage of various types of tissue in a mixture.

5.0 EXPERIMENTAL CONFIGURATION AND MEASUREMENT

5.1 General

This chapter gives the basic rationale behind the design of the experimental facility used to measure attenuation and nonlinear propagation. There then follows a description of the apparatus and the methods used to measure the axial nonlinear pressure distribution, the frequency dependence of attenuation and sound velocity in the fluids of interest.

As stated in the introductory chapter the main aim of this work was to compare experimentally measured pressure distributions, in biological fluids, with theoretically simulated pressure distributions. Chapter 4 revealed, in a review of published data on ultrasonic measurements in biological media, that there was a gap in the literature on measurements of parameters such as the frequency dependence of attenuation in biological fluids. In addition Chapter 3 illustrated that, in order to theoretically predict ultrasonic nonlinear propagation a knowledge of the frequency dependence of attenuation in the fluid of interest is also essential.

The main considerations, underlying the design of the experimental rig were, therefore, that it should enable both the axial pressure distribution and the frequency dependence of attenuation in a biological fluid to be measured. In principle the frequency dependence of attenuation can be determined in at least two ways, the

variable path length (Schwan & Carstensen, 1952) method and the substitution method (Kremkau *et al* 1981). For this work the variable path length method was chosen as it enabled both this measurement and the axial pressure distribution measurement to be performed without changes of fluid or major alterations to the rig. So allowing both measurements to be performed on the same sample of fluid without a significant time lag between measurements.

Measurements of the frequency dependence of attenuation and sound velocity were made on Dow Corning 350 silicone fluid, Human Albumin (4.5% and 20%) solutions, urine and amniotic fluid. Axial nonlinear pressure distributions were determined for the 4.5% Human Albumin solution, urine and amniotic fluid.

5.2 Experimental design and measurement procedures

5.2.1 *Rationale*

In order to perform the measurements outlined above three physical considerations needed to be taken into account. These factors, discussed in detail below, are:

(a) the volume of biological fluid available;

(b) the physical size of the transducer;

(c) the physical size of the hydrophone.

(a) Given that very large volumes of biological fluid were not available (e.g. 10's of litres), the standard ultrasonic test tank method of mapping the ultrasonic pressure

field (for example Baker *et al* 1988) was not realistic. This then required the containment of available fluid within a variable length chamber. Ideally both the transducer and hydrophone would be immersed in the fluid, however this results in several problems. Firstly adjustment of either device while inside a fluid tight container, would have been difficult (in terms of preventing fluid leakage) so causing severe problems in alignment. Secondly, the attenuation measurements required a different source and receiver so interchangeability between transducers and hydrophones was important. Finally, mounting the hydrophone inside the fluid would have been awkward due to its size. It was therefore decided to contain the fluid within a vessel with acoustically transparent mylar windows and to mount the transducer and hydrophone separately. A water path was used to acoustically couple the fluid with the transducer and hydrophone.

The physical dimensions of the variable length chamber were therefore governed by the size of the transducer and hydrophone as well as the volume of fluid available. For the fluids considered (amniotic fluid, Human Albumin solutions, urine and Dow Corning) volumes of the order of one to one and a half litres were available.

(b) The transducer used to generate the ultrasonic field for the nonlinear measurements was a circular single element Acuscan immersion transducer operating at 2.25 MHz, with a physical diameter of 44 mm (the active element diameter was nominally 38 mm). A single element transducer was used because of its well characterised (experimentally and theoretically) pressure field pattern (Baker *et al* 1988, Christopher & Parker 1991). The physical diameter of the transducer placed a

minimum diameter for the fluid chamber. The chamber needed to be larger than this so as to allow the whole irradiating field to enter it and also to minimise reflections (due to beam spreading) from its sides from interfering with the direct signal. Smaller 2.25 MHz transducers are available, however as the radius is reduced the power transmitted (for the same acoustic pressure) also decreases which results in less nonlinear generation. An alternative to this is to use a higher frequency of operation. However, as the frequency increases other problems become apparent. With a 5 MHz transducer the fourth harmonic would be at 20 MHz. This reaches the normal calibration limit of standard bilaminar membrane hydrophones (NPL 1994) with calibration information at higher frequencies being less accurate and more difficult to obtain. At high resonant frequencies the transmission properties of the mylar end windows (see section 5.3.5) also become important. Finally higher frequencies of operation also result in alignment problems and accentuate the spatial averaging effects of the hydrophone.

(c) The type of receiver also places limits on the general size of the rig. In order to map the pressure distribution an ultrasonic receiver requires the following properties:

(i) its active area should be small with respect to the wavelength;

(ii) it should be broadband;

(iii) it needs to be temporally stable.

This generally limits the detector to a PVdF hydrophone. Of these there are two main types, membrane and needle hydrophones. A more detailed description of the type of hydrophone will be given later (section 5.3.2), here it is suffice to say that a

membrane hydrophone was used. The physical size of these devices is nominally 150 mm in diameter while the active area is much smaller, typically 0.5 mm diameter.

5.2.2 *Experimental rig*

Given the above basic requirements, a description of the rig will now be given. Figure 5.1 shows a schematic representation of the arrangements used for the measurement of the frequancy dependence of attenuation and the axial nonlinear pressure distribution.

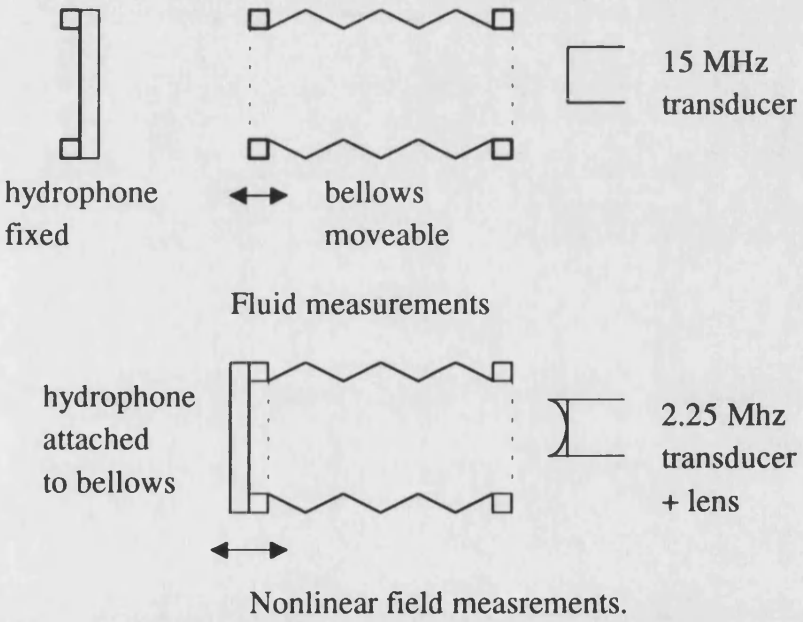

Figure 5.1 Schematic of the experimental arrangements used for fluid measurements and nonlinear field measurements.

As can be seen from Figure 5.1, the hydrophone is attached separately and fixed for the frequency dependent measurements. For the nonlinear pressure distribution measurements it is fixed onto the bellows and moves with it.

Figure 5.2 illustrates a more detailed experimental configuration while Figure 5.3 illustrates one end-piece and its attachment to a polyurethane bellows and Figure 5.4 is a schematic of the electronic set-up.

The rig, shown in Figure 5.2, consisted of an inner and outer water tanks *A* and *B*. The outer tank contained tap water and the inner one distilled water. The outer tank, containing a heater, water pump and thermocouple, provided a stable temperature controllable environment for the inner tank. The fluid tight chamber, placed in the inner tank, consisted of three perspex end-pieces, four brass rods and a variable length polyurethane bellows. The end-pieces *H* and *I* together with the bellows formed the fluid tight vessel, with end-piece *J* acting as an extra support for the arrangement. End-pieces *H* and *J* were located and fixed to the inner tank and also to the four brass rods, this left end-piece *I* to move freely along the length of the rods thereby allowing for a variable length fluid vessel.

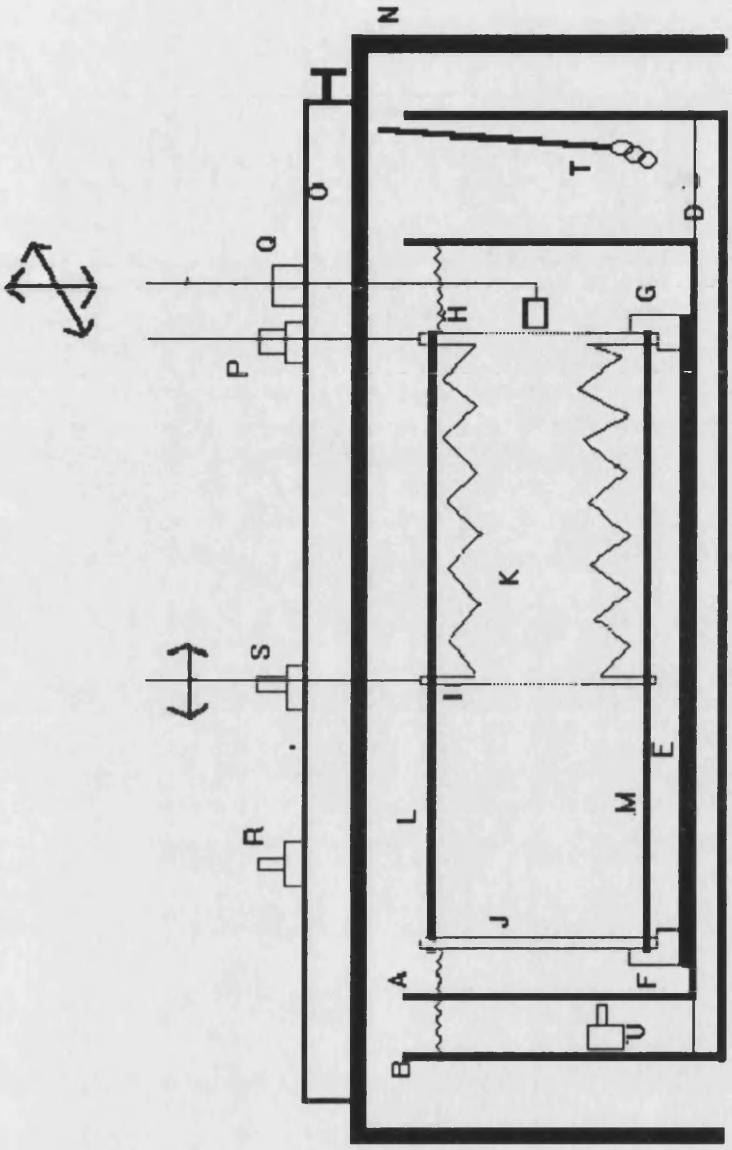

Figure 5.2 Schematic illustration of the experimental facility employed to measure the nonlinear pressure distributions and the frequency dependence of attenuation in the biological fluids. A key to the labels is listed below.

A-Inner tank. *B*-Outer tank. *D*-Polystyrene support. *E*-Aluminium base plate *F*/*G*-Aluminium support. *H*-Fixed perspex end-piece (transducer end). *I*-Moveable perpsex end-piece (0.5 mm hydrophone mounted here for nonlinear measurements) *J*-Fixed perspex end-piece. *K*-Variable length polyurethane bellows. *L*/*M*-3/8" brass rod (two of four). *N*-Frame for mounting translation stage and holders. *O*-Uni-slide translation stage. *P*-Holder for end-piece *I*. *Q*-Holder for transducer (four degrees of freedom). *R*-Holder for 4 mm hydrophone (attenuation measurements). *S*-Holder for moveable end-piece. *T*-Heater. *U*-Water pump.

An Aluminium frame *N* was placed over the two tanks. This frame was a support for the translation stage *O* which consisted of a Time and Precision uni-slide. The moveable end-piece, *I*, of the bellows was connected to the slide of the translation stage by a holder *S* and a vertical brass rod. Additional fixed holders *P* and *Q* were used to support rigid stainless steel rods which in turn screwed into the perspex end-piece *H* and a transducer mount. An optional holder *R* was also fixed onto the translation stage. This was for separate mounting of a hydrophone and was used for the attenuation measurements. With such an assembly the whole rig formed a rigid structure. Although the chamber had only one degree of freedom (due to its rigidity) the transducer mount had four degrees of freedom which allowed for satisfactory alignment of the ultrasonic field.

5.2.3 *Fluid containment*

Figure 5.3 illustrates the method of fluid containment in more detail. The containment was provided for by five pieces:

(i) The polyurethane bellows with flanged ends;

(ii) Perspex end-pieces (*H* or *I*);

(iii) Two Aluminium rings;

(iv) A 23 μm mylar window;

(v) Fluid inlet/outlet holes.

The polyurethane bellows was moulded from clear polythene, supplied and manufactured by Beakbane Ltd, (Beakbane, 1994), with a minimum length of 50 mm and, on extension, a maximum length of 300 mm. The flanged portion of the bellows, with the aid of an 'o'-ring and an Aluminium ring, was located against the inner side of the end-piece. A 23μm mylar window was stretched over the outer side of the end-piece and again located with an 'o'-ring and another Aluminium ring. A set of six screws were threaded through both Aluminium rings enabling the two rings to be brought together. This tightened the mylar window and the flanged portion of the bellows so ensuring a fluid tight arrangement.

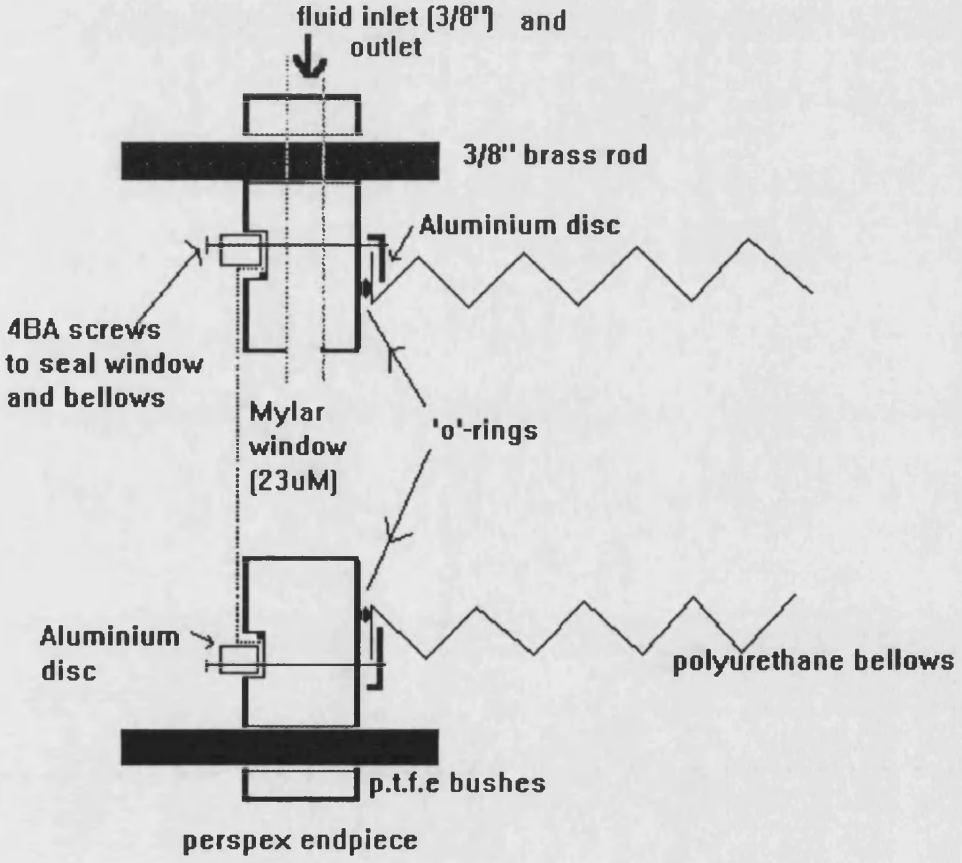

Figure 5.3 Schematic illustrating one end-piece and the method employed for fluid containment.

An identical arrangement at the other end-piece allowed for a fluid tight chamber. The advantage of achieving fluid containment via 'o'-rings and screws was that the chamber could be dismantled easily, this was necessary because easy disposal of the biological fluids and cleaning of the chamber were important for safety reasons.

Both end-pieces had 9.5 mm holes bored through them from the top, into the fluid chamber. This provided an inlet and outlet for fluid and air from the chamber. The fluid inlet at the transducer end-piece was connected to a fluid reservoir (3/4 litre volume). The reservoir had an outer jacket through which water from the outer tank flowed through via the water pump, maintaining all the fluid at the same temperature.

5.2.4 *Electronic apparatus*

Figure 5.4 illustrates the electronic arrangement used for generating and detecting the acoustic field. The function generator (Wavetek model 151) defined the frequency of operation and pulsing mode. In general a single cycle pulse (centred at 15 MHz) was used for the attenuation measurements. A tone burst centred at 2.25 MHz and of approximately eight cycles was used for the nonlinear axial pressure distribution measurements. After passing through a variable attenuator (maximum of 100 dB attenuation) the signal was amplified with a broadband (0.3 MHz to 35 MHz, 55 dB gain, model A150) ENI amplifier. The output of the amplifier excited a piezoelectric transducer to produce the ultrasonic field. The signal received by the hydrophone was passed through a buffer amplifier and captured with a Lecroy 9310 digital storage oscilloscope which was triggered from the function generator.

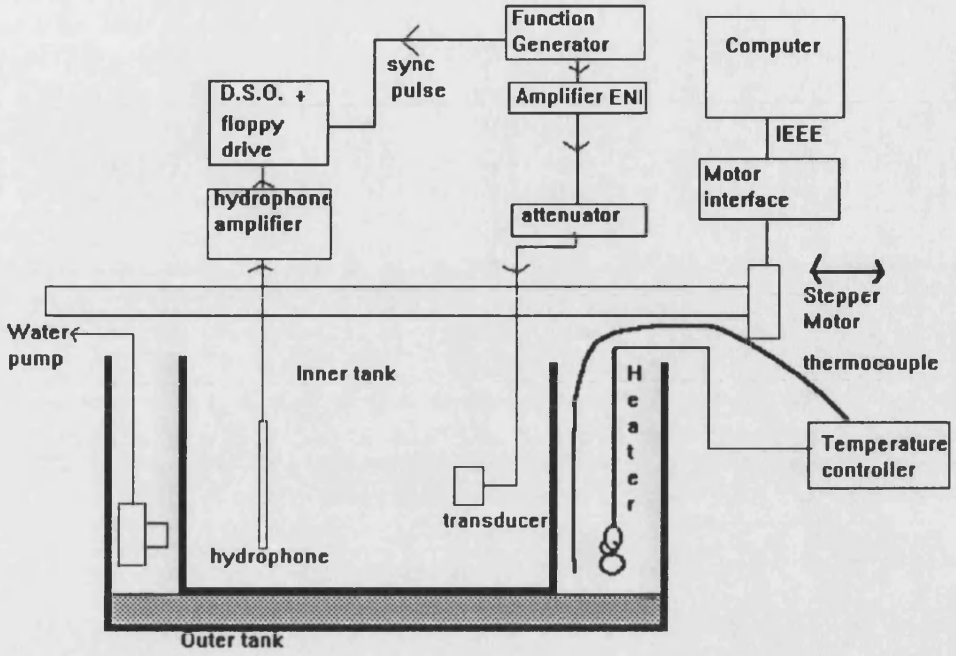

Figure 5.4 Schematic of the electronic arrangement used for movement of the stepper motor and the transmit and receive stages of the transducer and hydrophone.

The oscilloscope used a 100 megasamples per second sampling rate and contained an I.B.M. compatible floppy disk drive for storage of the waveforms. This facilitated easy transfer of data to a P.C. for subsequent processing. The Uni-slide translation stage was controlled by a P.C. via an IEEE bus interface.

5.2.5 Measurement procedure

The samples of amniotic fluid and urine used in the measurements were obtained as pooled samples. The amniotic fluid was taken from approximately forty patients undergoing the clinical procedure of amniocentesis, carried out at Odstock Hospital, Salisbury. The urine came from twelve female volunteers in the Wolfson centre at the Royal United Hospital, Bath. The two Human Albumin solutions (under the trade name of Zenalb 4.5% and 20% solutions) were purchased from BioProducts

Laboratory, Elstree. The general procedure with all these measurements was similar, with the fluid under investigation being stored in a stable condition prior to the measurement. For urine and amniotic fluid this entailed freezing of the fluid, for the Human Albumin solutions storage at temperatures below twenty five degrees centigrade was adequate provided the solutions were under sealed conditions. For all the measurements the fluid was allowed to settle in the chamber for approximately three hours. This enabled it to reach the desired temperature and helped to dissolve any air bubbles that may have been present. Previous workers (Frizzell *et al* 1979, Bamber *et al* 1977) have reported that longer times (of the order of 24 hours) are necessary for the removal of bubbles. However this length of time was not available if the measurements performed were to have a useful bearing on the behaviour of the fluid *in-vivo*. In addition the function generator and ENI power amplifier required a similar time to stabilise. In general the measurements were performed at room temperature (25 °C) and at physiological temperature (37°C).

Three basic types of measurement were made with the apparatus. These were:

(i) Measurement of acoustic velocity;

(ii) Measurement of the frequency dependent attenuation;

(iii) Measurement of axial nonlinear pressure distribution.

A description of these three measurements is given below. The axial pressure distribution measurements are discussed first as they incorporate the majority of features used in the experimental arrangement.

5.3 Measurement of the axial pressure distribution

For this measurement a long polyurethane bellows was used, which had a minimum length of 65 mm and a maximum length of 300 mm. The measurements were performed with a relatively large transducer with a suitable degree of focusing provided by a perspex lens. The signal was detected with a PVdF bilaminar membrane hydrophone attached behind the end-piece *I* (see figure 5.1) with a 2 mm water gap between the end-piece and the hydrophone.

5.3.1 Lens

As described earlier a 2.25 MHz transducer (38 mm active diameter) was used to generate the acoustic field. With such a transducer the last axial maximum occurs at approximately 540 mm. This implies that nonlinear measurements with the above bellows would only be restricted to the pre-focal region where harmonic generation is not prevalent. In order to investigate harmonic generation an acoustic lens was used to produce a focused field. This brought forward the diffractive field and allowed a significant amount of harmonic generation to occur in the region of the last axial maximum.

The plano-concave perspex lens was attached directly to the front of the transducer via a commercial coupling gel (Sonotrace, Diagnostic Sonar Ltd). The concave surface of the lens was machined using a lathe to a suitable radius of curvature to

give the required focal length as calculated by the thin lens formula (Papoulis, 1981). This relates the radii of curvature (R_1 and R_2) of the lens to the focal plane (D) by:

$$\frac{1}{D} = (n-1)\left(\frac{1}{R_1} + \frac{1}{R_2}\right). \qquad 5.1$$

For a plano-concave lens one of the radii of curvature is infinite. The refractive index, n, is the ratio of sound velocity in water to that in perspex. At room temperature (T = 25° C) the velocity in water is 1498 $m^{-1}s$. The velocity in the perspex lens was also measured and found to be 2727 ms^{-1}. Equation 5.1 may be rearranged to give:

$$D = \left(\frac{R_1}{1-\frac{c_m}{c_p}}\right), \qquad 5.2$$

where c_m and c_p are the are the velocities in the medium of propagation and the perspex respectively. This then gives a relation between the radius of curvature of the lens and the focal length. For these measurements, given the measurement range of the bellows, a focal length in the region of 140 mm was chosen. With this focal length measurements could be performed from the penultimate axial maximum to well past the last axial maximum. In addition alignment of the transducer would be possible with the last and penultimate maxima being used as reference positions.

The radius of curvature of the lens was machined to be 64 mm to give a focal length of 141 mm in water at room temperature, according to equation 5.2. An independent check on the radius of curvature of the lens was made using a spherometer which showed that R_1 was 63.9 mm ± 0.4 mm.

As explained earlier, it was decided to place the transducer outside the bellows chamber. This then meant that the actual path for acoustic waves, from the transducer, would be through a short water path (approximately 5 mm) and then into the fluid under investigation. This propagation through a two layer medium has the effect of modifying the direction of acoustic rays, due to refraction at the interface, which in turn modifies the focal length of the system. The magnitude of this change can be estimated, by considering a simple ray approach to the problem, as shown in figure 5.5.

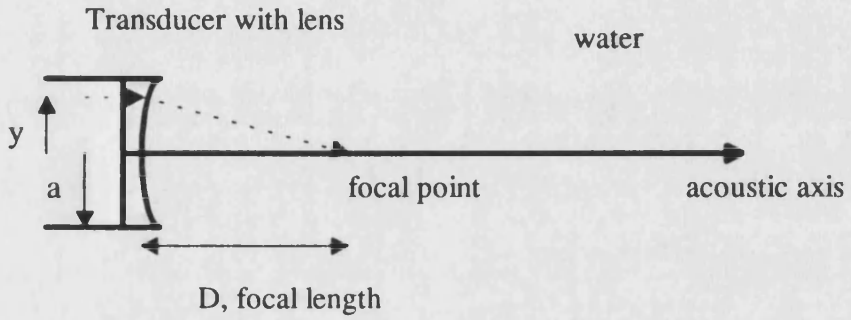

Figure 5.5a Focusing of a general ray in one medium propagation.

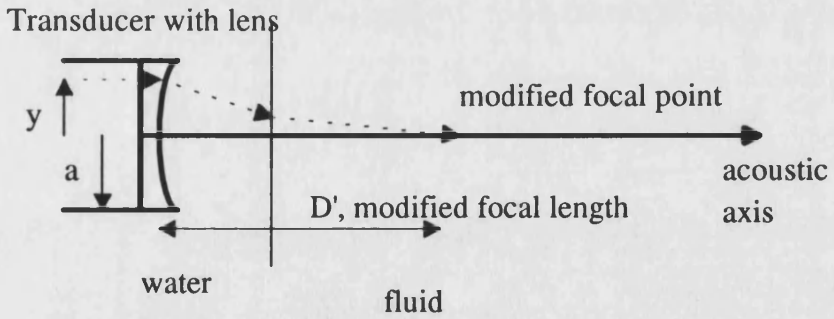

Figure 5.5b Focusing of a general ray in two media.

Figure 5.5 Diagram illustrating the change in focal length due to propagation through a two media.

Figure 5.5a illustrates one medium propagation. The lens is attached at the transducer face. The transducer radius is a, the focal length is D and y is the radial distance of a general ray from the acoustic axis. The angle a ray makes from the edge of the lens through to the focal point is θ_1. It follows that

$$\tan\theta_1 = \left(\frac{y}{D}\right). \qquad 5.3$$

Figure 5.5b illustrates the corresponding situation for two media propagation where the first medium is water and the second is the fluid under consideration. Here a general ray is refracted at the interface and arrives at the focal point D', at an angle θ_2, to the acoustic axis. From Snells law of refraction we have:

$$\sin\theta_2 = (\tfrac{v_2}{v_1})\sin\theta_1 \ . \qquad 5.4$$

Here v_1 and v_2 are the acoustic velocities in water and the fluid respectively. Now if the angles subtended are small (0.3 radians for example), then $\theta_1 \approx \sin\theta_1 \approx \tan\theta_1$. In this case equation 5.4 becomes:

$$\theta_2 \approx (\tfrac{v_2}{v_1})\left[\tfrac{y}{D}\right] \qquad 5.5$$

and

$$D' = (\tfrac{v_1}{v_2})D. \qquad 5.6$$

For the biological fluids considered in this work, the percentage change in velocity, with respect to water, is of the order of two to three percent, implying that the change in focal distance is also of this magnitude.

The addition of a lens in front of the transducer has two effects on the excitation at the source. Firstly it reduces the amplitude of the pressure wave emanating from the

source as the attenuation in perspex is approximately 1 dB cm^{-1} (Kaye & Laby 1986). The effect of this reduction is considered in Chapter 7. Secondly, because focusing is achieved by changing the lens thickness across the face of the transducer, waves passing through the edge of the lens travel through more perspex than those arriving from the centre. The effect of this aperture shading across the transducer/lens assembly was modelled theoretically using the finite difference model however it was found that it had little effect to the structure of the ultrasonic field produced.

5.3.2 Hydrophone and hydrophone calibration

A 0.5 mm diameter PVdF bilaminar membrane hydrophone (manufactured at GEC Marconi) was used to map the axial pressure distribution. This is the standard detector for such measurements and has been recommended by the AIUM/NEMA (1983). The advantages of this type of device are:

(i) It is mechanically stable.

(ii) The impedance of the device (PVdF) is similar to that of water. This reduces any perturbations to the ultrasonic field caused by an impedance mismatch.

(iii) Although the active area of the hydrophone is small the hydrophone itself is approximately 150 mm in diameter due to the method of mounting the active area. The majority of this area is made from PVdF which again reduces any perturbations

to the ultrasonic field. This feature of the membrane hydrophones gives them an added advantage when compared to PVdF needle hydrophones. These latter devices have a backing material which causes them to be directional, therefore making alignment of the device a problem.

(iv) PVdF membrane hydrophones are also broadband (up to 30 MHz), and can be calibrated by the National Physical Laboratory up to 20 MHz. This is advantageous for nonlinear measurements, where harmonic generation results in energy being present at these high frequencies.

The active area of the hydrophone used was 0.5 mm in diameter. The choice of active area is a trade off between sensitivity, spatial averaging effects and directionality. The sensitivities of a 4 mm bilaminar device and a 1 mm bilaminar device, relative to 1 V μPa^{-1} , are -230 dB and -260 dB respectively (Preston *et al* 1983). Because the fluids used in this work are thought to have attenuation values that are intermediate between water and soft tissue, problems of signal to noise ratio were thought not to be so important. This is further alleviated by the use of a standard buffer amplifier on the output of the hydrophone. The advantages of using a smaller hydrophone are that it is far less directional (so reducing alignment problems) and also that spatial averaging effects are less significant. The IEC recommendations (IEC 1991) on spatial averaging effects, when mapping the ultrasonic field, also support this. They derive a maximum permissible hydrophone size based on transducer radius and frequency of operation. They recommend that the maximum hydrophone radius b_{max} is

$$b_{\max} = \left(\frac{\lambda}{4}\right)\left[\left(\frac{l}{2a}\right)^2 + \left(\frac{l}{4}\right)\right]^{1/2} . \qquad 5.7$$

For a 19 mm radius transducer operating at 2.25 MHz and at an axial distance of 80 mm, the value of b_{max} is 0.36 mm. This is slightly larger than that employed in the measurements. As the value of l increases so the value of b_{max} increases, so decreasing the effect of spatial averaging. It should be noted that spatial averaging effects become more important for the higher harmonics.

The calibration of the 0.5 mm PVdF membrane hydrophone was performed at the NPL by intercomparison with a primary standard hydrophone. Figure 5.6 illustrates the results of the NPL calibration for the frequency range 1 MHz to 20 MHz (note that this is the end of cable open circuit sensitivity). The general behaviour of the hydrophone was fairly typical of these devices, the sensitivity being fairly flat then rising to a broad resonance and finally falling off fairly rapidly (the rapid fall off is not illustrated as the calibration is only up to 20 MHz). The uncertainties associated with these values are typically 7 % up to 8 MHz and rising to 12 % from 17 MHz to 20 MHz. Normally the resonance occurs around 25 MHz. With this particular device it is however closer to 20 MHz.

The frequency response of membrane hydrophones has been modelled by Bacon (1982). The method considers the voltage across the active element (as a function of the piezoelectric constants of PVdF and the thickness of the active element) given a mean pressure at the element. The sensitivity (S) can be expressed as:

$$S = \left(\frac{T_1 \sin(\theta)}{\theta(\exp(-j\theta) - R_2 \exp(j\theta))} \right), \qquad 5.8$$

where

$$\theta = \left(\frac{kx}{2} \right), T_1 = \left(\frac{2}{1+Z} \right), R_2 = \left(\frac{Z-1}{Z+1} \right). \qquad 5.9a,b,c.$$

Here x is the film thickness, k is the wavenumber and Z is the ratio of the acoustic impedance of water to that of the film. The acoustic impedance of a medium is simply the product of the acoustic velocity and density for the medium. For the piezoelectric film ρ is 1780 Kg m $^{-3}$ and its velocity is 2400 m s^{-1} . Given the above parameters one can compare the theoretical sensitivity with that measured experimentally. For the above hydrophone it was found that (Figure 5.6) a film thickness of sixty micrometers gave the closest agreement with theory. This thickness is approximately 20% higher than that normally used (fifty micrometers), but explains the resonance at approximately 20 MHz.

In order to increase the signal to noise ratio, the output of the hydrophone was fed into a buffer amplifier before connection to the oscilloscope. This required the hydrophone to be re-calibrated, in order to take account of the frequency response of the amplifier and the effects of the oscilloscope and amplifier on the device. The hydrophone was not calibrated from first principles but a relative calibration was performed in the modes of operation, i.e. with and without the buffer amplifier. The transducer was driven at a relatively high voltage (200 V peak to peak). The received waveform was therefore appreciably distorted and contained energy at a wide range of harmonic frequencies which allowed the calibration to be performed over the frequency range of 2.25 MHz to 20 MHz.

In each case the transducer was driven with a toneburst and the received signal was recorded. A single cycle was extracted and an FFT applied to it to give a spectral level at each harmonic present (frequencies up to 20 MHz are considered). The measurement made with the hydrophone connected to the oscilloscope had to be corrected for the loading effect of the hydrophone. The loaded sensitivity of the hydrophone depends on the impedance of the hydrophone and the electrical load of the oscilloscope (in this case).

If it is assumed that the impedance of the hydrophone and the load are mainly capacitative then a simple expression results and the loaded end of cable sensitivity M_l is given by

$$M_l = M_c\left(\frac{C}{C+C_l}\right). \qquad 5.10$$

Here M_c is the open circuit end-of-cable sensitivity, C is the capacitance of the hydrophone and C_l is the capacitance of the load. For the Lecroy 9310 oscilloscope C_l is 15pF, for the hydrophone C is 103pF and the loading effect reduces the open circuit end-of-cable sensitivities (M_c) by 13%.

Once the loaded sensitivity of the hydrophone had been calculated it was possible to calibrate the acoustic wavefield. An identical measurement of the waveform was taken with the buffer amplifier attached. Fourier analysis of this signal yielded another set of voltage values as a function of frequency. As the acoustic pressures of the wavefield were known, these values enabled the overall sensitivity of the hydrophone/amplifier/oscilloscope (detection) system to be obtained.

Figure 5.6 illustrates the new calibration of the detection system. As can be seen the addition of the buffer amplifier increased the sensitivity by approximately 23 dB. The general dependence of sensitivity with frequency was not, however, altered. It should be noted that the experimental results are the average of five independent measurements. The figure also illustrates the sensitivity at physiological temperature (37°C). These results were inferred with data given from the NPL (1994) concerning the variation of sensitivity with temperature. In general, for a 0.5 mm bilaminar hydrophone the sensitivity increases by 0.1 % per degree Celsius at 2 MHz and rises to 0.4 % per degree Celsius at 10 MHz.

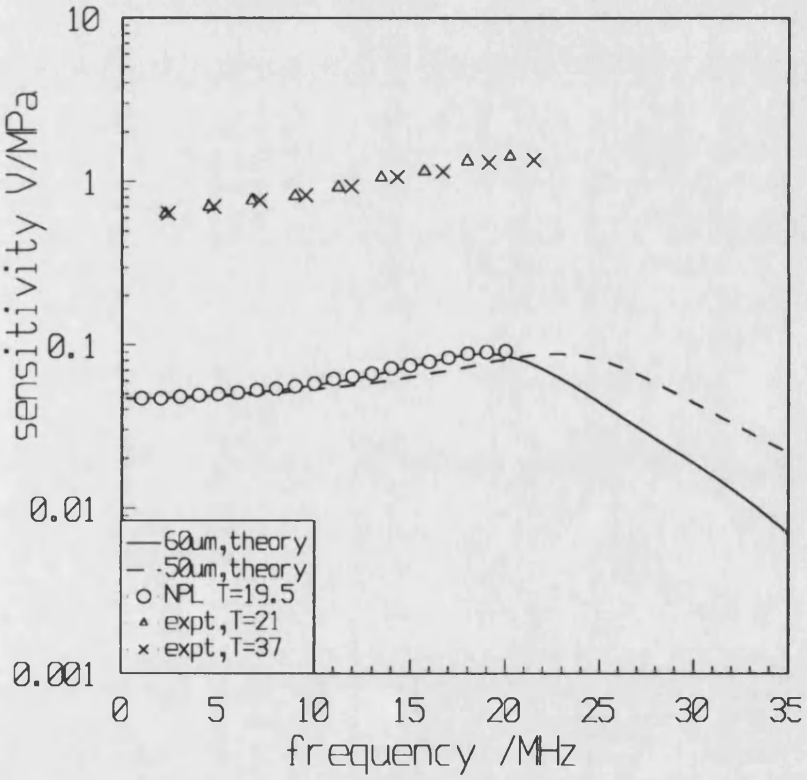

Figure 5.6 Sensitivity of 0.5 mm bilaminar PVdF membrane hydrophone as a function of frequency.

This method of calibration does not require knowledge of the impedance of the buffer amplifier stage because in effect the buffer amplifier and the oscilloscope are a taken

as one unit. The calibration is however only valid for the particular amplifier and oscilloscope used.

5.3.3 Alignment

Since the bellows and the hydrophone were connected to the translation stage, the transducer was aligned to be parallel to the stage axis. In general alignment was achieved by considering various special points in the axial field. These were the penultimate maximum, the last minimum and the last maximum (any maxima and minima present beyond the focal plane are not included in the definition of maxima or minima). The method of alignment was an iterative process whereby the rotation and tilt of the transducer were altered to find the acoustic axis. In general a further check of the alignment was also made in the far-field. This was useful because for such strongly focused sources the minima and maxima were very close together (in the axial direction) so a slight misalignment may not have been apparent. In addition it should be pointed out that the transducer alignment was achieved manually.

5.3.4 Transducer output

For the measurement of the axial pressure field, the transducer was driven with a short toneburst of eight cycles at its resonant frequency with a pulse repetition rate of approximately 1KHz. The voltage applied to the transducer was varied from 8 volts peak to peak (corresponding to P_o of 0.007 MPa), for linear propagation to 240 volts peak to peak (0.224 MPa) for nonlinear propagation. A longer

toneburst would have been desirable as this would have allowed the transducer and amplifier to reach a more stable output. This, however, was not possible because of reflections between the hydrophone and mylar window which interfered with the direct signal for longer pulses. It should be noted that this reflected signal only manifested itself at high drive levels where there was significant energy present in the higher harmonics. This is illustrated in Figure 5.7 which shows a typical signal received on the hydrophone, after passing through a fluid path, when the transducer is driven at a higher drive level. As can be seen the first pulse is simply distorted (as a result of nonlinear propagation), but in the latter lower amplitude pulse only the higher frequency components are observed. Fourier analysis of the reflected signal revealed that it contained energy in the frequency range 5 MHz to 10 MHz. Preston *et al* (1983) have measured the transmission properties of bilaminar PVdF hydrophones. They found that although the membrane had a high transmission coefficient, the amplitude reflection coefficient was nevertheless significant. For a membrane thickness of 50μm the amplitude reflection coefficient was found to be approximately 0.7 in the frequency range 5 MHz to 9 MHz.

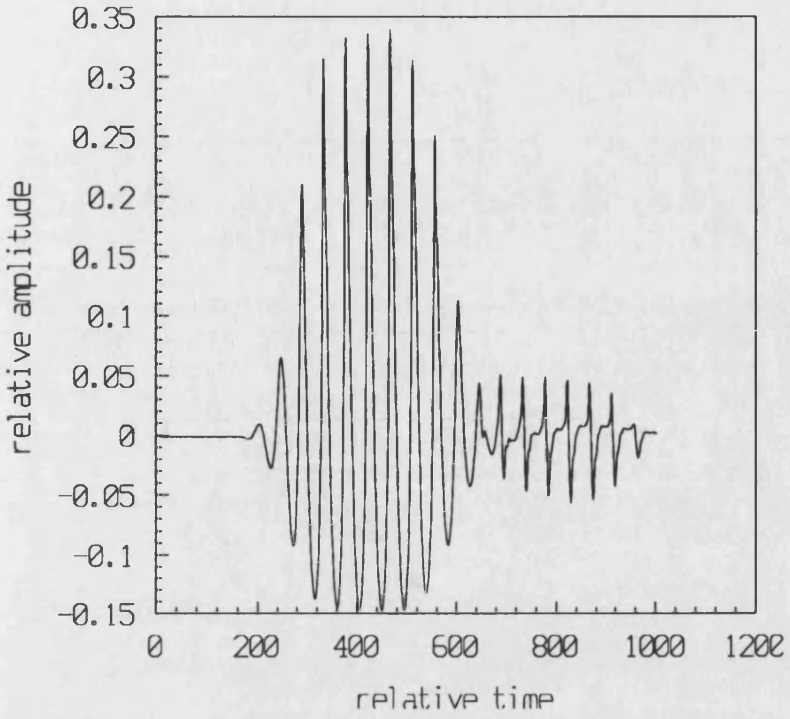

Figure 5.7 Typical waveform captured for the axial nonlinear pressure distribution measurement. The second pulse results from a multiple reflection between the hydrophone and mylar window.

5.3.5 *Mylar end windows*

As described , mylar end windows (with a nominal thickness of 23μm) were used as part of the fluid containment chamber. The transmission properties of these end windows were important for the nonlinear measurements where actual voltages and pressures were measured and then compared with theoretical predictions.

The transmission of the end windows was measured as a function of frequency by the standard substitution method. A broadband transducer (radius 6.35 mm) with a frequency of 15 MHz was used to produce a single cycle pulse in water which was detected by a 4 mm diameter bilaminar PVdF membrane hydrophone. The distance

between the transducer and hydrophone was kept to a minimum (approximately 100 mm) in order to minimise any nonlinear propagation in the water path, and also kept constant. The use of a fixed transducer to hydrophone distance and the use of a large area hydrophone minimised any correction that may have been necessary due to a change in the diffractive field, as discussed in Chapter 2.

The mylar was stretched across a perspex end-piece in an identical manner to that used for fluid containment. Waveforms were captured with and without a single sheet of mylar film in the propagation path. The amplitude transmission properties were determined from examining the frequency content of the two waveforms, by applying a fast Fourier transform to both the pulses. The frequency dependent transmission loss $T_m(f)$ was expressed in dB's using

$$T_m(f) = -20\log_{10}\left(\frac{V_m(f)}{V_w(f)}\right). \qquad 5.11$$

Here $V_m(f)$ was the voltage at frequency f with the mylar present in the water path and $V_w(f)$ is the voltage at frequency f with only the water path.

Figure 5.8 illustrates the experimental results over the frequency range 2 MHz to 20 MHz. As can be seen the transmission loss is low over the whole frequency range of interest. At 11 MHz it is about 1 dB, this corresponds to the fifth harmonic for a waveform originally centred at 2.25 MHz. From 8 MHz to 20 MHz the loss increases with frequency, reaching a maximum of 2 dB at 20 MHz.

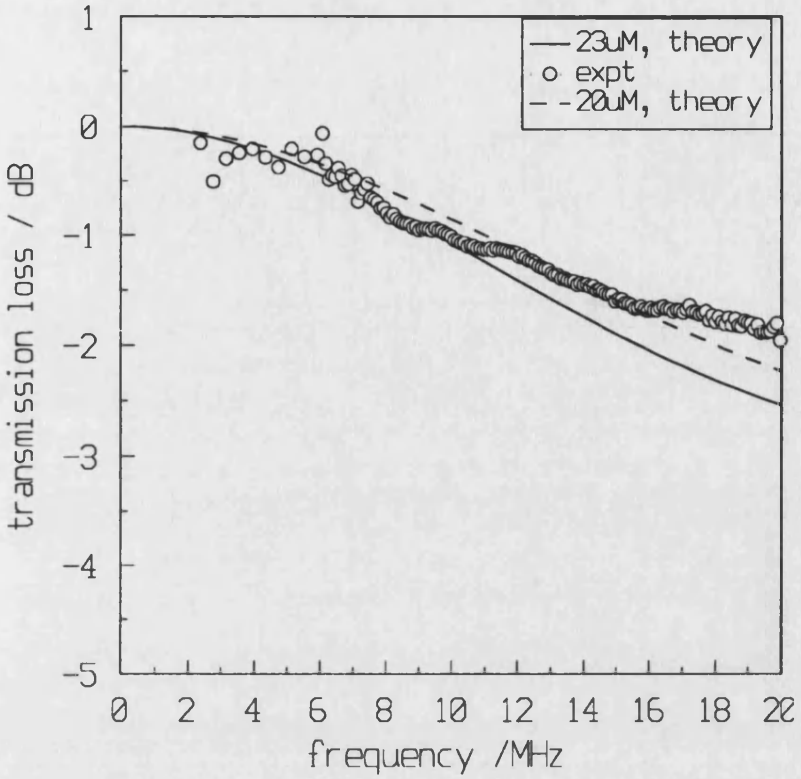

Figure 5.8 Transmission loss for a mylar window as a function of frequency, comparison between experiment and theory.

The acoustic transmission through the mylar can also be modelled by considering it as propagation through a fluid loaded plate at normal incidence (Kinsler 1962). In this case the transmission loss is expressed as

$$T_m(f) = -20\log_{10}\left[\frac{4Z_1Z_2}{(2Z_1)^2\cos^2(k_2l_2)+\left(Z_2+\left(\frac{2Z_1}{Z_2}\right)\right)^2\sin^2(k_2l_2)}\right]^{1/2}, \qquad 5.12$$

where Z_1 and Z_2 are the impedances of water and mylar respectively, $k_2 = \left(\frac{2\pi}{\lambda_2}\right)$ is

the wavenumber in mylar, l_2 is the thickness of mylar and λ_2 is the wavelength in mylar. The velocity in mylar is 2540 m s^{-1} (Zeqiri 1995) and its density is 1.1 kg m^{-3} (Kensulat 1994).

Using these values a theoretical transmission loss curve was calculated and is also shown in Figure 5.8. As can be seen the general behaviour of the curve is similar to that obtained experimentally, especially at the low frequency end. There are, however, differences between the experiment and theory above 10 MHz, with the theory consistently giving a higher loss, the maximum difference being 0.5 dB at 20 MHz. This disagreement could be due to a number of factors. For example as the frequency increases so the orientation (the angle at which the mylar window intersects the acoustic beam) of the mylar window with the transducer and hydrophone becomes more critical. In general, for small angles of non-normal incidence the transmission loss decreases (Humphrey & Berktay 1985), as observed experimentally. Alternatively, if the thickness of the mylar is reduced to 20μm (a reduction of 13 %) then the theoretical transmission loss decreases. This is also illustrated in figure 5.8, the agreement between experiment and theory being good, with only a 0.25 dB difference at 20 MHz. The quoted error for the mylar thickness is +/- 2μm. (Kensulat 1994).

For the frequencies of interest in this work the differences are small, when compared to other errors (such as the calibration of hydrophone and transducer output) and it is reasonable to say that the effect of the mylar windows is well characterised.

5.3.6 Processing

Measurements of the axial pressure distribution were made from the penultimate axial maximum well past the focal plane, approximately 300 mm from the transducer. At each axial position the waveform detected by the hydrophone was captured and

recorded as a binary data file on an IBM compatible floppy disc (fitted to the oscilloscope). This data was then downloaded to a P.C. where it was converted into ASCII form. Further processing then involved picking a single cycle from each waveform and Fourier analysing it. This yielded the harmonic components (converted to harmonic pressures) which were subsequently plotted as a function of axial distance to give the axial nonlinear pressure distribution for the fluid of interest.

5.4 Frequency dependent attenuation

5.4.1 General

A variable path length method, originally devised by Schwan & Carstensen (1952) was used to measure the frequency dependence of attenuation. With this method the physical distance between the transducer and hydrophone is kept constant, but the path length of test fluid and reference fluid is altered. The method used differs slightly from that used by Schwan and Carstensen (1952) in that there were actually two water paths; one between the transducer and test fluid (of 15 mm in length) and the other between the test fluid and the hydrophone. However because the length of the first water path was constant, as the fluid path length was altered it had no bearing on the analysis of the results.

The experimental configuration for this measurement was as follows. The transducer was mounted on holder *Q* (see figure 5.1), as with the nonlinear measurements, but the hydrophone was now mounted on holder *R*. This was fixed and only the fluid

path length was altered by movement of the translation stage. The distance between the transducer and hydrophone was approximately 300 mm. The fluid path length was in general varied by 100 mm to 150 mm, with a minimum path length of at least 100 mm. Measurements were performed with steps in the fluid path length from 2 mm to 10 mm. Low frequency attenuation measurements involved steps of 10 mm changes in fluid length, whereas the high frequency measurements (where the attenuation was greater) were calculated using 2 mm steps. Typically each measurement of attenuation used ten steps in fluid path length, to increase the statistical precision of the results.

For the measurements reported here the reference fluid was distilled water and the test fluids were Dow Corning 200/350 silicone fluid, amniotic fluid, urine and Human Albumin (4.5 % and 20 % solutions). Again measurements were performed at both room temperature and physiological temperature.

5.4.2 Transducer

A 13 mm diameter transducer with a centre frequency of 15 MHz was used for these measurements. This gave a usable frequency range of 5 MHz to 25 MHz for the measurement of attenuation. The transducer was mounted in a similar manner to the axial pressure distribution measurements, however no focusing was employed here. The transducer was driven with a single cycle pulse, this allowed for broadband measurements to be made, of low amplitude. Typically the voltage at the transducer face was between 10 volts peak to peak and 30 volts peak to peak, so ensuring that

there was minimal nonlinear generation in the water and fluid paths. Zeqiri (1992) has pointed out the importance of avoiding nonlinear effects since attenuation values can otherwise be in error by as much as 50 %, depending on the actual attenuation of the fluid and the degree of nonlinear propagation.

5.4.3 Hydrophone

A 4 mm diameter PVdF bilaminar membrane hydrophone was used for this measurement. A PVdF device was used primarily because of its wide bandwidth with a fairly constant sensitivity over the frequency range 1 MHz to 20 MHz. The actual sensitivity was however not required, as the measurements were based on relative changes as a function of fluid path length. This was advantageous as calibration of such a large diameter hydrophone is not straight forward. The use of a large diameter hydrophone also reduced errors in the attenuation measurements due to diffraction loss (see chapter 2 section 2.1.3). The output from the hydrophone was fed into a buffer amplifier and then captured by the oscilloscope for storage. Because of the high sensitivity of a 4 mm hydrophone it was necessary to ensure that the input to the buffer amplifier did not exceed 350 mV. Above this value the device ceased to operate linearly.

5.4.4 Processing

The results consisted of a series of waveforms captured over a range of fluid path lengths. Each waveform was Fourier analysed to give the pulse spectrum and hence

the change in each frequency component with propagation distance. This data was then corrected, in order to take account of the attenuation of the signal due to the water path replaced by the fluid path and also to take into account diffraction effects. The two corrections are discussed below.

(i) Water correction

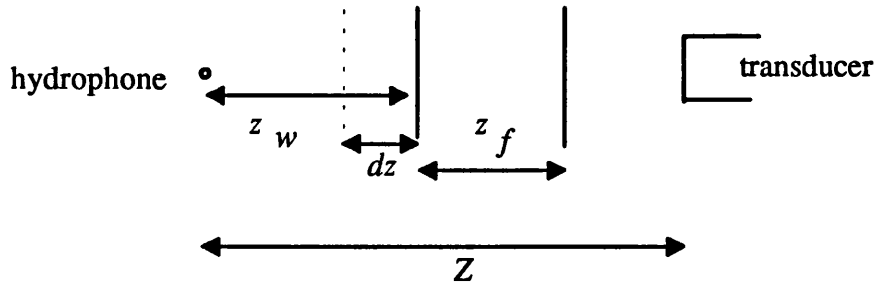

Figure 5.9 Schematic illustrating the arrangement for the frequency dependent measurements.

Consider the arrangement shown in Figure 5.9. For this analysis we will consider a single frequency, a similar analysis can be applied to all the frequency components in the pulse. The distance Z, between the transducer and the hydrophone, is constant. The fluid path length, z_f, increases by δz from a minimum value $z_{f(min)}$. The signal received at the hydrophone, V_1, for the minimum fluid path length can be expressed as:

$$V_1 = V_o e^{-\alpha_f(z_{f(\min)})} e^{-\alpha_w(z_{w(\max)})}, \qquad 5.13$$

where V_o is the signal that would be obtained for no attenuation and $z_{w(max)}$ is the maximum water path, and is $(Z - z_{f(min)})$. The attenuation coefficient in the fluid and water are α_f and α_w (Nepers cm^{-1}) respectively.

Now, as the fluid path length is increased by δz the signal received decreases and can be expressed as:

$$V_2 = V_o e^{-\alpha_f(z_{f(\min)}+\delta z)} e^{-\alpha_w(z_{w(\max)}-\delta z)}. \qquad 5.14$$

The attenuation coefficient α_f of the fluid can then be expressed by taking the ratio of equations 5.13 and 5.14, as

$$e^{-\alpha_f \delta z} = \left(\frac{V_2}{V_1}\right) e^{\alpha_w \delta z}. \qquad 5.15$$

Equation 5.15 is similar to that describing the attenuation of a monochromatic wave, that has travelled a distance δz, but includes a second factor on the right hand side to correct the raw data for the attenuation of the replaced water path.

(ii) Diffraction correction

In general the acoustic velocity, in the fluid of interest, is not the same as that in water. This then implies that changes in the propagation path of water and fluid will result in changes in the diffractive field of the transducer. In effect the observation position will 'move' through the diffractive field. A change in the magnitude of the received signal, due to this diffraction error, can be allowed for if the diffractive field of the transducer and the acoustic velocity in the medium are known.

The diffractive field of a given transducer and hydrophone configuration in a single medium, can be calculated theoretically as discussed in Chapter 2 section 2.13. The

method (Beissner 1981) can be extended to include propagation in more than one medium, by introducing a modified s parameter, s', where s' is given by:

$$s' = \left(\frac{z_w \lambda_w}{a^2}\right) + \left(\frac{z_f \lambda_f}{a^2}\right) + \left(\frac{\left(Z - \left(z_w + z_f\right)\right)\lambda_w}{a^2}\right), \qquad 5.16$$

where z_w and z_f are the propagation paths in the water and medium respectively and Z is the distance between transducer and hydrophone.

Changes in s' as a result of changes in z_w and z_f can be calculated from the above expression. These changes in s' can then be used to determine the change in signal amplitude in the diffractive field (from Beissners expression). A correction to the amplitude of the received signal, at the hydrophone, can then be applied to obtain the 'true' attenuation coefficient of the medium. Figure 5.10 illustrates the variation in pressure amplitude for a 4 mm diameter receiver. The values of s' are associated with a source of 13 mm diameter, operating in the frequency range 1 MHz to 25 MHz with variable water and fluid path lengths as used in the experimental arrangement. Since the fluids considered have similar velocities to water, changes in the value of s' are small, and the subsequent diffraction corrections applied to the original signal are of the order of a few percent. It should be noted that because the diffractive field of a transducer is complex, and can change quite rapidly with axial distance, there are regions in the field where the changes in amplitude can be significant.

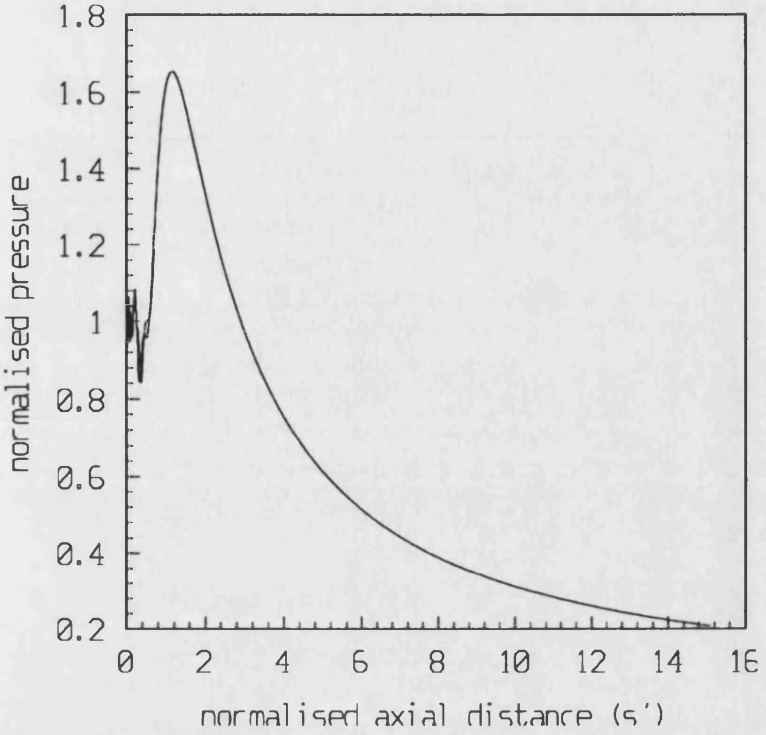

Figure 5.10 Axial variation of the pressure amplitude for a 4 mm diameter receiver and a 13 mm diameter transmitter for a range of s' values.

The problem is however minimised by using a large diameter hydrophone and choosing a range where the diffraction term is slowly varying. A QuickBasic program was written to perform the necessary processing, taking into account water attenuation and the diffraction correction.

(iii) Processing methods

The corrected data consisted of a series of signal amplitudes as a function of propagation distance (in the fluid) for each frequency component in the signal. In general the attenuation due to the fluid can be expressed as:

$$\left(\frac{V}{V_1}\right) = e^{-\alpha_f z}, \qquad 5.17$$

where the attenuation coefficient is in Nepers per centimetre. The attenuation coefficient is generally determined by transforming the data to a linear equation of the form:

$$\ln\left(\frac{V}{V_1}\right) = -\alpha_f z. \qquad 5.18$$

The attenuation coefficient can then be calculated by linear regression of the signal amplitude versus propagation distance data. The above transformation is mathematically rigorous, but when dealing with real data, it may not yield the most accurate estimates for the attenuation coefficient. The reason for this is as follows. Each experimental measurement has associated with it an intrinsic random error which will be proportionally more for smaller signal magnitudes. It follows from this that the error in the value of V_1 will be smaller than that associated with the error in the value of V (a smaller amplitude) , the signal amplitude after propagation through a greater fluid path. Now, transforming equation 5.17 into equation 5.18 and applying a simple linear regression to the data will intrinsically apply an equal weighting to all the data. In reality the data points should have unequal weightings associated with them, the larger the signal detected the larger the weighting applied to it.

An alternative approach is to apply a nonlinear regression, of the form describing equation 5.18, to the data and so taking into account the 'importance' of each point. The results presented in chapter 7 will illustrate this point. It should, however, be

pointed out that the significance of this effect is in general not large as signal levels would have to fall appreciably before the error due to noise becomes significant.

Once the attenuation coefficient has been found as a function of frequency, the frequency dependence of attenuation of the fluid can be determined. It is common to fit the data in the following form:

$$\alpha = \alpha_o f^m. \qquad 5.19$$

Here α_o is the attenuation coefficient and is defined in dB cm $^{-1}$ MHz^{-m} , where m is the frequency dependent index. Again it is common, in the literature, to transform the data into a linear equation (using a logarithmic transform) and determine the values of α_o and m from the intercept and gradient of the regression line. However, here again strictly speaking a nonlinear regression should be applied (a power law form) because the high frequency measurements are more accurate than those at a lower frequency. As above, the effects of the two types of processing will be discussed in Chapter 7.

5.5 Measurement of sound velocity

This measurement was performed at the same time as the axial nonlinear pressure distribution measurement and was based on the time of flight technique. Essentially the time of arrival of a short toneburst was measured as a function of the change in fluid path length for low amplitude pulses. The change in fluid path length was determined by and under the control of the translation stage. The pulse, itself, consisted of approximately 8 cycles centred on 2.25 MHz, emanating from the 38

mm transducer. It was detected with the 0.5 mm bilaminar PVdF membrane hydrophone and captured using the delayed timebase on the LeCroy 9310 oscilloscope. The time of arrival of the pulse was determined by selecting a cycle in the pulse and measuring the temporal position of its zero-crossing by interpolation.

For this measurement the sampling rate of the oscilloscope was set to 100 megasamples per second, and when operated with a timebase of 1 μs, gave a temporal resolution of 10 ns. This, together with the high precision of the translation stage (better than 0.1 mm), resulted in very low random uncertainties for the velocity measurements. In addition it should be pointed out that changes in the fluid path length were in the post focal plane region where diffraction effects cause a negligible change to the pulse shape.

6.0 RESULTS (I)-FLUID CHARACTERISTICS

6.1 Outline

The previous chapter described the measurement rig and the methods employed to make the desired measurements. In this chapter results for the sound velocity and the frequency dependence of attenuation for Dow Corning 200/350 silicone fluid, amniotic fluid, urine and the Human Albumin solutions will be presented. The chapter consists of the following sections:

(i) Velocity of sound measurements;

(ii) Frequency dependence of attenuation measurements.

The results are presented in this order because the sound velocity results are used in the attenuation measurement procedure to correct for diffraction loss.

6.2 Sound Velocity

Figure 6.1 illustrates the variation in time of arrival of a short toneburst as a function of the relative distance travelled, through the fluid, by the pulse. Four sets of data are illustrated, for amniotic fluid, urine and the 4.5% and 20% Human Albumin solutions. Simple linear regression of the data gives the velocity of sound in the fluid as the gradient of the line fitted by linear regression. The results for the four fluids are tabulated in Figure 6.2, at both room temperature and at physiological temperature.

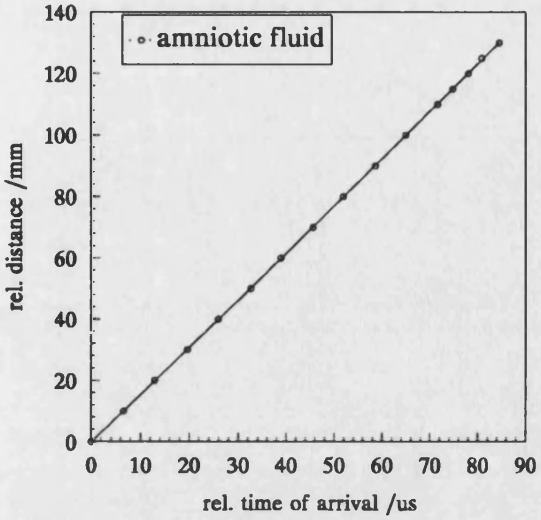

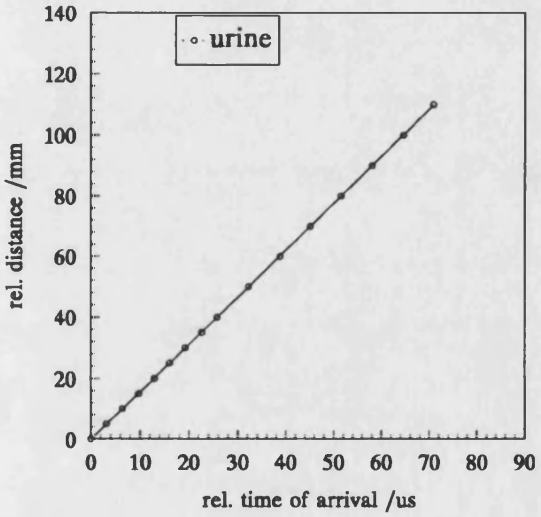

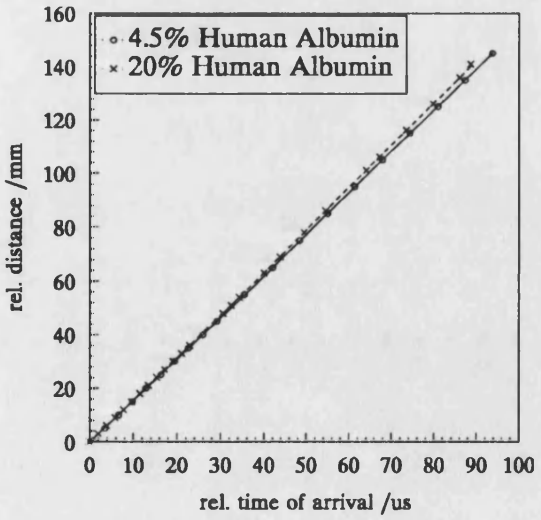

Figure 6.1. Determination of the sound velocity in the four biological fluids.

The good accuracy (better than 1 %) of the results is due to the number of data points (at least 15 measurements) for each fluid. Included in the table is a comparison of the velocity of sound in water, measured as part of this work, with published values from the literature.

	Physiological temperature T=37°C		Room temperature T=25°C	
Fluid	velocity (m s^{-1})	one S.E.(m s^{-1})	velocity (m s^{-1})	one S.E.(m s^{-1})
Amniotic fluid	1541.1	1.3	1519.5	1.7
Urine	1551.3	1.3	1520.5	0.8
4.5% Human Albumin	1547.3	1.0	1522.1	3.6
20% Human Albumin	_	_	1580.3	1.0
Water (measured)	_	_	1495.5	1.0
Water (published)	1520	_	1498	_

Figure 6.2. Tabulated values of the measured sound velocity and its standard error at room temperature and physiological temperature for the four biological fluids.

6.2.1 Discussion of measured velocities

It was not the purpose of this study to investigate, in detail, the velocity of sound in biological fluids. Rather the measurements were required more as an input parameter for the nonlinear propagation model and for diffraction correction purposes in the attenuation measurements. To this end there is not much detailed comment on the results. However the following general points can be stated and provide support for other work found in the literature.

As expected the velocity of sound in all four fluids is similar to that in water. In general the velocity is approximately 2 % higher, rising to 4 % for the 20 % Human Albumin solution. The similarity with water is not surprising, considering the large water content in these fluids (80 % and higher), and is also reflected by other published work in the literature (Goss *et al* 1978). Indeed the 20 % and 4.5 % Human Albumin solutions support previous work in the literature (Dunn & O'Brien 1976, Goss *et al* 1980) that states that sound velocity is related to protein content, with the velocity increasing as the protein concentration is increased. Although the variation of sound velocity with temperature has not been measured in a systematic manner the percentage increase from room temperature to physiological temperature (approximately 2 %) is also in accordance with published work on biological fluids (Povall *et al* 1984). It should be noted that measurements at room temperature encompass a temperature range of 22°C to 25°C.

6.3 Frequency dependence of attenuation

6.3.1 General

This section presents results of the frequency dependence of attenuation for Dow Corning 200/350 silicone fluid, 4.5 % and 20 % Human Albumin solutions, amniotic fluid and urine. The results for each fluid are presented and where appropriate the following points will be illustrated:

(i) Corrections for diffraction effects;

(ii) Corrections for attenuation in the water path;

(iii) Curve fitting procedures employed in order to obtain the attenuation and its frequency dependence. It should be stressed, in order to avoid confusion, that there are two separate occasions where curve fitting is used. Firstly it is used with voltage-range data to determine attenuation at a given frequency. Secondly, it is employed to obtain a functional relationship between attenuation and frequency.

6.3.2 Dow Corning (200/350) Silicone fluid

Measurements in Dow Corning 200/350 silicone fluid were made because it is often quoted as a reference fluid (Zeqiri, 1995) for attenuation measurements as a result of its stable acoustic properties. In the measurements a single cycle pulse, centred at 7 MHz was used. The signal was detected using a 4 mm diameter bilaminar Pvdf membrane hydrophone (as with all the other fluids) so as to minimise diffraction correction effects. The minimum and maximum fluid path lengths were 50 mm and 70 mm respectively. This together with a relatively small drive voltage at the transducer face, and a short water path of approximately 100 mm, eliminated the possibility of any nonlinear distortion in the pulse that may have influenced the determination of the attenuation (Zeqiri 1992). The measurement was made at 25 ° C. Figures 6.3 and 6.4 illustrate the results of the attenuation, in dB cm^{-1}, for the frequency range 1 MHz to 10 MHz. Above and below this frequency range the signal level was close to the noise floor.

Figure 6.3 illustrates the effect of applying a diffraction correction to the raw data and shows attenuation data with and without the correction applied. The difference in sound velocity between water (1498 m s^{-1}) and Dow Corning (1013 ms^{-1}) is approximately 30 % and, as can be seen, can result in significant differences to the measured value of the attenuation coefficient. In general at low frequencies, 1.5 MHz to 3 MHz, the correction can increase the attenuation coefficient from 30% to 15%, conversely at the higher frequency end correcting for diffraction effects reduces the attenuation coefficient by approximately 6%. Although corrections for diffraction effects do to some extent depend on the geometry of the measurement procedure, these results indicate that appreciation of diffraction corrections are necessary when making high accuracy attenuation measurements.

Figure 6.4 illustrates the effect of correcting for the water path that is replaced by the fluid path (a maximum of 20 mm). As can be seen the effect of correcting for the attenuation in water is less significant. It results in a correction which rises from 2% to 4% at the higher frequencies. This is of course due to the low attenuation of water (0.0025 dB cm^{-1} MHz^{-2}) compared with the silicone fluid.

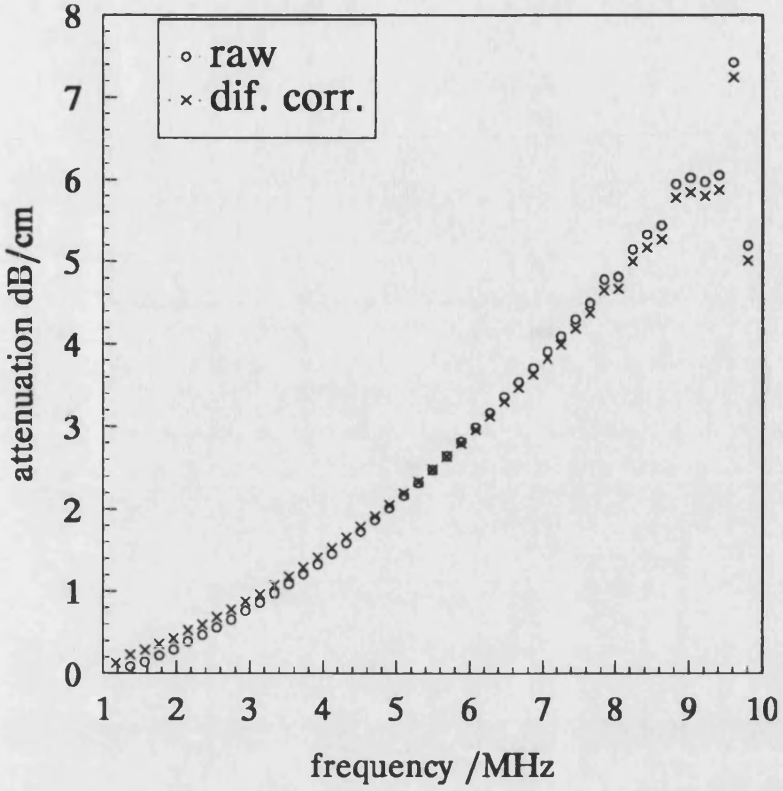

Figure 6.3. Frequency dependence of attenuation in Dow Corning 350/200 silicone fluid. The graph represents raw data results and diffraction corrected results.

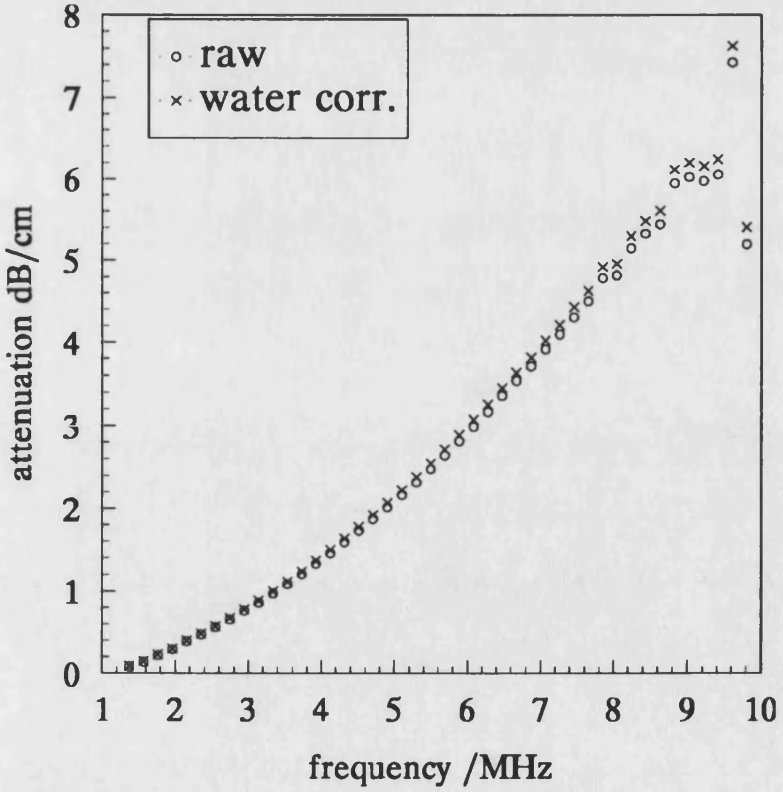

Figure 6.4. Frequency dependence of attenuation for Dow Corning 350/200 silicone fluid. The graph represents raw data results and water corrected results.

Figure 6.5 illustrates the effect of the type of processing applied to the measurements of attenuation, in both cases water and diffraction corrections have been applied to the raw data. The two data sets (ignore for the moment the curve of best fit, this is discussed on page 128) represent two different methods for determining the value of the attenuation coefficient (dB cm^{-1}). With data set (o) the attenuation was calculated at each frequency from the range data by using equation 5.18 whereas with data set (x) the attenuation was calculated by applying a nonlinear algorithm to fit equation 5.17. The algorithm determines the curve of best fit by minimising both the constant in front of the exponent and the attenuation coefficient, which appears in the exponent. As can be seen there is little difference between the two processing methods at low and intermediate frequencies. The situation at the high frequency end (8 MHz and above) is however different, with the nonlinear curve-fitting algorithm giving more consistent estimates of the attenuation coefficient. The reason for this has been discussed in Chapter 5, and is due to the fact that at high frequencies, where the attenuation coefficient is large, the errors associated with individual measurement points (on a signal level versus fluid path length plot) are not equal. For example at 10 MHz, over a 20 mm fluid path, the signal level drops by about 13 dB. The signal after propagating through the maximum fluid path, is therefore much closer to the noise floor and will, therefore, have a larger relative error associated with it. These measurements should therefore be given a low weighting when estimating the attenuation.

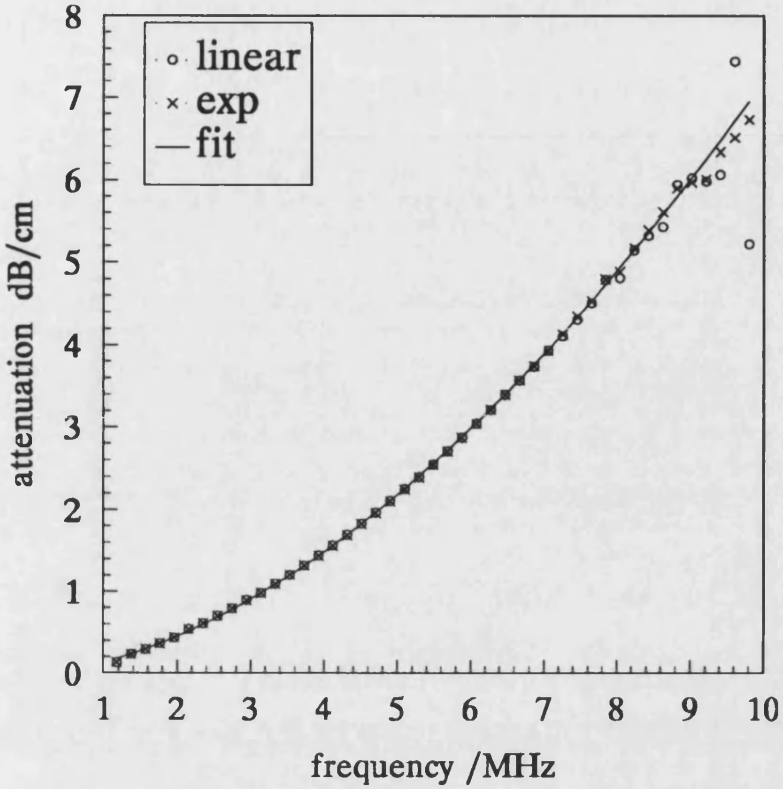

Figure 6.5. Graph illustrating the effect of linear and exponential (nonlinear) processing on the calculation of attenuation.

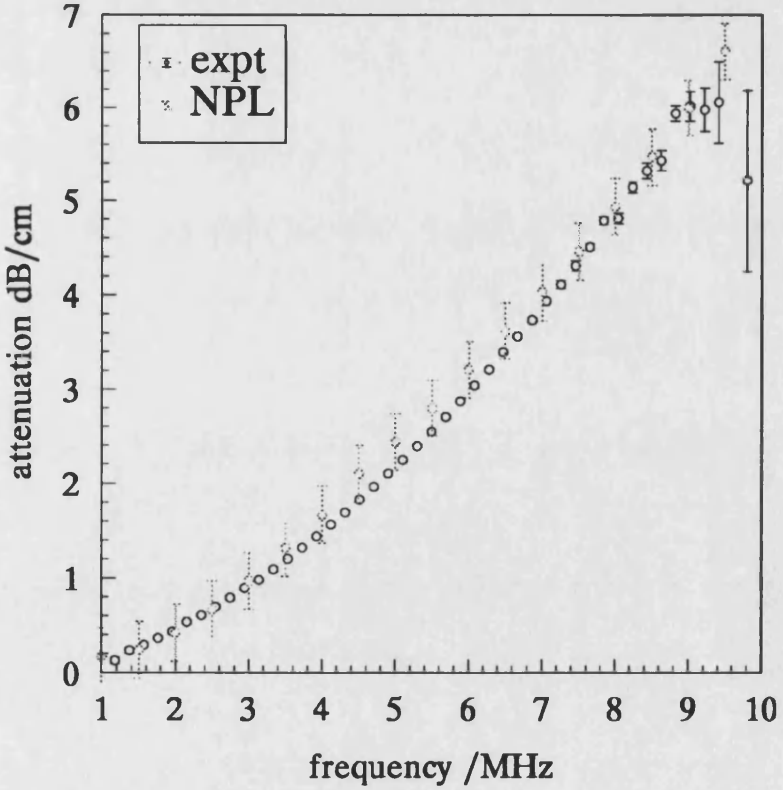

Figure 6.6. Frequency dependence of attenuation in Dow Corning 350 silicone fluid. Experimental results and those performed at the NPL on the same sample.

As mentioned in Chapter 5 it is common to express the variation of attenuation with frequency in a functional form of the type described in equation 5.19. This again can be achieved in two ways. The original equation can be transformed (log transform) and the two constants (α_o and m) determined from a straight line fit, or again a nonlinear regression of the form given by the original equation can be applied, to find a curve that minimises the sum of the squares of the errors from the data. Both types of processing were performed on the corrected attenuation data, and it was found that similar values of two constants were obtained, within experimental error. The reason for this can be found by inspecting the data in Figure 6.5. As can be seen the error associated with each measurement of attenuation is small, especially at the low frequency end. In general nonlinear power law curve fitting is sensitive to data at this end of the frequency spectrum, whereas logarithm transformed data applies equal weighting to these points. If however, as is the case, the data here has a high precision then there is little difference between the two types of fitting procedure.

The best curve fit is also illustrated in Figure 6.5 (applied to dataset 'x'), and gives the following relationship for the attenuation coefficient as a function of frequency:

$$\alpha = 0.137 f^{1.72 \pm 0.01} \quad (\text{dB cm}^{-1}). \qquad 6.1$$

The standard error in the attenuation coefficient at 1 MHz is 0.002 dB cm^{-1} MHz^{-1} .

A sample of the fluid used in these measurements, was sent to the NPL for direct comparison and assessment of the measurement rig. Figure 6.6 illustrates two results for the attenuation over the frequency range of interest. The results correspond to

measurements made in this study and measurements made at the NPL with the same fluid batch. It should be noted that the NPL error bars illustrated for the NPL data points include systematic errors, the measurements made in this study give only the random errors. As can be seen the agreement is in general very good, the results all being within two standard errors (95 % confidence limits) over the whole frequency range. It should however be noted that from 4.5 MHz to 6.5 MHz the NPL results and the results presented here do seem to show a systematic difference. The reason for the difference is unclear, but it does seem that the NPL measurements, over this frequency range, deviate from the rest of the data points, given a power law relationship for the frequency dependence of attenuation. Despite this difference it would seem satisfactory to conclude that the measurement procedure employed here was reliable.

6.3.3 Biological fluids

Measurements of the frequency dependence of attenuation for the four biological fluids considered in this work were made using a single cycle pulse, centred at 15 MHz and, as with the silicone fluid, a 4 mm diameter PVdF bilaminar hydrophone was used for detection. In general the minimum fluid path length for the measurements was 130 mm increasing to 230 mm, the distance between transducer and hydrophone being approximately 300 mm. Corrections for diffraction losses were made to the results, however these are not illustrated as the correction is small (of the order of 1 %) due to the similar velocities of sound in these fluids compared with water. In addition nonlinear curve fitting procedures were employed to

determine the attenuation and its frequency dependence (using equations 5.17 and 5.19).

(i) Amniotic fluid

Figure 6.7 illustrates the variation of attenuation with frequency, from 5 MHz to 25 MHz, for amniotic fluid at both room temperature and at physiological temperature. Both these results were processed using equation 5.17 and its logarithmic transform, however no significant difference between the results was found. The maximum difference, found above 20 MHz, was approximately 2 %. At these frequencies the attenuation is about 1 dB cm^{-1}, so over a change in fluid path length of 100 mm the drop in signal level is of the order of 10 dB. Given an initially small signal level at these high frequencies it seems plausible that some of the measurement points approach the noise floor.

Figure 6.8 tabulates the form of the frequency dependence of attenuation for amniotic fluid at both temperatures. Results are given for data processed by nonlinear regression, although linear transformation of the data gives similar values. The nonlinear curve fits, at both temperatures, represent the measured data well (see figures 6.9a and 6.9b for results at physiological temperature). However the values determined for the constants are puzzling. With the functional form given the attenuation at 1 MHz would be greater at 37 °C than at 25° C. It is generally thought that an increase in temperature should decrease the value of the attenuation coefficient, but leave the value of m unaltered. There is no obvious explanation,

although it does seem that the measurements at 37°C are not as accurate as those at room temperature, partly due to the decrease in the overall attenuation. It should also be pointed out that such differences, at low frequencies, have little bearing on the outcome of the prediction of the axial nonlinear pressure distributions, presented later.

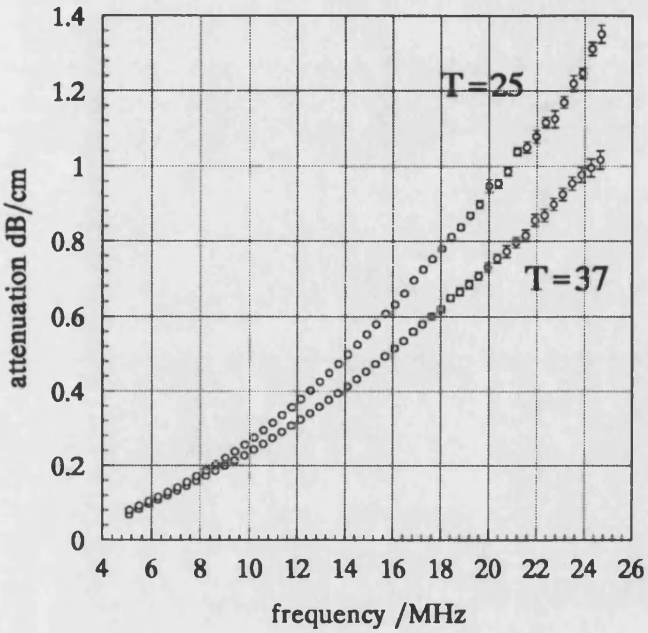

Figure 6.7. The frequency dependence of attenuation in amniotic fluid at room temperature and physiological temperature.

Temperature	T=25°C		T=37°C	
Fluid	α_o +/− *oneS.E.*	*m +/- one S.E.*	α_o +/− *oneS.E.*	*m +/- one S.E.*
Dow Corning 350 silicone fl.	0.137 +/- 0.002	1.72 +/- 0.01	____	____
Amniotic fluid	0.0041 +/- 0.0001	1.81 +/- 0.01	0.0053 +/- 0.0002	1.65 +/- 0.01
Urine	0.008 +/- 0.0001	1.62 +/- 0.01	0.0047 +/- 0.0002	1.67 +/- 0.01
4.5% Human Albumin	0.0347 +/- 0.0005	1.43 +/- 0.01	0.019 +/- 0.0004	1.57 +/- 0.01
20% Human Albumin	____	____	0.167 +/- 0.003	1.27 +/-0.01

Figure 6.8. Tabulated values of the functional relationship between attenuation and frequency. The curve fitting was performed by using nonlinear regression of the data.

Referring back to Figure 6.7 it can be seen that the attenuation in amniotic fluid is small, e.g. at 5 MHz it is 0.08 dB cm^{-1} (at room temperature). The corresponding attenuation in water is 0.048 dB cm^{-1}. Given the similar values for attenuation it seems likely that corrections due to the water path, replaced by fluid path during the measurements, will be significant. Figure 6.10 illustrates this by comparing attenuation measurements for amniotic fluid with and without corrections for the water path, at physiological temperature. The result shows that the measured attenuation is now reduced by a factor of approximately three at 5 MHz, and rises to a factor of four at 16 MHz. This also implies that the results are sensitive to an accurate correction for water attenuation. It is interesting to note that in the literature there are very few references to the measurement of attenuation in water, the one most often quoted is Pinkerton (1947).

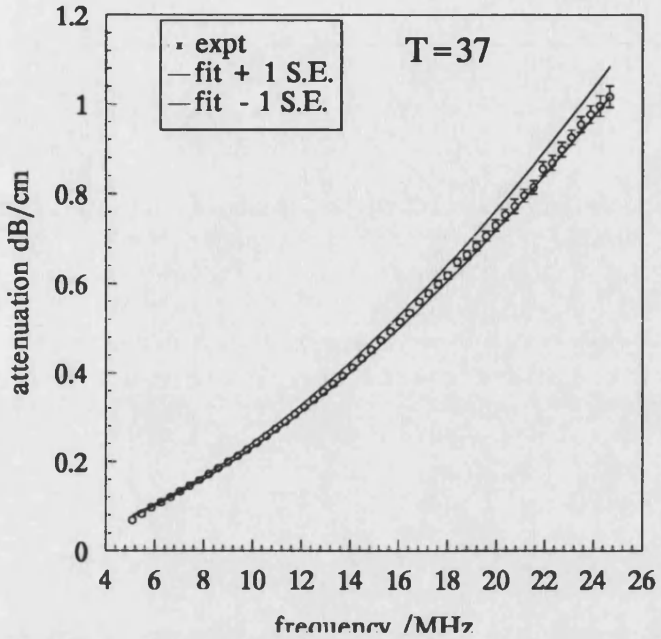

Figure 6.9a. A comparison between the data and the curve fit for amniotic fluid. The two curves represent the variation in the curve fit for changes in the value of *m*.

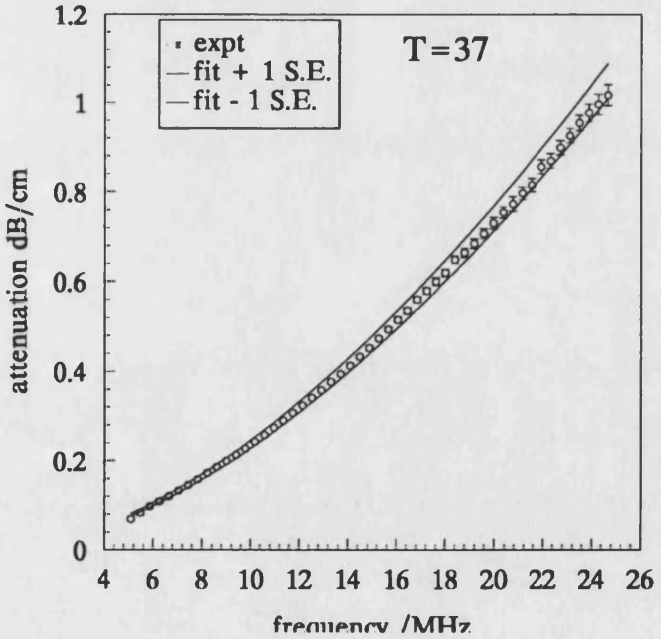

Figure 6.9b. A comparison between the data and the curve fit for amniotic fluid. The two curves represent the variation in the curve fit for changes in the value of α_o.

(ii) Urine

Figure 6.11 illustrates the frequency dependence of attenuation for urine at 22° C and 37°C. The results, as with amniotic fluid, show relatively small random errors and have absolute values in the same region. The processing method, for obtaining the attenuation, is again not critical.

Figure 6.8 tabulates the functional form obtained for the frequency dependence. In general the behaviour as a function of temperature is clearer to see, the attenuation coefficient increases as the temperature decreases. The situation with the frequency index m is again not so clear. For urine the value of m increases slightly as the temperature increases, but the two values are within 2 standard errors of each other.

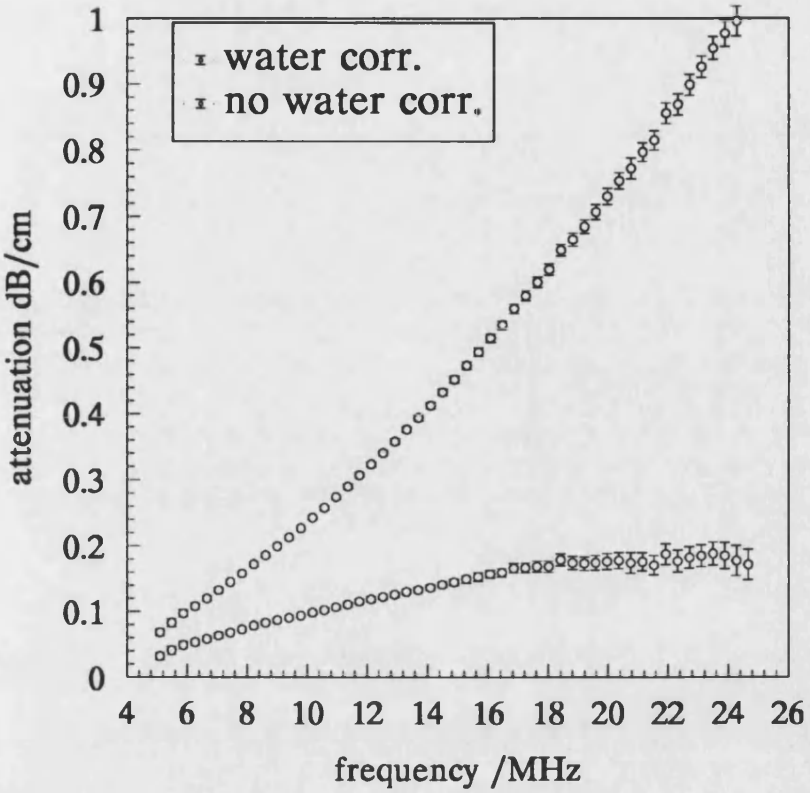

Figure 6.10. Illustration of the effect of correcting for the water path for the attenuation measurements in amniotic fluid.

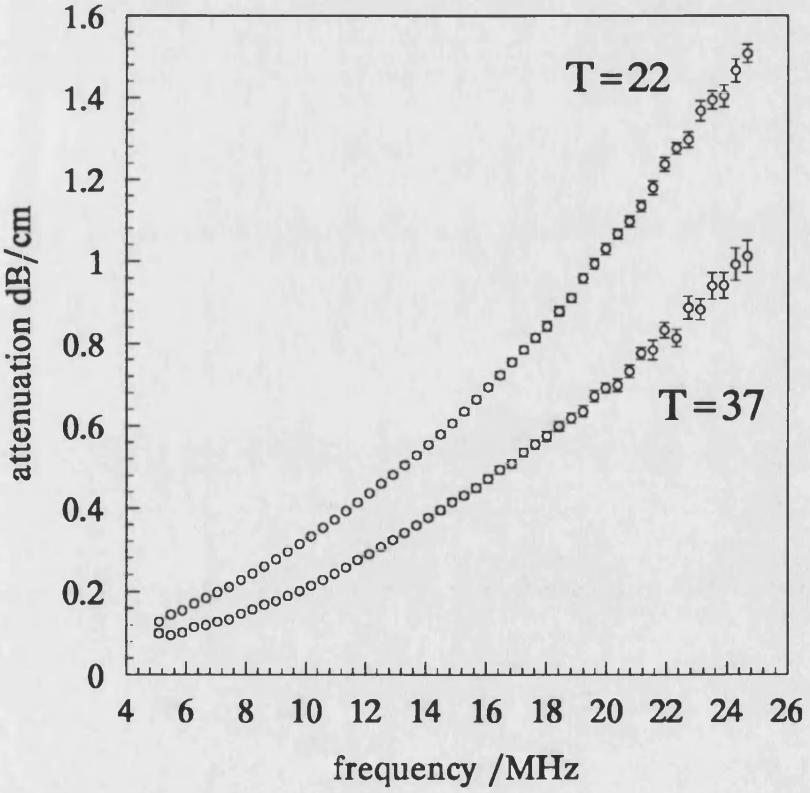

Figure 6.11. The frequency dependence of attenuation for urine.

(iii) 4.5 % Human albumin solution

Figure 6.12 illustrates the frequency dependence of attenuation at 25°C and 37°C for 4.5% Human Albumin solution. The results at 25 °C were obtained using a transducer driven at 10 MHz resulting in a smaller frequency bandwidth for those measurements. The results have had both a diffraction correction and water path corrections applied. In general the attenuation is larger than for both amniotic fluid and urine, for example at 5 MHz the attenuation is greater by a factor of five and at 15 MHz by a factor of three. The functional form of the frequency dependence of attenuation is tabulated in Figure 6.8. The influence of the type of curve fitting procedure employed to obtain the frequency fit is clearer to see with these results. Consider the results at room temperature. If the whole data set is taken (from 1.6 MHz to 15 MHz) then the results of the linear and nonlinear fits are as follows (expressed in dB cm^{-1}):

linear fit : $\alpha = 0.024f^{1.6}$
power law fit: $.\alpha = 0.034f^{1.44}$.

Taking a smaller, more accurate range of the data (2.4 MHz to 12 MHz) results in the following fits:

linear fit: $a = 0.036f^{1.42}$
power law fit: $\alpha = 0.035f^{1.43}$.

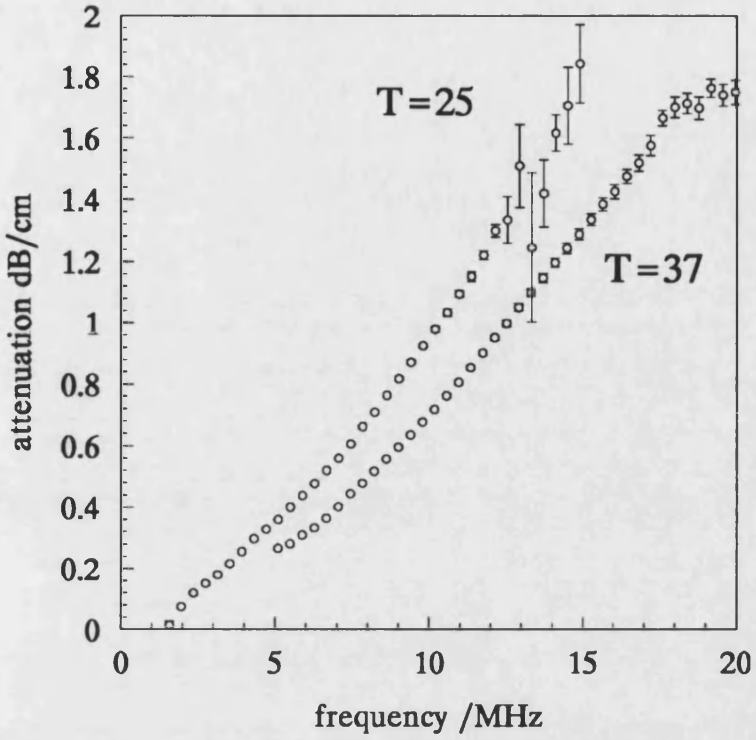

Figure 6.12. The frequency dependence of attenuation for 4.5% Human Albumin solution at room temperature and physiological temperature.

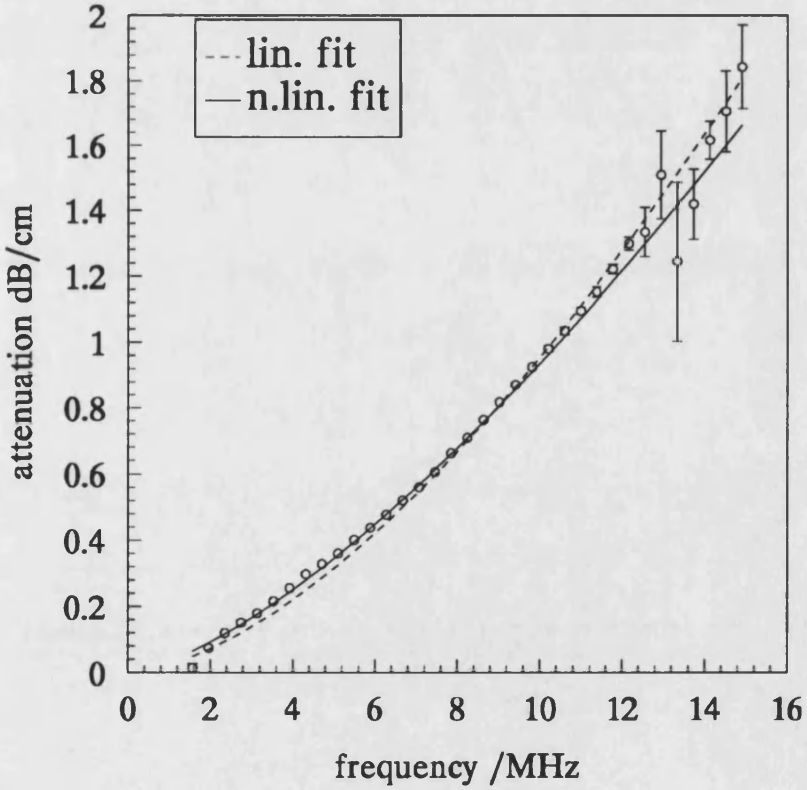

Figure 6.13. Illustration of the difference between linear and nonlinear curve fitting procedures employed in determining the form of the frequency dependence of attenuation.

As can be seen the power law fit is very much less susceptible to 'rogue points' in the data. Figure 6.13 illustrates the two curve fits (obtained from the whole data set), together with the original data. It is not immediately apparent that the power law fit represents the data better, however on close inspection one can see that at the low frequency end it is closer to the data points. At the high frequency end the linear fit does seem better but one has to remember the much larger errors associated with these data points. At physiological temperature, a similar behaviour to the two other body fluids is observed. The value of the attenuation coefficient decreases, as expected, but again the value of m increases.

The effect of attenuation due to the water path, replaced by the fluid path, is similar in form to that for the other two body fluids. The magnitude of the correction is however reduced. For example at 15 MHz the correction for 4.5% human albumin is approximately 20%, for amniotic fluid at the same frequency the correction was in the region of 80%.

(iv) 20 % Human Albumin solution

Figure 6.14 illustrates the frequency dependence of attenuation for 20 % human Albumin solution from 1 MHz to 14 MHz at physiological temperature. The data presented has been corrected for diffraction effects and attenuation due to the water path. In both cases the corrections are small; the diffraction correction is negligible and the water path correction increases the attenuation by a maximum of 6 % at 14 MHz. The results show that with this fluid the attenuation, at 5 MHz, is five times

that for 4.5 % human albumin and 20 times that for amniotic fluid. The functional form of the frequency dependence of attenuation is given in Figure 6.8. If the whole data set is taken then we obtain (expressed in dB cm^{-1}):

linear fit: $\alpha = 0.122f^{1.41}$
power law fit: $\alpha = 0.167f^{1.27}$.

Disregarding the first data point, the two processing methods give:

linear fit: $\alpha = 0.175f^{1.24}$
power law fit: $\alpha = 0.167f^{1.27}$.

As can be seen again the power law fit represents the data much better, without having selectively ignored outlying data points.

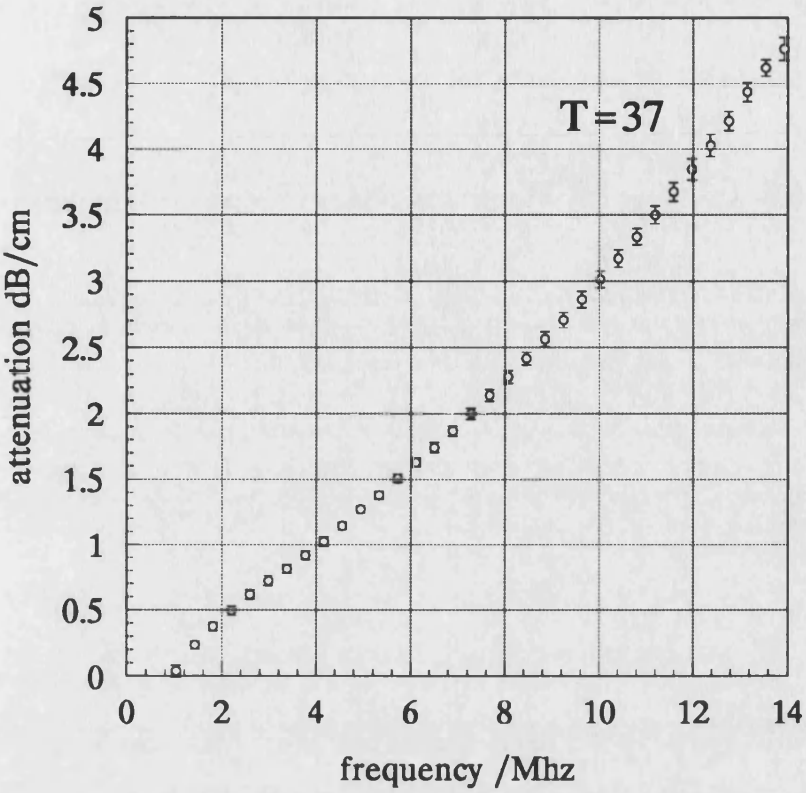

Figure 6.14. The frequency dependence of attenuation for 20% Human Albumin solution. The result is at physiological temperature.

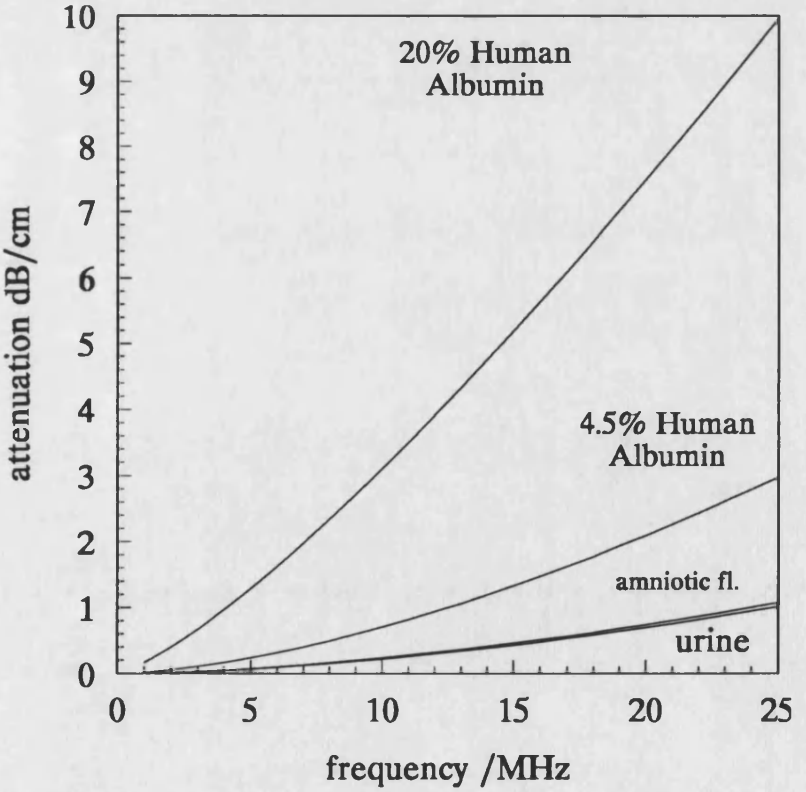

Figure 6.15. Functional form of the frequency dependence of attenuation, at physiological temperature, for all the four biological fluids.

6.3.4 General comments

(i) The results illustrate that there is a relationship between the attenuation and the protein concentration for the four biological fluids. Figure 6.15 illustrates the variation of attenuation with frequency for the four body fluids at physiological temperature. For amniotic fluid and urine, the measured attenuation is similar to that obtained in water. At 5 MHz the attenuation in both these fluids is about twice that in water (0.075 dB cm^{-1} compared to 0.035 dB cm^{-1}). For the 4.5 % human albumin solution the attenuation at 5 MHz is 0.25 dB cm^{-1} and for the 20 % human albumin solution it is 1.3 dB cm^{-1}. The result shows that as the protein concentration increases it begins to dominate the attenuating behaviour of the medium, due to the increase in the value of the attenuation coefficient.

(ii) Related to this is the observation that as the protein concentration increases the value of the frequency index *m* decreases. In amniotic fluid it has a value close to 1.7, whereas in the 20 % human Albumin solution it is closer to 1.3. The reason for this is again due to the water content in these solutions, and its contribution to the total attenuation in the fluid. For amniotic fluid and urine, water is the major component, the attenuation is dominated by it, and so the value of *m* is close to 2. As the protein concentration increases the contribution, to the attenuation, from water decreases and so the value of *m* departs from 2 and begins to approach 1.

An interesting consequence, for all fluids, is that as the frequency increases the attenuation due to water becomes more dominant due to its squared law dependence.

For example at 50 MHz the attenuation in water is 3.5 dB cm^{-1} , the attenuation in amniotic fluid (using extrapolation of the relationship given in Figure 6.8) would be 3.4 dB cm^{-1}. Presumably if measurements in amniotic fluid or urine were made at higher frequencies the value of *m* would approach 2. The situation, in principle, is the same for the 20 % human albumin solution, however one would have to consider frequencies of hundreds of megahertz before this happened.

This behaviour of the value of the attenuation coefficient and the frequency index, is reflected in the literature. Measurements on biological fluids (Zana & Lang 1974, Lang *et al* 1978) and macromolecule solutions (Kremkau & Carstensen 1971) indicate that the attenuation coefficient is low and that *m* is close to 2. At the other end of the spectrum, measurements on tissue generally report high values for the attenuation coefficient and a near linear frequency dependence.

(iii) The measurement procedure employed with these measurements involves propagation of the acoustic pulse through a relatively large fluid/water path length, up to 300 mm. Employing such a method allows a relatively large fluid path length to be used and also enables measurements to be made for a number of path lengths (typically fifteen measurements). This is advantageous because it reduces the random uncertainty in the measurements considerably, as is evident from all the results. For example if the random uncertainty of the measurements is taken as two standard errors then the percentage change in the estimated value of the attenuation would be of the order of 2 % to 3%.

Although this procedure reduces the random uncertainties, it can however be subject to a systematic error. If the propagation path of the pulse is large, there is a possibility that nonlinear distortion of the pulse can become significant. This can be either due to the low attenuation of the fluid and/or the propagation through the water path. An analysis of the nonlinear effects is not trivial as one has to consider the effects of nonlinear pulse propagation and also the frequency response of the receiving hydrophone. For example a percentage loss in signal amplitude at the fundamental frequency will not automatically appear as the same percentage increase in signal amplitude at the harmonic frequency.

The general effect, on the estimation of the attenuation, of such pulse distortion can however be deduced qualitatively. Consider the 5 MHz component of the pulse. As this becomes distorted, due to nonlinear propagation, two effects occur. Firstly, there will be a reduction in the magnitude of the 5 MHz component. This will result in an overestimate of attenuation at 5 MHz, as part of the reduction in signal level will be due to energy being lost to the harmonics and not due to attenuation.

Secondly, the distortion will introduce energy at the second harmonic level (at 10 MHz) which will in turn result in an underestimate of the attenuation at this frequency. Figure 6.16 illustrates the point, the results are for 4.5 % Human Albumin solution at physiological temperature. The two sets of data represent results obtained by using a small voltage, tens of volts, and a high voltage, of approximately one hundred volts, at the transducer face. As can be seen the attenuation at both the lower and intermediate frequencies are in error by about 30 %, the lower frequencies

being overestimated. The magnitude of the error introduced by using nonlinear pulses is to some extent governed by the attenuation of the fluid for this measurement system. For fluids such as urine, amniotic fluid and 20 % Human Albumin solution the error was found to be relatively small, less than 10%. For the low loss fluids (amniotic fluid and urine) the reason behind this is that the initial pulse (i.e. with the minimum fluid path length) is itself quite distorted and the extent of its distortion does not alter much over the change in fluid path length. This is because of the attenuation in water is of the same magnitude as that in the fluid. For 20% Human Albumin the situation is different. Here the large attenuation of the fluid does not permit high amplitude pulses to distort. Indeed after travelling through a minimum fluid path of 100 mm the 5 MHz component of a pulse, emanating from the transducer, is attenuated by approximately 14 dB before it enters the water path.

(iv) The results presented in this chapter illustrated the frequency dependence of attenuation of four biological fluids. In general these fluids can be thought of a macromolecule (mainly protein structures) in solution. The measured attenuation then becomes the sum of the attenuation due to the macromolecule and the attenuation due to the water content. One can determine the contribution to the frequency dependence of attenuation of the macromolecule by simply subtracting the attenuation due to water (this assumes that the attenuation due to water and macromolecule are additive and that there is no contribution due to mixing of the two). In addition if the attenuation is calculated per cycle it possible to see if any relaxation peaks in the frequency dependence of attenuation exist. Figure 6.17 illustrates results for amniotic fluid. As can be seen there does seem to be a roll-off

in the curve as one approaches the high frequency end of the curve. Unfortunately the experimental data reaches the noise floor after this, however it does seem that there may be broad resonance peak above 20 MHz. Similar results were obtained for the higher concentration Human Albumin solutions (by subtracting the appropriate percentage contribution from water). Unfortunately one requires much wider bandwidth results to encompass the whole resonance peak.

(v) A number of sets of measurements of the frequency dependence of attenuation were made for the two Human Albumin solutions. Although the results are not presented here, for brevity, they illustrated two points.

Firstly, different batches of fluid illustrated remarkably similar values for the measured attenuation. Secondly, the fluids were stable in terms of their acoustic properties (velocity and attenuation) for over twenty four hours. This together with the general availability of the fluid and the dependence of attenuation on protein content may make this fluid a useful tissue mimic. A wide range of tissue attenuation's, ranging from low loss fluids to soft tissue, could in principle be mimicked.

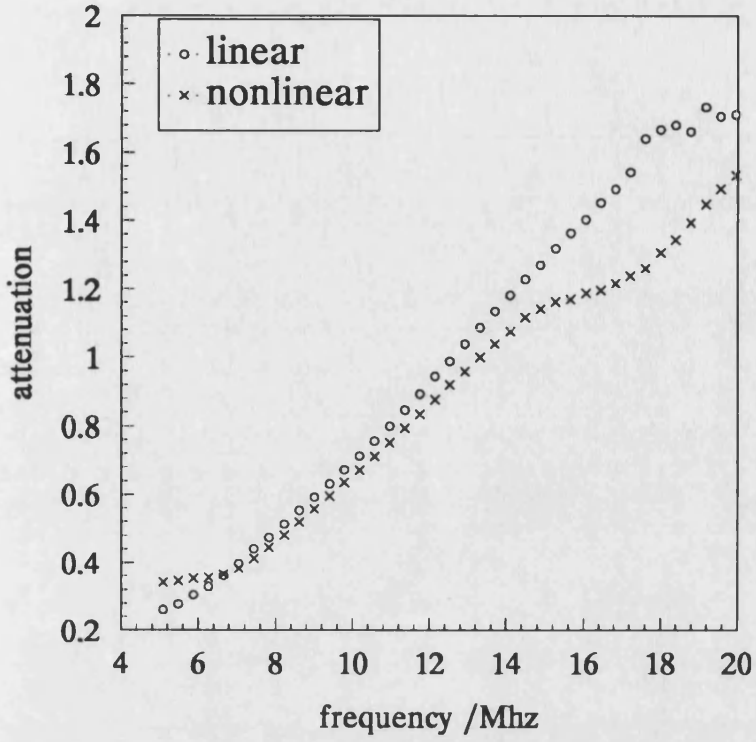

Figure 6.16 The effect of nonlinear propagation of the measurement of the frequency dependence of attenuation in 4.5% Human Albumin solution.

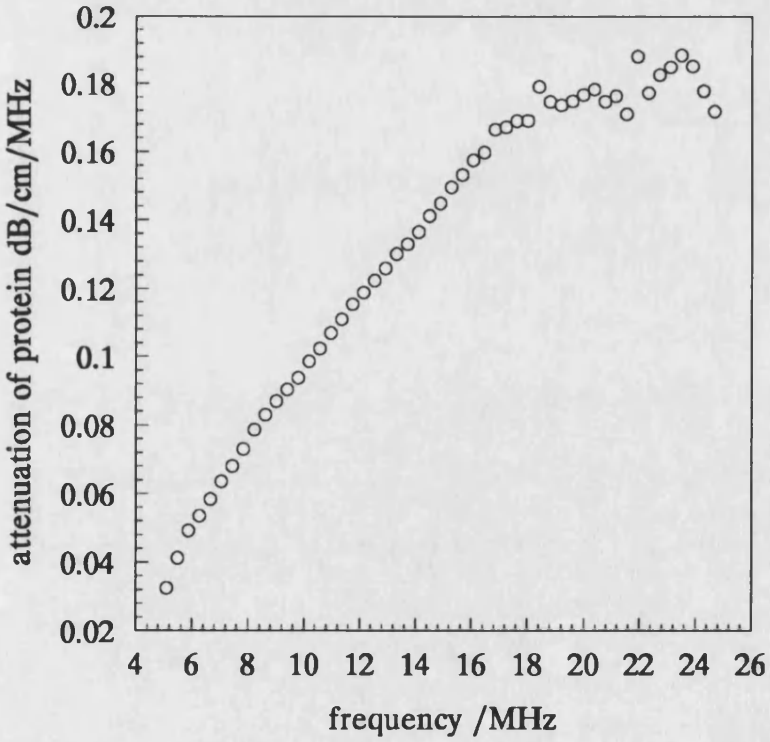

Figure 6.17 Illustration of the attenuation per cycle versus frequency from the macromolecular constituent in amniotic fluid.

7.0 RESULTS (II)-NONLINEAR PROPAGATION

7.1 Outline

In Chapter 3 it was stated that the main aim of this research project was to compare experimentally determined nonlinear pressure distributions in biological fluids with those predicted theoretically. We also saw that in order to predict these pressure distributions certain input parameters were required for the theoretical model. These parameters can, in general, be divided into two categories, those relating to the source of sound generation and those relating to the medium of sound propagation.

In the last chapter results were presented for the sound velocity and frequency dependence of attenuation in four biological fluids. These formed two of the medium input parameters required by the model for predictions (some results for the medium nonlinearity parameter (B/A are presented in Appendix A). In this chapter we will present experimental results of the axial nonlinear pressure distributions in the biological fluids considered and then compare them with predictions made with the model, using the input parameters determined in the previous chapter. Also presented in the chapter are details of the various source parameters that were required for the modelling. The chapter firstly describes the experimental nonlinear pressure distributions observed and then goes on to give a comparison between the experimental and theoretical simulations.

7.2 Experimental results

This section presents results of the measured axial nonlinear pressure distribution for three biological fluids, amniotic fluid, urine and 4.5 % Human Albumin solution. Unfortunately due to lack of resources further measurements on the 20% Human Albumin solution could not be made. Measurements were made at both room temperature and physiological temperature (37° C) using a 38 mm diameter single element transducer operating at a frequency of 2.25 MHz. Focusing was achieved via a plano-concave perspex lens with a radius of curvature of 63.95 mm, giving a focal gain of approximately 12 in water at room temperature. The transducer was operated with short tonebursts of approximately eight cycles, the pulse repetition rate being 1 kHz. In general the transducer was driven under various drive conditions ranging from 0.007 MPa to 0.224 MPa at the transducer face in order to allow both linear and nonlinear measurements to be made. Experimental results are presented from the penultimate axial maximum to well past the focal plane. A 0.5 mm bilaminar Pvdf membrane hydrophone with a buffer amplifier was used for detection of the signal, which was subsequently captured with a Lecroy 9310 digital oscilloscope for processing. Harmonic amplitudes were determined by isolating a single cycle from the pulse and then applying fast fourier transform techniques to the desired cycle.

Because of the large volume of data not all the results will be presented in graphical form. In general the salient points from each of the presented graphs will be mentioned and discussed.

7.2.1 Linear measurements

Figure 7.1 and figure 7.2 illustrate the axial variation of the fundamental for amniotic fluid and urine at room temperature and physiological temperature. The source pressure for the amniotic fluid and urine measurements was 0.0077 MPa and 0.007 MPa respectively. In both cases the value of the second harmonic was more than 30 dB below the fundamental (in the region of the focus) implying that for these measurements nonlinear propagation was not significant. The following general points can be made:

(i) At both temperatures the variation of the axial field is in accordance with that expected from a single element circular transducer. Relatively rapid variations in the pressure occur from the penultimate maximum through to the final maximum. Beyond the last maximum the pressure drops off more slowly as the phase changes in the fundamental are not so rapid.

(ii) The axial position of the last minimum has increased a small amount (approximately 5 mm) from about 95 mm for the room temperature results to 100 mm for the physiological temperature results. The situation for the last axial maximum is even more noticeable. At room temperature it is at about 14 cm whereas at 37°C it is closer to 15 cm from the source for all three fluids. In addition to this the pressure at the last axial maximum has reduced by approximately 15 % as the temperature is increased from room temperature to 37°C. The result is at first sight a little surprising as the increase in temperature results in an increase in sound

velocity (for example see Figure 6.2) which would tend to bring the diffractive field closer to the source by reducing the Rayleigh distance.

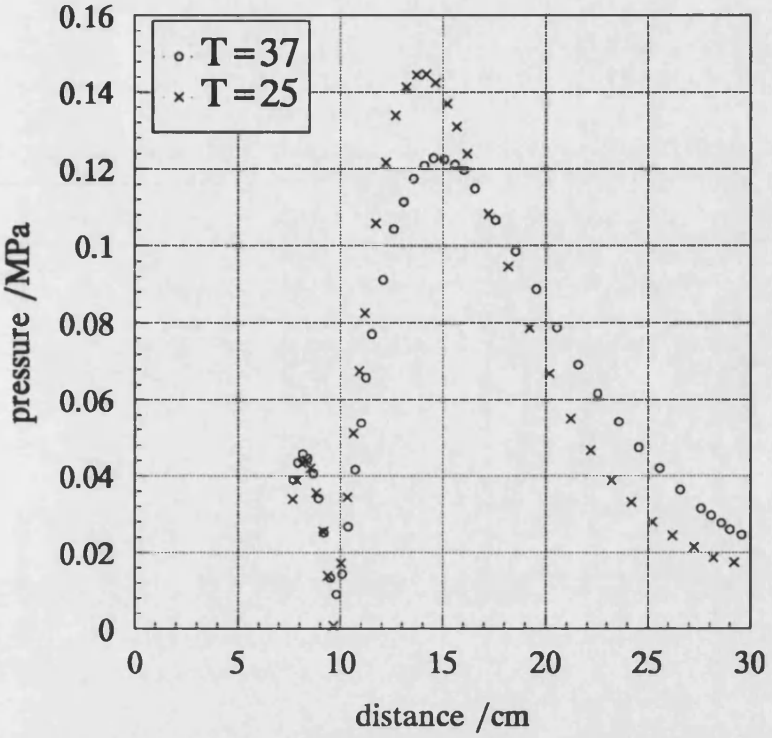

Figure 7.1. Experimental determination of the axial variation of the fundamental in amniotic fluid under low drive conditions.

However the increase in temperature also modifies the gain of the transducer. Equation 3.2 expresses the gain in terms of the Rayleigh distance and the focal length. As stated the Rayleigh distance decreases, however the focal length also changes due to the change in sound velocity in the perspex lens and the fluid under investigation. The effect of these changes is to reduce the overall gain of the lens system with an increase in temperature. The observed change in the axial pressure distribution with temperature can in part explain the reduction in gain. The change in the value of the pressure at the last axial maximum is also likely to be influenced by the change in sensitivity of the hydrophone with temperature, which can only be inferred from NPL data.

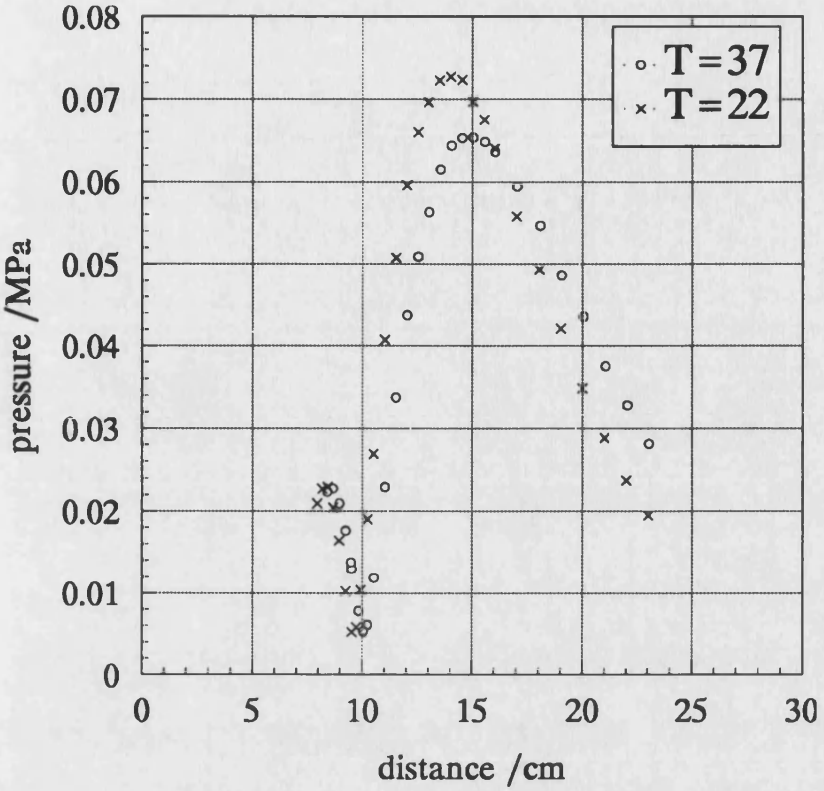

Figure 7.2. Experimental determination of the axial variation of the fundamental in urine under low drive conditions.

(iii) In general the behaviour of the axial variation in pressure seems to indicate a change in the diffractive field with a change in temperature. This change with temperature cannot easily be attributed to the fluid as it occurs for all three fluids.

Also supporting this is the observation that similar behaviour can be found in the variation of the second harmonic. Figure 7.3 illustrates the point. It shows the second harmonic amplitude in amniotic fluid, at both temperatures, for measurements made with a source pressure of 0.137 MPa. As can be seen, an increase in temperature has more marked effects here, the reduction in the maximum pressure is now of the order of 20% and the shift in the position of this pressure peak is from 14

cm to 16 cm. An explanation for the observed behaviour will be given later in section 7.3.2.

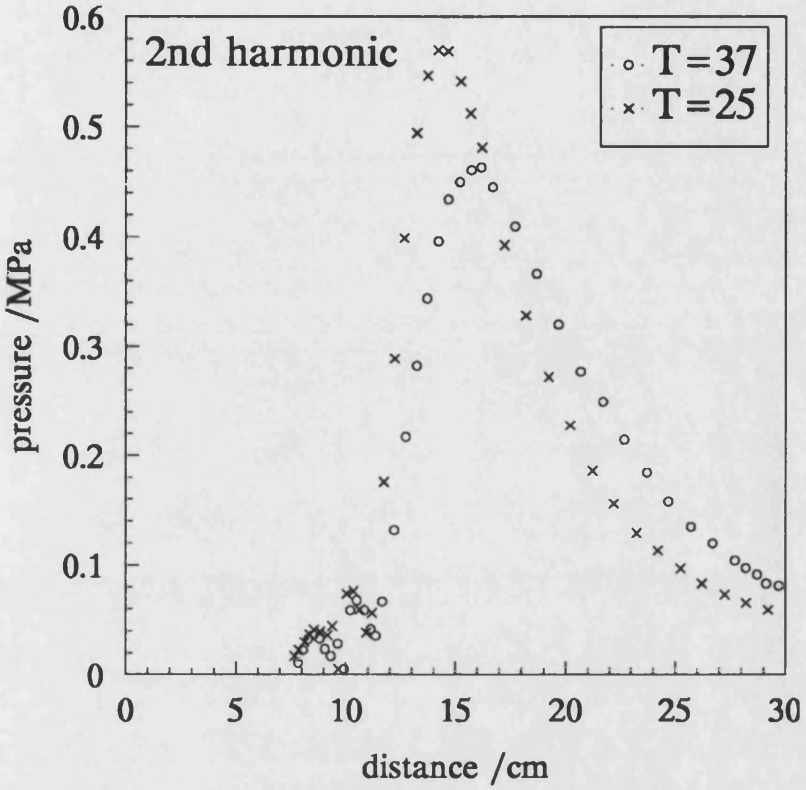

Figure 7.3. Experimental plot of the axial variation of the second harmonic in amniotic fluid at room temperature and physiological temperature, source pressure is 0.137 MPa.

7.2.2 Nonlinear measurements

Figures 7.4, 7.5 and 7.6 illustrate results of the axial variation of the fundamental and first four harmonics in amniotic fluid, at physiological temperature. The y-axis plots the measured pressure and the x-axis is the axial distance from the transducer. The three graphs represent different degrees of nonlinear propagation, as determined by the source pressure. The source pressure for the three graphs were 0.077 MPa, 0.137 MPa and 0.244 MPa respectively.

Each increase in source pressure corresponds to an increase in drive level of 5 dB. The increase in the maximum pressure of the fundamental does not, however, correspond to this. The first measured increase is approximately 4.3 dB and the second increase is 3.7 dB. This removal of energy from the fundamental, due to nonlinear propagation, to the harmonics is evident from the graphs. As can be seen there is a progressive increase (approximately 6 dB on each occasion) in the value of the second harmonic as the drive pressure increases. This process is also observed for the other three harmonics. For example the fifth harmonic level, for a source pressure of 0.077 MPa, is only about 0.02 MPa (in the region of the focus) whereas with a source pressure of 0.244 MPa the fifth harmonic reaches pressures of about 0.3 MPa in the same axial region. This increase in the importance of nonlinear processes is illustrated in figure 7.7 which shows the ratio of second harmonic to fundamental in the region of the focus as a function of source pressure. Although only four points are plotted the general effect can be inferred. At low drive levels the increase in the second harmonic is fairly rapid; however as the source pressure increases further (at still relatively small levels compared to the output of many diagnostic transducers) the rate of increase in second harmonic level reduces and seems to reach a plateau. The value of the second harmonic, is approximately 5 dB down relative to the fundamental, at a source pressure of 0.244 MPa. The result indicates very clearly that nonlinear distortion is easily achieved in amniotic fluid. This value, of 5 dB, exceeds that expected from a plane wave that has undergone full distortion and reached a mature shock. The higher than expected value is due to the high degree of focusing and the difference in the diffraction effects for the fundamental and second harmonic.

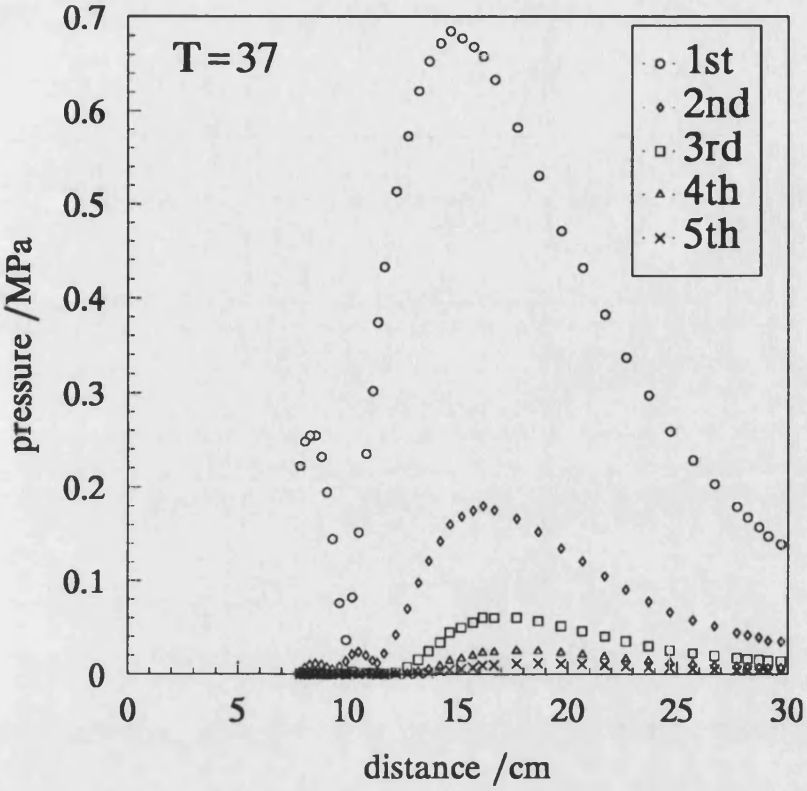

Figure 7.4. Experimental plot of the axial variation of the fundamental and first four harmonics in amniotic fluid, source pressure is 0.077 MPa.

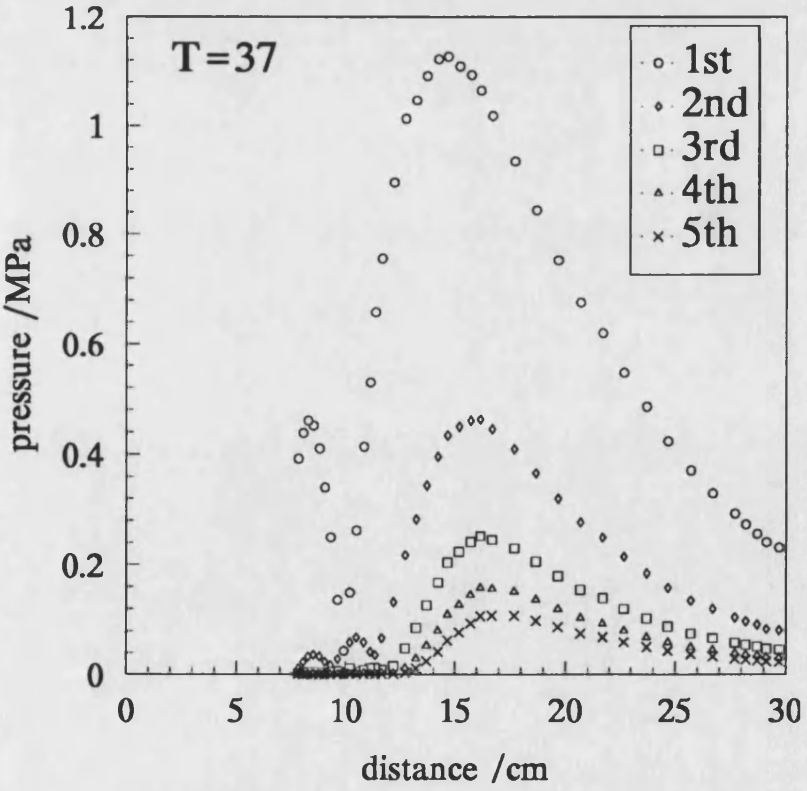

Figure 7.5. Experimental plot of the axial variation of the fundamental and first four harmonics in amniotic fluid, source pressure is 0.137 MPa.

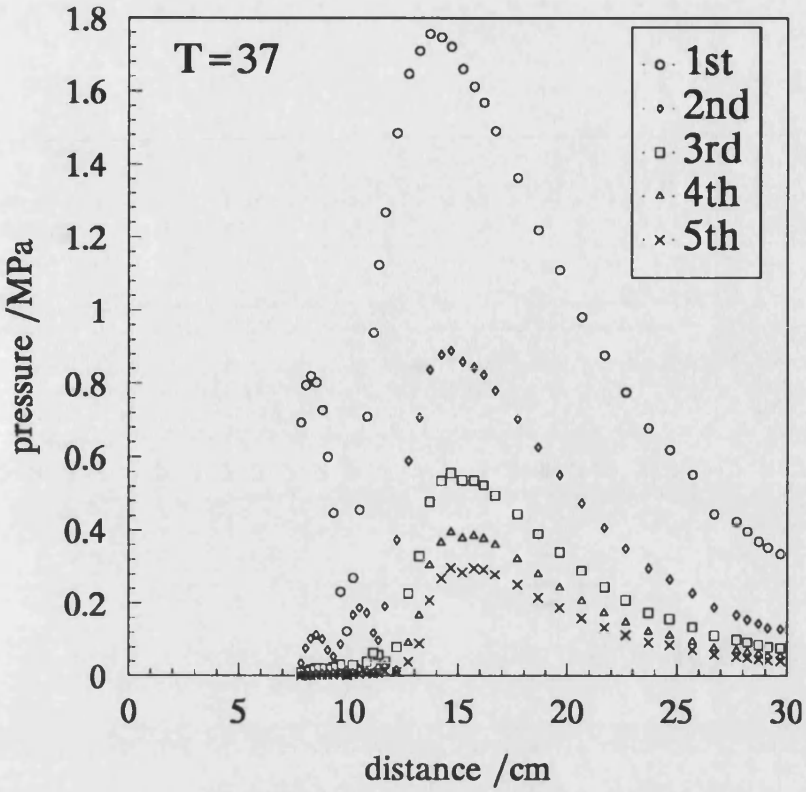

Figure 7.6. Experimental plot of the axial variation of the fundamental and first four harmonics in amniotic fluid, source pressure is 0.244 MPa.

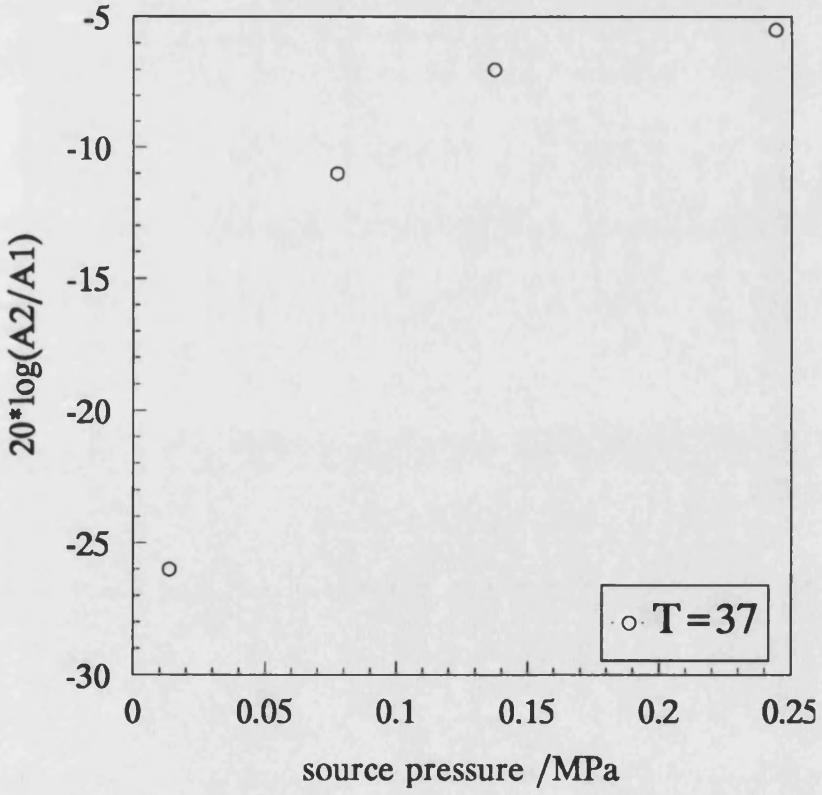

Figure 7.7. Experimental plot of the ratio of the second harmonic amplitude to fundamental amplitude as a function of source pressure for amniotic fluid.

The large extent of harmonic generation and propagation is presumably due to the low attenuation in amniotic fluid, as once the harmonics are generated they are not attenuated significantly but are allowed to propagate.

Figures 7.4, 7.5 and 7.6 also illustrate the change in the nature of the ultrasonic field as the drive pressure is increased. In particular the position at which the harmonics peak is altered. The situation is clearest with the fifth harmonic, at a source pressure of 0.077 MPa the fifth harmonic reaches a maximum value at approximately 16.5 cm, whereas at a source pressure of 0.244 MPa the maximum is reached at a position of about 15 cm from the source. This tightening of the axial beam profile, for all the harmonics, is expected and follows that determined by other workers (Baker *et al* 1988) for measurements made in water. It should be pointed out that similar results were obtained in urine, the attenuation and sound velocity being similar.

The effect of attenuation on the production and propagation of distorted waves is however not so easy to see from these set of measurements. The reason for this is two fold:

(i) Although measurements were made in amniotic fluid and 4.5% Human Albumin solution, where the attenuations differ by a factor of four at the fundamental frequency, the values of attenuation are so low (0.017 dB cm^{-1} and 0.1 dB cm^{-1} respectively) that changes in the ultrasonic field over distances of 15 cm produce little change to the signal level.

(ii) One can consider a higher harmonic, for example the fifth harmonic in amniotic fluid has an attenuation of 0.3 dB cm^{-1} whereas for 4.5% Human Albumin the attenuation is 1.1 dB cm^{-1}. The propagation and attenuation of this harmonic should allow for a comparison of the two fluids, under the same initial conditions of propagation. Figure 7.8 illustrates the variation of the fifth harmonic for both fluids, with a source pressure of 0.137 MPa at the source. As can be seen the value of the fifth harmonic, for 4.5% Human Albumin solution, at 25 cm from the source is reduced by approximately 3 dB from that measured in amniotic fluid. Athough it might appear that this is due to the larger, and measurable, attenuation in 4.5% Human Albumin, one has to be careful. Although the transducer and lens for the two measurements were identical, the difference in sound velocity between the two fluids results in a different gain for the lens system, so it not necessarily correct to compare the results. Further to this, the measurements presented here are with a highly focusing beam (this was desirable so as to make measurements into the far field and to avoid reflections from the sides of the bellows) where the changes in the harmonic magnitudes with axial distance are influenced by diffraction effects. In addition to this the curves in Figure 7.8 assume that both measurements were made on the acoustic axis, for example the difference between the values of the fifth harmonic, in the far field, may have been due to a misalignment problem with one of the measurements. Overall Figure 7.8 illustrates that if the source pressure level is high enough then nonlinear effects dominate over attenuation.

In general the results show that the measurements have a dynamic range of about 80 dB, for example pressure levels of the order of 0.1 KPa can be detected for the fifth

harmonic. The maximum pressures measured for the fundamental, in the region of the focus, approach 2 MPa for very high drive results (not illustrated for brevity).

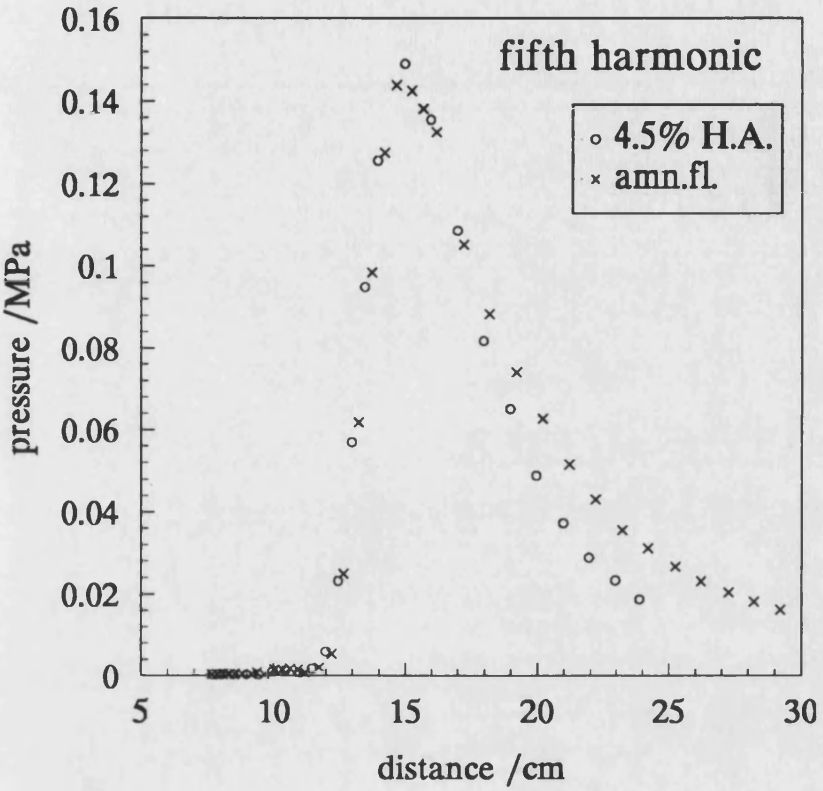

Figure 7.8. Experimental plot of the axial variation of the fifth harmonic in amniotic fluid and 4.5% Human Albumin.

Fluid	Measured source pressure at T=25^{0}C with 0.5 mm bilaminar hydrophone (MPa)				
Amniotic fluid	0.0077	_	0.077	0.137	0.244
Urine	0.0069	_	0.069	0.122	0.217
4.5% Human Albumin soln	0.0077	_	_	0.137	0.244

Figure 7.9 Tabulated values for the various source pressures used in the three biological solutions at room temperature.

7.3 Comparison between experiment and theory

In the previous section experimental results of the axial pressure distribution for the biological fluids were presented for various degrees of nonlinear propagation. In this section a comparison between experimental and theoretical distributions will be made. The results presented in this section were selected to illustrate as many useful features as possible and also include results not illustrated previously. Although the parameters required in the model have been discussed previously, it was thought that it would be useful to reiterate them here.

7.3.1 Model input parameters

The input parameters for the model fall into two categories, those relating to the medium of propagation and those relating to the source conditions.

(i) Medium parameters

The medium parameters that the model requires are:

(i) The sound velocity;

(ii) The frequency dependence of attenuation;

(iii) The medium density;

(iv) The nonlinearity parameter.

The first two of these were measured accurately and the results presented in chapter 6; refer to the tabulated results in Figures 6.2 and 6.8. These values will be used in all of the modelling work.

For amniotic fluid and urine the density was taken to be the same as that of water, 1000 kg m^{-3} . This was thought to be reasonable based on their large water content. The densities of the 4.5% Human Albumin solution was obtained from BPL, the suppliers of the solutions. For the 4.5% solution the density was 1019 kg m^{-3}.

The nonlinearity parameter, B/A, for the fluids was also chosen to have the same value as water (5.5 at room temperature and 5.66 at physiological temperature). It was originally intended to measure *B/A* as well using the experimental facility. Appendix A describes how the parameter could be measured for the fluids considered in this study; however, as explained there, the measurements highlighted some problems with the measurement procedure. These will not be discussed here, but the reader is referred to the appendix. For this reason it was necessary to use existing values for the nonlinearity parameter for water. There is some justification in using the value for water. Since the nonlinearity parameter for a medium depends on the bulk properties of the medium. It would be reasonable to assume that the nonlinearity parameter in these fluids is not more than 10% to 15% different from that of water. The literature also supports this, measurements made by Sun Yongchen (1985, 1986) and Everbach (1989) report that (*B/A*) for urine is 6.14, for bile (pig) is 6.0 and for blood plasma (cow) is 5.74.

The effect of changes of the order of 10% in *B/A* on the simulated axial pressure distribution will be illustrated to show the influence of this parameter on the results.

(ii) Transducer parameters

The transducer parameters required are:

(i) Source pressure;

(ii) Transducer radius;

(iii) Focusing gain.

(i) The source pressures used for the measurements described in this chapter are tabulated in figure 7.9. The measurement of source pressure was determined by two techniques, direct measurement near the transducer face using a bilaminar PVdF hydrophone and measurement with a power balance.

The hydrophone measurement was performed with the 0.5 mm bilaminar hydrophone, calibrated at the NPL. In general the hydrophone was placed approximately 5 mm from the transducer and centred on the transducer with the measurements being made in water. Measurements closer to the transducer resulted in problems due to interference of the direct signal with those reflected between the transducer and the hydrophone.

The measurements with the power balance (Perkins 1989) were performed by aligning the transducer with the central axis of the power balance. In general for the

high source pressure measurements the transducer was driven in pulsed mode (so as to avoid overheating of the amplifier), whereas for the low source pressure measurements the transducer was driven continuously. In both cases the source pressure was determined from the measurement of the output power and timing measurements of the pulsing regime.

For continuous wave excitation, the source pressure P_o is related to the measured power by:

$$P_o = \left(\frac{2P' \rho_o c_o}{\pi a^2} \right)^{1/2}, \qquad 7.1$$

where P' is the measured power, ρ_o is the density of water, c_o is the velocity of sound in water and a is the transducer radius.

In general the agreement between the two sets of measurements was within 10%. For example with the same source condition settings the hydrophone measurement gave a source pressure of 0.28 MPa while the power balance gave a measurement of 0.26 MPa. The hydrophone measurements were used in the modelling work.

Measurements of the source pressure, by the hydrophone technique, were also made with the addition of a perspex lens in front of the transducer. These results showed that the measured source pressure was significantly reduced; for example under the same condition the source pressure was reduced from 0.28 MPa to 0.224 MPa. This was thought to be due to the relatively high attenuation coefficient of perspex (often

quoted as 1 dB cm^{-1}). In addition there is also an impedance mismatch at the transducer/lens interface and the lens/water interface, which results in reduced transmission of power through the lens into the water.

In order to check the attenuation of the perspex, measurements were made by the comparison method. Using this method the attenuation, as opposed to the insertion loss (which includes loss of signal due to reflections at the interface) was measured at a frequency of 2.25 MHz The results of the attenuation per mm as a function of temperature are presented in figure 7.10. As can be seen the attenuation does not vary greatly from physiological temperature to room temperature, but is on average 0.36 dB mm^{-1} . For the lens used in the measurements presented in the previous section, the thickness at its centre was 4.4 mm. This gives a total attenuation of approximately 1.6 dB. The consequent reduction in signal level that would be expected due to the addition of a lens is in agreement with that observed for the source pressure measurements.

(ii) The nominal value of the transducer radius, quoted by the manufacturers (Panametrics) was 19 mm. In order to check the actual transducer radius, the 0.5 mm bilaminar hydrophone was used to scan across the transducer. The hydrophone

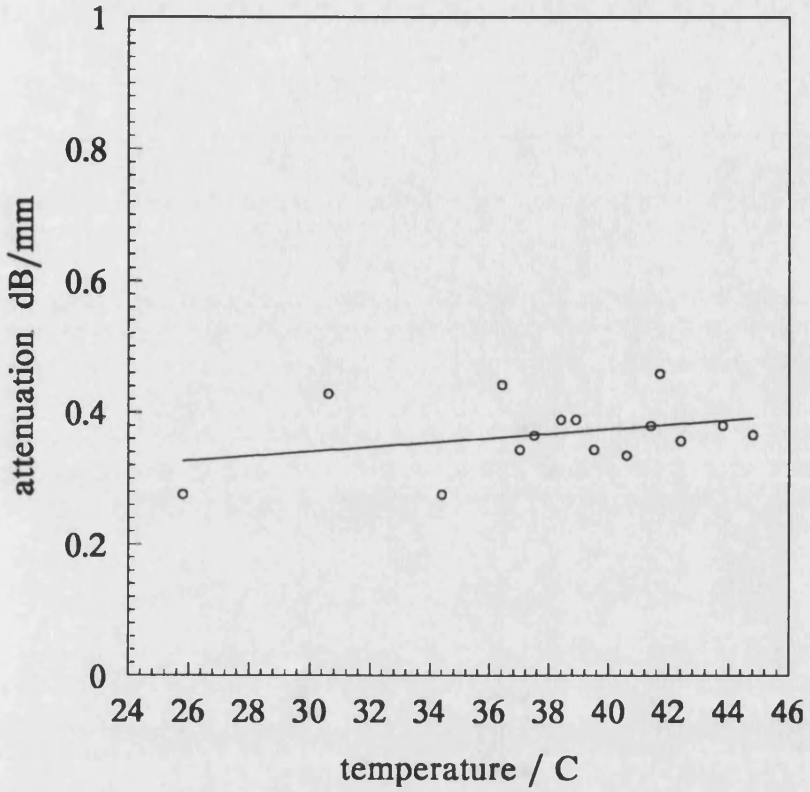

Figure 7.10. Experiemntal plot of the measured attenuation in perspex as a function of temperature.

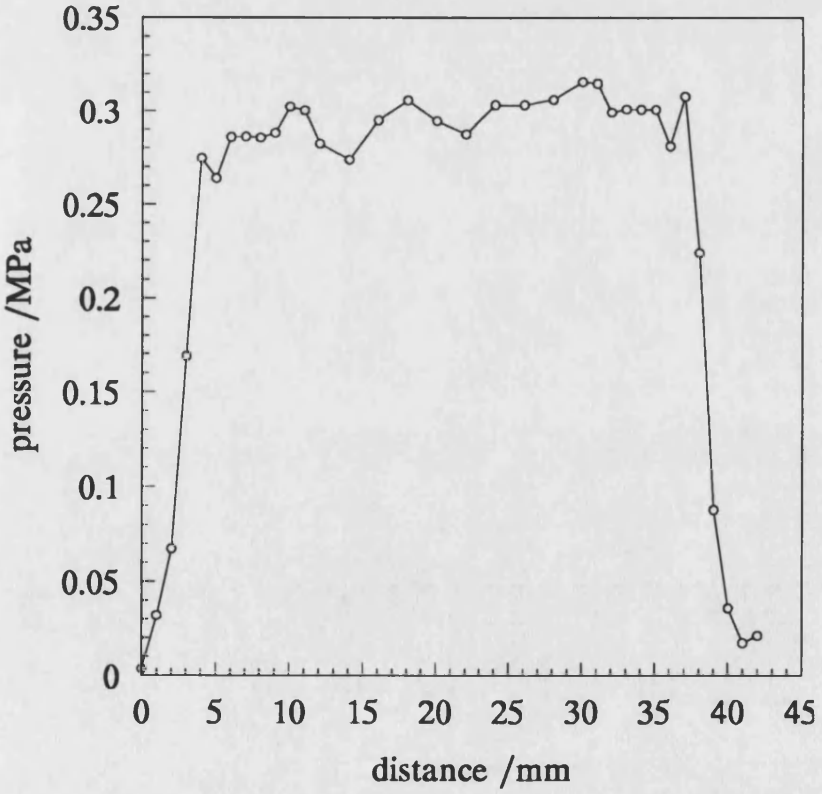

Figure 7.11. Experimental plot of the measured pressure across the transducer face, at an axial distance of 5 mm from the transducer.

was again placed at an axial distance of 5 mm from the transducer and the resulting pressure field is illustrated in figure 7.11. The graph illustrates two points.

Firstly, using a 6 dB drop in pressure as the basis for determining the transducer radius, it can be seen that the effective radius is 18.5 mm. This corresponds to a 3% reduction on the expected value. The normal value of 19 mm was initially used for the simulations presented later, however the influence of the transducer radius on the pressure distribution due to changes in the transducer radius will also be considered.

Secondly, figure 7.11 also illustrates that the pressure across the transducer face is not constant. There is a 6% variation around the mean value. This deviation can become more significant if one considers that as one approaches the edge of the transducer, the fraction of the total power, from the transducer, increases as the elemental area increases. Again the effect of changes in the source pressure on the simulation results will be discussed later.

(iii) As described in chapter 5, equation 5.2, the focusing gain of the system can be determined by knowledge of the radius of curvature of the perspex lens and the velocity of velocity in perspex and the fluid. The velocity of sound in perspex was measured at room temperature and physiological temperature for this purpose. The speeds were 2727 ms^{-1} and 2687 ms^{-1} respectively, with a standard error of $\pm$ 10 m s^{-1}. The results for the focusing gain are tabulated in figure 7.12.

Medium	room temperature	physiological temperature
Amniotic fluid	11.6	10.5
Urine	11.6	10.8
4.5% Human Albumin	11.8	11.2

Figure 7.12. Tabulated values of the focusing gain in the three biological fluids.

7.3.2 Linear field comparison

Having described the various input parameters initially chosen for the modelling, we shall now consider the comparison between experimental and theoretical results. Firstly a comparison for linear measurements (where the source pressure is low enough to minimise any nonlinear effects) will be presented and then, on the basis of the agreement obtained nonlinear pressure distributions will be compared. In all the graphs presented the experimental results are illustrated as points and the theory as solid lines.

Figures 7.13 and 7.14 illustrate the axial variation of the fundamental in amniotic fluid at room temperature and physiological temperature. Figures 7.15 and 7.16 are the corresponding results in 4.5% Human Albumin solution. In both cases the agreement between experiment and theory is reasonable. For example the positioning of features such as the penultimate maximum, last axial minimum and the last axial maximum are good. It is however noticeable that in both cases the discrepancy in the position of these features increases as the temperature is increased. For example the last axial maximum is found to be about 1 cm further away, from the source, in the experimental measurements at physiological temperature. The other

disagreement between experiment and theory lies in the values of the measured and predicted pressures at the penultimate and last axial maxima.

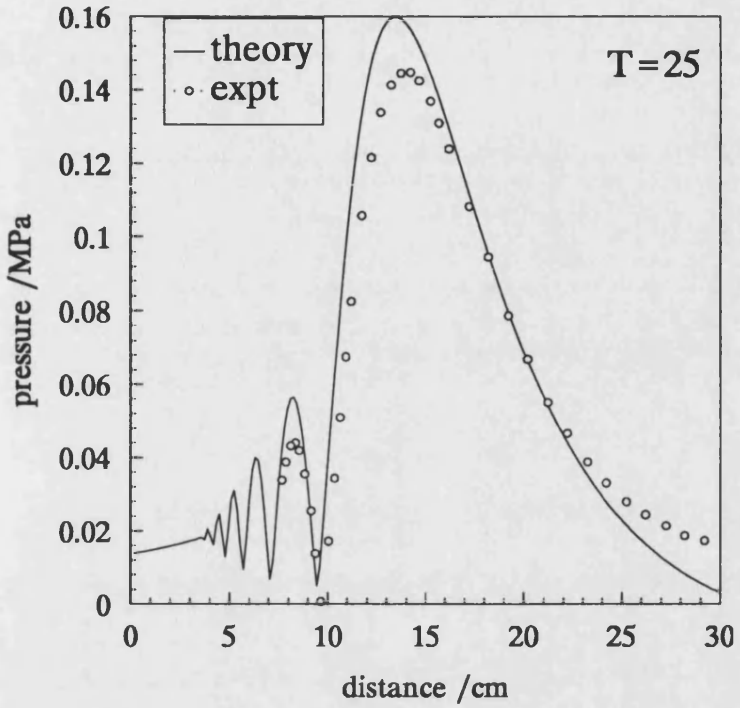

Figure 7.13. Comparison between experiment and theory for the axial variation of the fundamental in amniotic fluid, at T=25°C, source pressure is 0.0137 MPa.

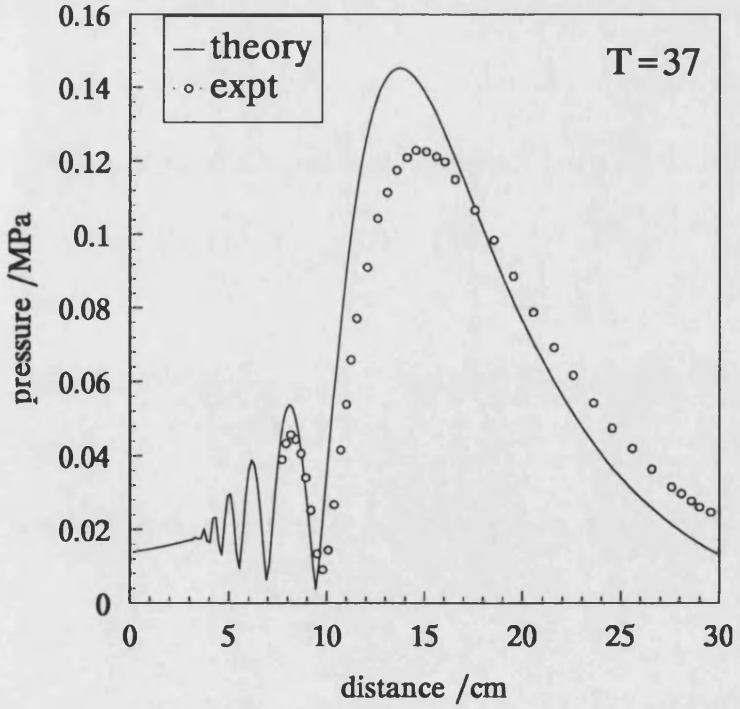

Figure 7.14. Comparison between experiment and theory for the axial variation of the fundamental in amniotic fluid, at T=37°C, source pressure is 0.0137 MPa.

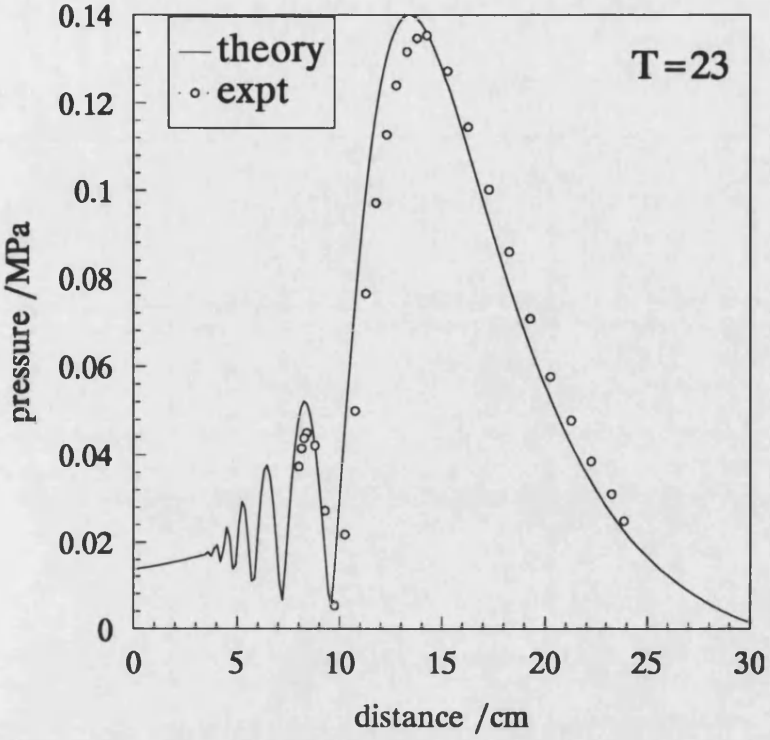

Figure 7.15. Comparison between experiment and theory for the axial variation of the fundamental in 4.5% Human Albumin, at T=25°C, source pressure is 0.0137 MPa.

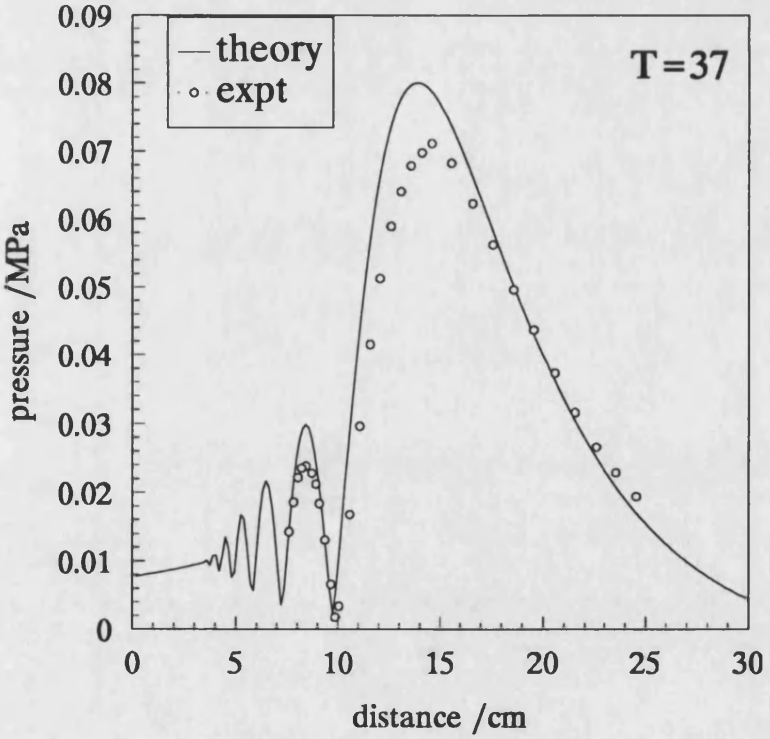

Figure 7.16. Comparison between experiment and theory for the axial variation of the fundamental in 4.5% Human Albumin, at T=37°C, source pressure is 0.0077 MPa.

Here again the discrepancy increases with temperature, with the predicted pressures being consistently higher. In amniotic fluid the difference rises from 10% at room temperature to 16% at physiological temperature. The situation in 4.5% Human Albumin is not so bad. The room temperature results, at the last maximum, are similar but at physiological temperature the difference is about 10%. The predicted pressure at the penultimate maximum in all four results is greater by approximately 15%.

It may appear at first sight that the discrepancy between experiment and theory is due to the value of source pressure used in the predictions. The possible error in this parameter is 10%, as discussed in the previous section. However the difference between experiment and theory cannot immediately be explained by such an argument, for three reasons.

Firstly, a reduction in the source pressure by say 10% would bring the pressure amplitudes into line at the penultimate and final maxima but it would also have the effect of reducing the predicted pressures everywhere else in the field. This would manifest itself very clearly in the post focal region. With the present results the theoretical predictions are either similar to or less than the experimental values in this region. A reduction in source pressure (for these linear propagation results) would make the comparison between experiment and theory much worse in the far field. In particular it is harder to imagine a situation where one can measure a higher pressure than that predicted, on-axis, without there being a significant inaccuracy in one of the input parameters. The converse of this is more likely, misalignment of the transducer

and hydrophone can result in the off-axis pressure being measured which will in general be less than that on-axis.

Secondly, reducing the source pressure will not alter the shape of the axial distribution. We saw in the previous section (Figures 7.1 and 7.2) that an increase in temperature seems to produce a broadening of the axial pressure distribution. In the simulations presented here (figures 7.13, 7.14, 7.15, 7.16) the pressure distributions are similar at both temperatures.

In addition to this there is also the possibility that the transducer and hydrophone were misaligned. Misalignment however would tend to cause the axial harmonic variation in the experimental results to peak earlier rather than later as is seen in the above figures.

The difference between experiment and theory at both temperatures seems to imply a cause that is related to the diffractive field of the transducer. Ward *et al* (1995) has demonstrated that phase variations across the face of transducers such as these can cause significant departures to the expected axial pressure distribution from perfect piston behaviour.

As a result of these observations the phase across the 2.25 MHz diagnostic sonar transducer was measured. The measurement was performed by scanning the 0.5 mm bilaminar PVdF membrane hydrophone across the transducer at an axial distance of 5 mm. Figures 7.17 and 7.18 illustrate the phase variation across the transducer at

both temperatures of interest. The x-axis represents the radial distance across the transducer, the 20 mm point being close to the centre of the transducer. The y-axis is the absolute phase of a chosen cycle from a toneburst of eight cycles. The absolute phase was determined by measuring the time of arrival at the hydrophone. As can be seen the phase across the transducer is not constant, and shows a marked deviation from plane piston behaviour.

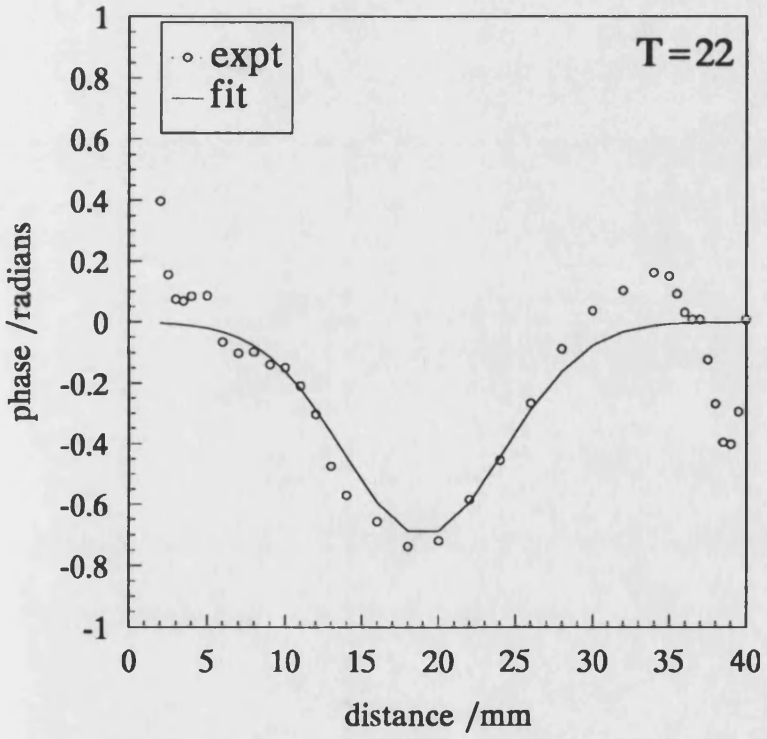

Figure 7.17. Phase distribution across the face of the 38 mm transducer at room temperature T=25°C. Experimental data and gaussian fit.

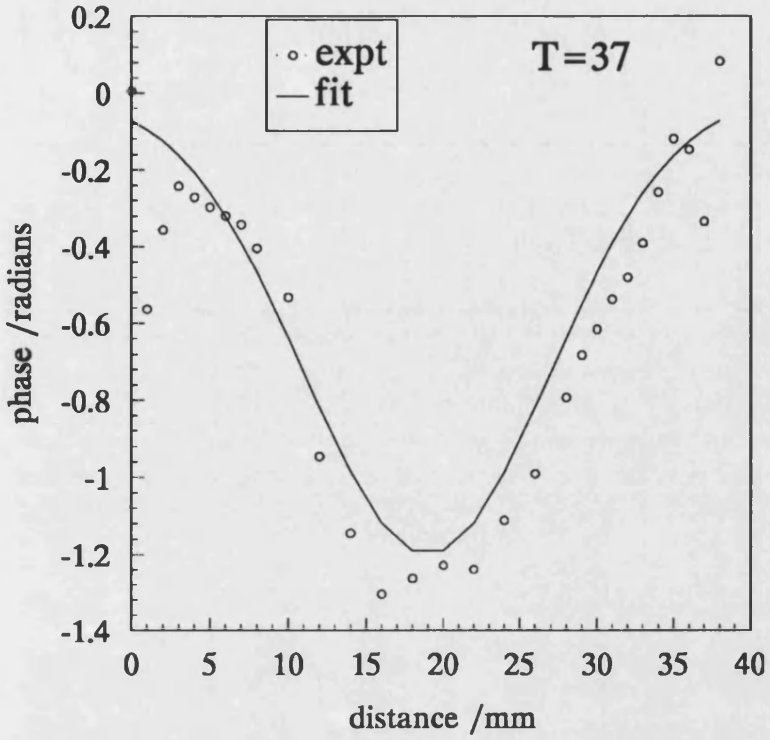

Figure 7.18. Phase distribution across the face of the 38 mm transducer at physiological temperature T=37°C. Experimental data and gaussian fit.

At room temperature the centre of the transducer is roughly 0.7 radians ahead of the edge. This phase advance increases to 1.2 radians at physiological temperature. As can be seen the phase distribution across the transducer is fairly symmetric. This is fortuitous for two reasons.

Firstly it allows the variation to be fitted by a relatively simple function. The figures both show a gaussian fit to the experimental data. As can be seen the fitted representation of the phase variation in is reasonable in both cases.

Secondly it allows such a phase variation to be applied, in the model, at the transducer. If the phase behaviour had been unsymmetric then its implementation

would have caused problems as the governing equations of the model rely on circular symmetry.

The gaussian phase distribution was implemented into the model with the other input parameters unaltered. The corresponding results for linear propagation are presented in figures 7.19, 7.20, 7.21 and 7.22. As can be seen in all four cases the agreement between experiment and theory is much improved. The following three points are apparent:

(i) The positioning of the maxima and minimum are in better agreement at both temperatures;

(ii) The predicted and measured pressures are much closer;

(iii) The broadening in the axial diffractive field that is observed experimentally with temperature is also followed in the theoretical predictions.

Similar results to those shown were obtained with urine.

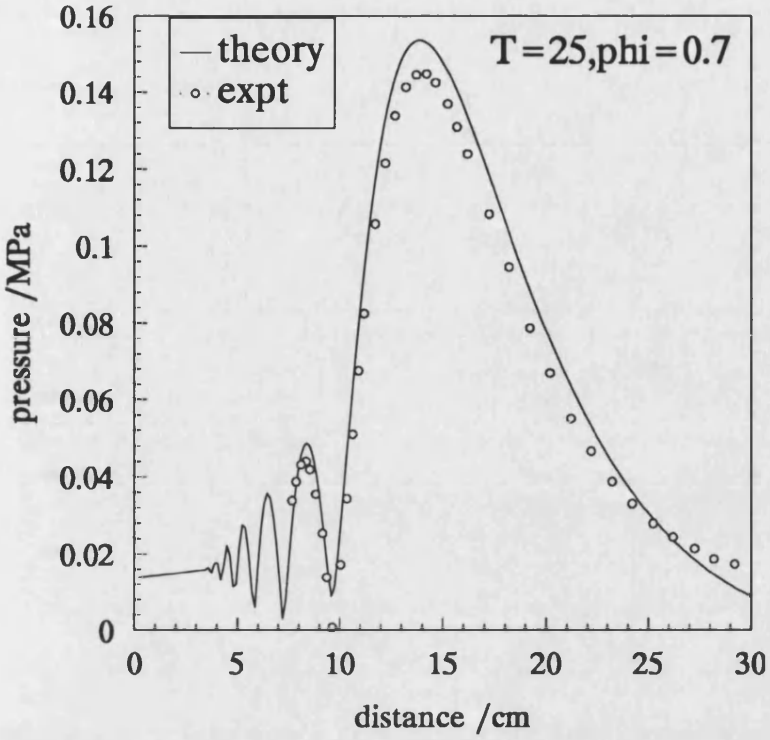

Figure 7.19. Comparison between experiment and modified theory for the axial variation of the fundamental in amniotic fluid, at T=25°C, source pressure is 0.0137 MPa. Gaussian phase distribution across transducer face.

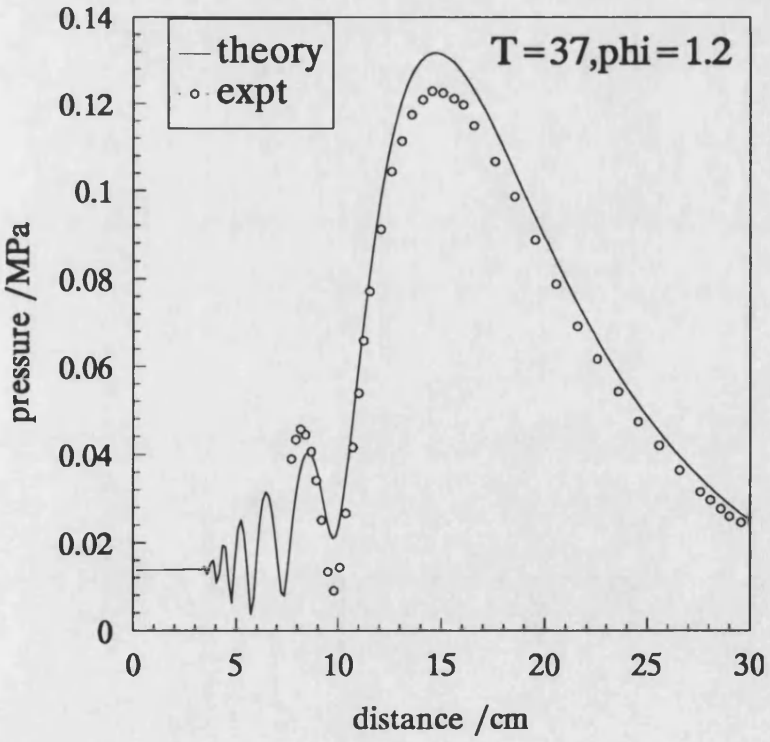

Figure 7.20. Comparison between experiment and modified theory for the axial variation of the fundamental in amniotic fluid, at T=37°C, source pressure is 0.0137 MPa. Gaussian phase distribution across transducer face.

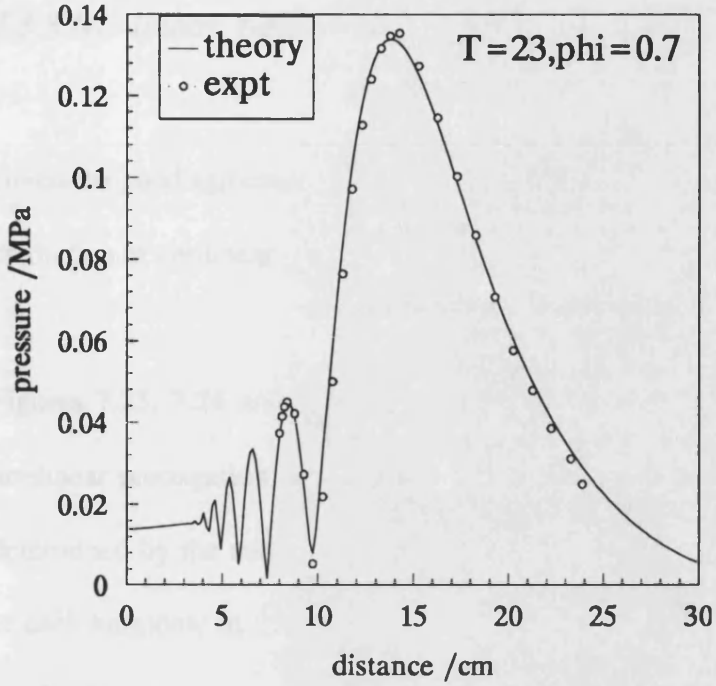

Figure 7.21. Comparison between experiment and modified theory for the axial variation of the fundamental in 4.5% Human albumin, at T=25°C, source pressure is 0.0137 MPa. Gaussian phase distribution across transducer face.

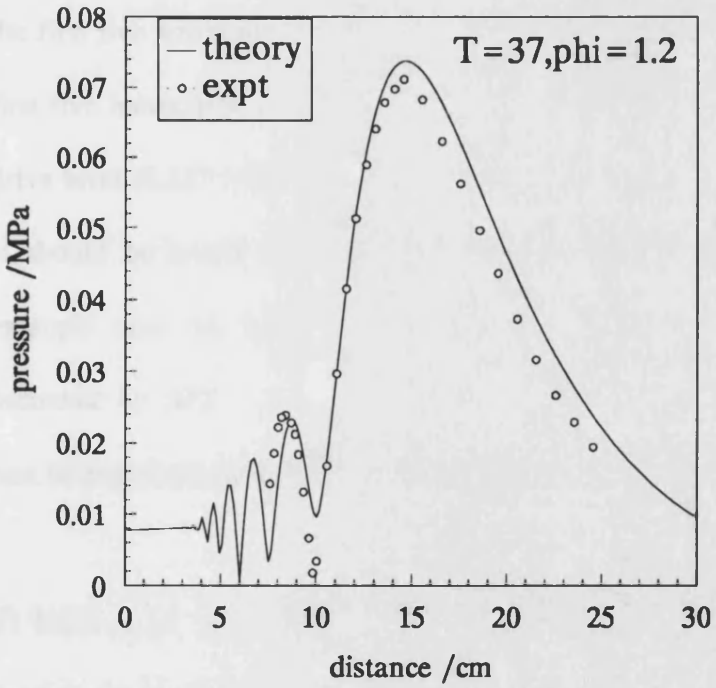

Figure 7.22. Comparison between experiment and modified theory for the axial variation of the fundamental in 4.5% Human albumin, at T=37°C source pressure is 0.0077 MPa. Gaussian phase distribution across transducer face.

7.3.3 Nonlinear field comparison

Given the good agreement between experiment and theory for linear propagation, the prediction of nonlinear pressure distributions can now be considered.

Figures 7.23, 7.24 and 7.25 are a comparison between experiment and theory for nonlinear propagation in urine at room temperature. The degree of nonlinearity is determined by the source pressure and is given in the figure captions. The pressure of each harmonic in the field is illustrated on a logarithmic scale so as to present the results clearly.

In general the results show very good agreement between experiment and theory for the first five harmonics. Both the axial variation and the absolute amplitude of the first five harmonics are well predicted. There is some disagreement for the highest drive level (0.217 MPa), with the theory predicting higher pressure values on axis. It should be noted that the disagreement increases with harmonic number. For example near the focus the fundamental is overestimated by 12% and the 5th harmonic by 30%. This disagreement in the fundamental and the harmonics can in part be explained by a combination of the following factors:

(i) There is an 7% to 8% (NPL 1994) uncertainty in the hydrophone calibration of the 0.5 mm hydrophone in the frequency range 2 MHz to 12 MHz. This uncertainty will affect the measured value of the fundamental and the first four harmonics.

(ii) The transmission properties of the mylar end windows becomes significant at 10 MHz and higher, the loss at these frequencies is of the order of 1 dB (10%). It should be noted that correction for this loss has not been made to the experimental results.

(iii) The error in the source pressure is also of the order of 10%.

(iv) Increasing the drive level results in tighter focusing of the harmonics in the region of the focus. This makes the alignment of transducer and hydrophone more critical, a slight misalignment will result in a decrease in the measured on-axis pressure.

(v) The averaging effect of the 0.5 mm diameter hydrophone will begin to cause significant spatial averaging effects for the higher harmonics.

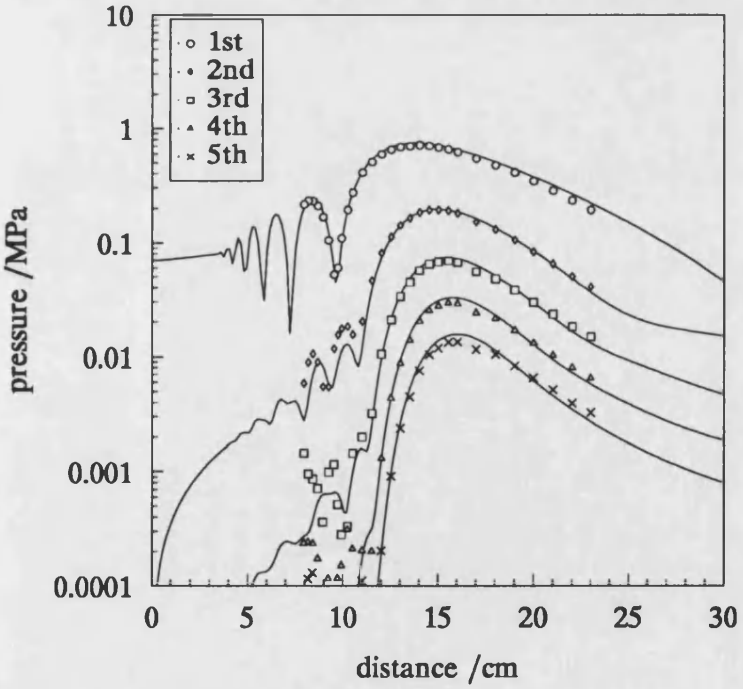

Figure 7.23. Comparison between experiment and theory for the axial variation of the fundamental and first four harmonics in urine at room temperature, source pressure is 0.069 MPa.

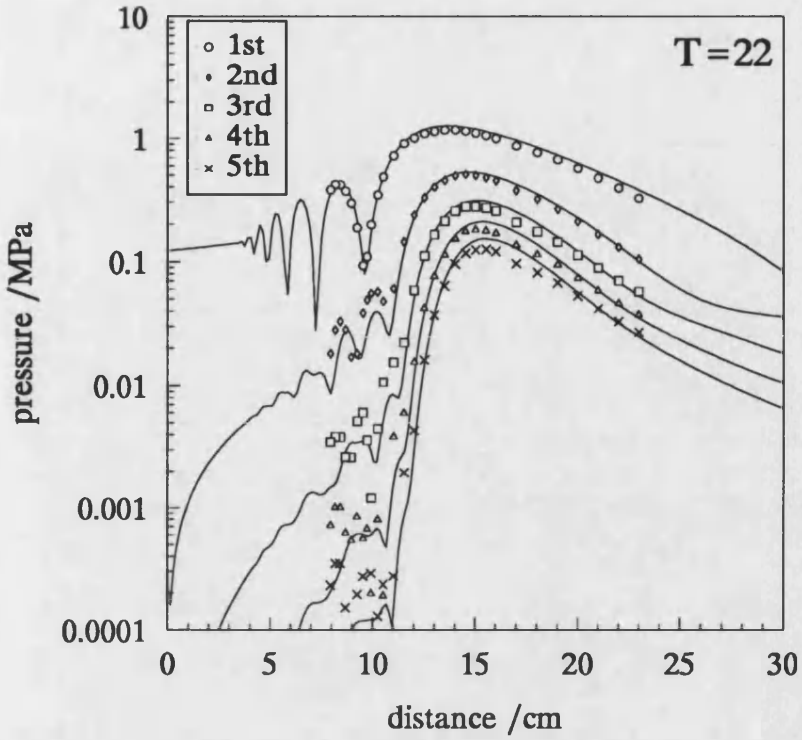

Figure 7.24. Comparison between experiment and theory for the axial variation of the fundamental and first four harmonics in urine at room temperature, source pressure is 0.122 MPa.

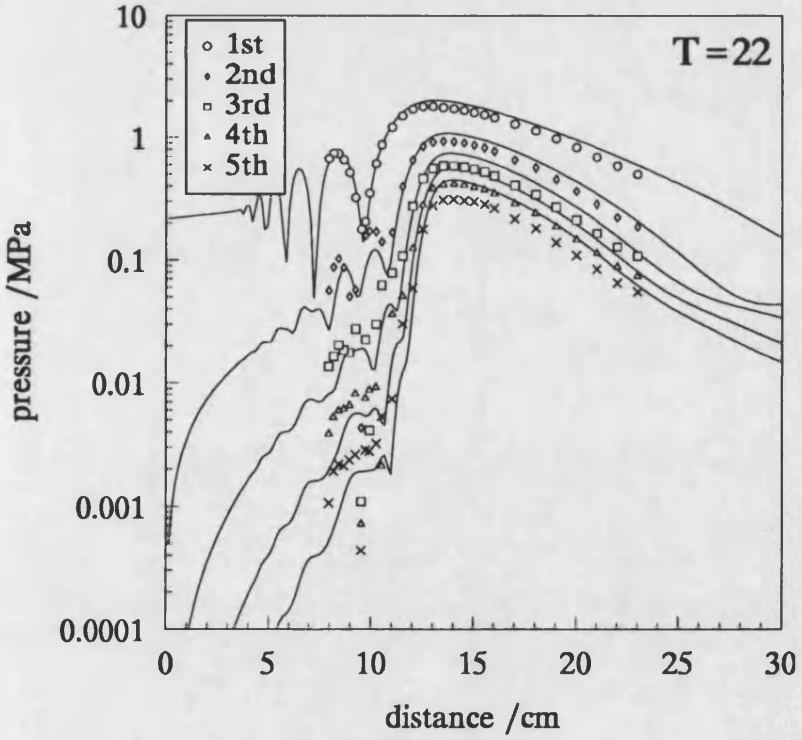

Figure 7.25. comparison between experiment and theory for the axial variation of the fundamental and first four harmonics in urine at room temperature, source pressure is 0.217 MPa.

Alignment of the transducer and hydrophone, as stated, can be an important factor in the measurement of the axial pressure distribution. Figures 7.26 and 7.27 illustrate comparable results, at physiological temperature, in amniotic fluid and 4.5% Human Albumin for a source pressure level of 0.137 MPa. As can be seen the agreement in the build-up and fall off in the harmonics is reasonable. However the actual pressure amplitudes predicted are higher than those measured experimentally. The situation is worst for amniotic fluid, here the predicted 5th harmonic amplitude in the region of the focus is about 50% higher than that measured experimentally. The suggested cause for this difference is due to misalignment of the transducer and hydrophone.

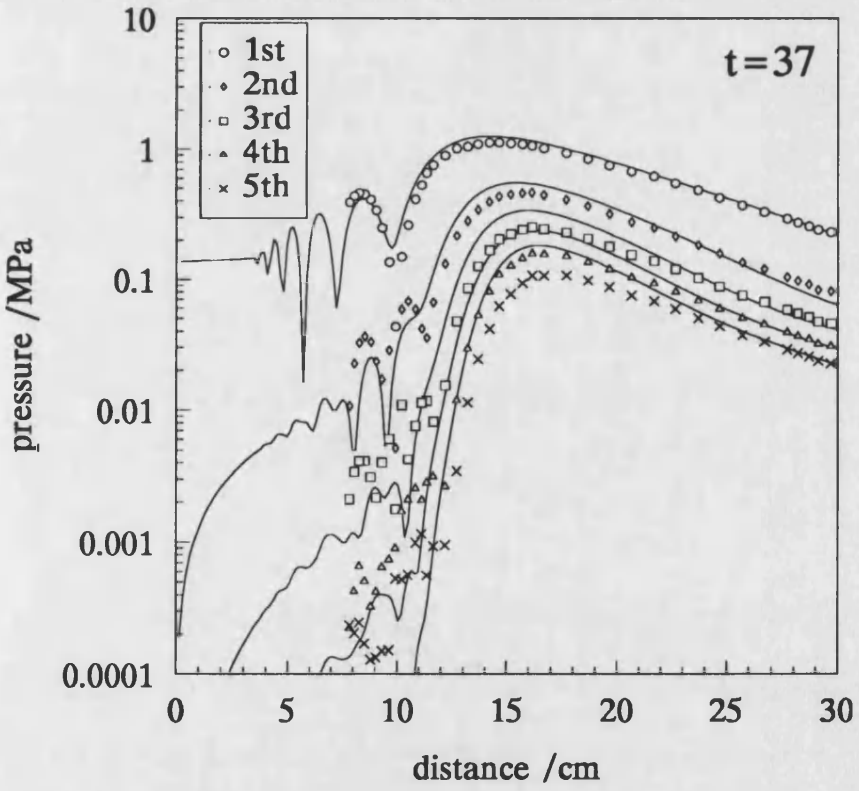

Figure 7.26. Comparison between experiment and theory for the axial variation of the fundamental and first four harmonics in amniotic fluid at T=37°C source pressure is 0.137 MPa.

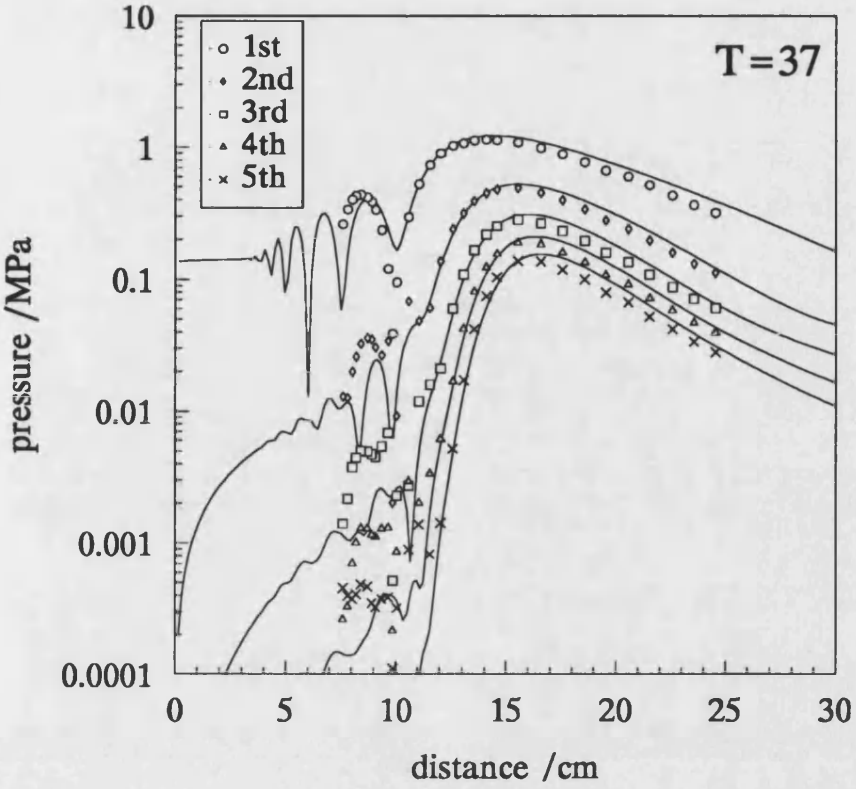

Figure 7.27. Comparison between experiment and theory for the axial variation of the fundamental and first four harmonics in 4.5% Human albumin at T=37°C source pressure is 0.137 MPa.

The reason is as follows. One of the consequences of a non planar phase distribution across the transducer is that the last axial minimum, of the fundamental, does not remain a minimum. If one refers back to figures 7.19, 7.20, 7.21 and 7.22 it can be seen that in the simulations results the pressure at the last minimum does not drop down to zero. In fact what happens is that at this axial position sharp minima exist on either side (radially) of the expected minimum. In aligning the transducer and hydrophone it is common to use the last minimum as a reference point as it is normally a very well defined position in the field. With non perfect piston behaviour this can result in a misalignment as one of the off-axis minima may be chosen. The situation will become more pronounced with the higher harmonics as they are focused more tightly. The non uniform phase distribution across the transducer was

however not apparent at the time of the amniotic fluid measurements and it is likely that one of the off-axis minima was chosen during the alignment procedure.

Measurements performed in urine support the above argument (the phase behaviour of the transducer was known for this measurement). Figure 7.28 illustrates the axial variation of the first five harmonics in urine at physiological temperature. In particular one can consider the axial variation of the second harmonic. With a planar phase distribution across the transducer the second harmonic shows a double peaked behaviour (Baker 1988) in the region of the last minima of the fundamental. The theoretical results illustrated in figures 7.28, 7.26 and 7.27 all indicate that the second peak does not drop down to a trough but rather a shoulder appears in the axial variation of the second harmonic. The experimental results in figure 7.28 (urine) also show a shoulder, supporting the view that with this measurement the transducer and hydrophone were better aligned. The reason for this behaviour in the second harmonic is likely to be due to the fact that it follows the behaviour of the fundamental. Since the fundamental does not fall to a null there is not a rapid phase inversion at the last minimum and this is reflected in the presence of a shoulder, rather than a null, in the second harmonic.

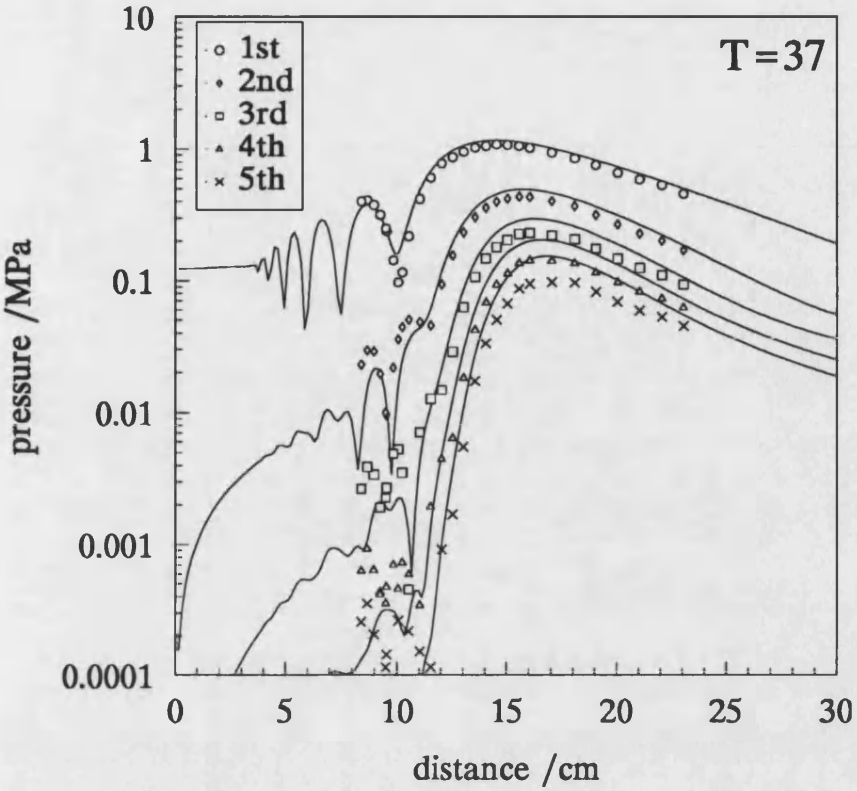

Figure 7.28. Experimental and theoretical axial variation of the fundamental and first four harmonics in urine at physiological temperature, source pressure is 0.122 MPa.

In addition to this the results illustrated in Figure 7.24 can be compared with those in Figure 7.28. Both measurements were made in urine with the same focusing lens and source pressure, the former were at room temperature and the latter at physiological temperature. As can be seen one of the differences between them is the much sharper focusing of all the harmonics at room temperature. This occurs for two reasons. Firstly the change in temperature results in a lower gain for the physiological temperature measurements (see Table 7.12) due to the change of sound velocity in the fluid and the perspex lens. Secondly, as has been discussed, the phase delay from the edge of the transducer increases with increasing temperature resulting in a reduction in the effective gain.

The other feature of the two results (comparing Figures 7.24 and 7.28) is the better agreement between experiment and theory for the room temperature results. This was in general found with all the fluids. It seems likely that the change in temperature will bring about other changes, apart from the phase behaviour of the transducer, in the experimental measurements. For example:

(i) The source pressure at the transducer may be altered. Some measurements of source pressure at physiological temperature were performed and seemed to indicate an increase of a few percent. However whether these changes were due to a change in the output of the transducer or due to changes in the sensitivity of the hydrophone (given the significant calibration errors and the extrapolation from room temperature calibration to physiological temperature, NPL 1994) is not clear.

(ii) The transmission properties of the mylar end-windows may also have altered with the increase in temperature. If one assumes that the velocity of sound in mylar decreases with increasing temperature (as is the case for perspex) then it would be usual for the transmission loss to increase. This would have the effect of reducing the effective source pressure that enters the fluid.

In summary, the results presented in Figures 7.23 to 7.28 represent the main results in this thesis and they show very good agreement between experimental measurements and theoretical predictions for the three biological fluids studied.

7.4 The influence of input parameters

In the last section it was shown that good agreement between experiment and theory was achieved for the nonlinear pressure distributions in amniotic fluid, urine and 4.5% Human Albumin solution. Given the extent of agreement, it is possible to use the model to consider the influence of various input parameters on the resultant simulated pressure distributions. The parameters considered are the attenuation and nonlinearity parameter of the fluid and the pressure and effective radius of the source.

Figure 7.29 illustrates the percentage change in the predicted axial pressure of the fundamental and fifth harmonics as a result of a reduction in source pressure from 0.137 MPa to 0.122 MPa (approximately 10%). The solid lines represent results for amniotic fluid, the dashed lines are for 4.5% Human Albumin solution. The reduction in the fundamental for both fluids is approximately 10%. In addition to this there is some structure in the precise variation with axial distance. For example in the region of the focus the reduction is not as great. This is due to a reduction in harmonic generation, as a result of the lower source pressure, and therefore a decrease in the loss of energy from the fundamental. For the 4.5% Human Albumin solution the drop in fundamental pressure increases after about 17 cm. The reason for this is not immediately obvious but could be due to the fact that at the higher drive level some energy is returned to the fundamental from the interaction of higher harmonics. For the lower drive level these harmonics may not be produced and so

cannot return energy back to the fundamental.

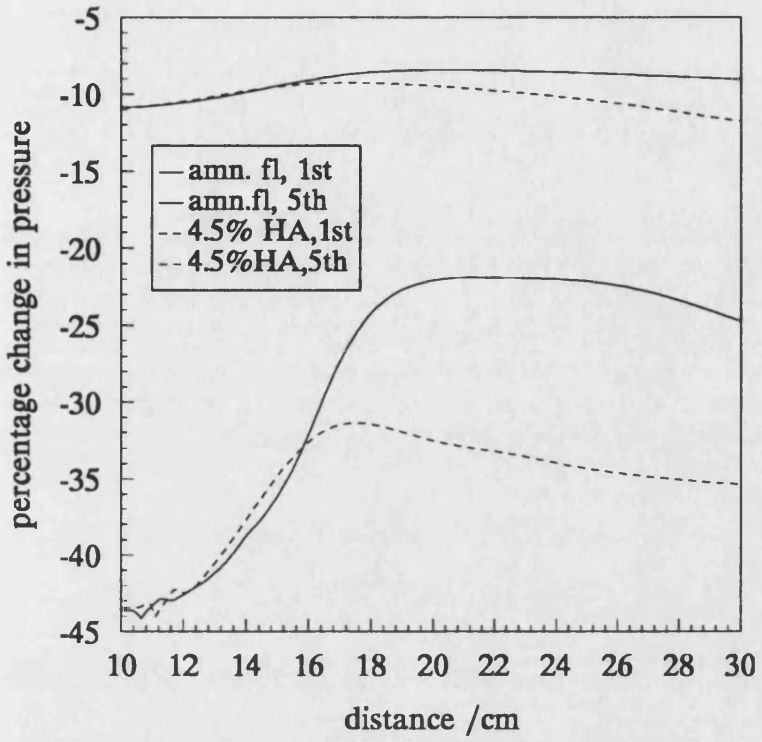

Figure 7.29. The effect of a 10% reduction in the source pressure on the axial variation of the fundamental and fifth harmonics; theory.

The situation for the fifth harmonic is different. The curves can be split into two parts, the pre-focal and post-focal region. In the pre-focal region the 5th harmonic starts of about 40% lower, for a reduction of 10% in the source pressure, for both fluids and then rises fairly rapidly into the focal region. In the post-focal region both curves plateau out with the level in amniotic fluid reaching a stable value of 20% lower (with respect to the original source pressure simulations). In the 4.5% Human Albumin solution the fifth harmonic is lower by approximately 35% and here there does seem to be a further change with propagation distance. One can get an understanding as to why the fifth harmonic decreases by these amounts by considering plane wave analysis.

In Chapter 2 reference was made to two solutions for finite amplitude propagation: the Fubini solution (for low levels of nonlinearity and weak distortion) and the Fay solution (for high levels of nonlinearity and strong shocks). Using the Fubini solution, the pressure amplitude can be expressed as follows:

$$\left(\frac{P}{P_o}\right) \propto \left(\frac{2l_d}{nz}\right) J_n\left(\frac{nz}{2l_d}\right). \qquad 7.2$$

For very low levels of nonlinearity and very close to the source the Bessel function can be expanded to include only the first term. This then gives:

$$\left(\frac{P}{P_o}\right) \propto \left(\frac{2l_d}{nz}\right)\left(\frac{nz}{2l_d}\right)^n. \qquad 7.3$$

This reduces to the following:

$$P \propto P_o\left(\frac{nz}{2l_d}\right)^{n-1}. \qquad 7.4$$

The shock distance, l_d, can be expressed in terms of the source pressure and (see for example equation 1.8, in Chapter 1) we get:

$$P \propto P_o^n\left(\frac{nz\beta k}{2\rho_o c^2}\right). \qquad 7.5$$

This implies that close to the source and for low levels of nonlinearity, a 10% change in the source pressure will result in approximately a 50% change in the level of the fifth harmonic (since n=5).

In contrast the Fay solution for highly distorted waves (for example σ=3) states that the amplitude of a harmonic is inversely proportional to its harmonic number (i.e. $1/n$). Here a 10% change in the source pressure will result in a 10% change in the level of the fifth harmonic.

One can see that in the pre-focal region the Fubini solution gives an indication as to the magnitude of behaviour shown in Figure 7.29. In the post-focal region the behaviour of the fifth harmonic falls in between the Fay and Fubini solutions. It is also apparent that the result in amniotic fluid is closer to the Fay solution than the result in the 4.5% Human Albumin solution. This is presumably due to the lower attenuation in amniotic fluid (approximately 0.3 dB cm^{-1}) so allowing a harder shock to form. Also supporting this is that the percentage change in amniotic fluid is much more stable from 20 cm to 30 cm. In the 4.5% Human Albumin solution the attenuation of the fifth harmonic is approximately 1 dB cm^{-1} and here variations in the percentage change are more influenced by attenuation processes.

Figure 7.30 illustrates results for a 10% reduction in the nonlinearity parameter. As can be seen for both fluids and both harmonics the behaviour is similar to that obtained with a 10% reduction in source pressure. The main differences here are in the magnitude of the changes. In the pre-focal region, where harmonic generation is beginning to occur, a reduction in the value of the nonlinearity parameter results in a higher pressure for the fundamental in both fluids as less energy is lost to the harmonics. However in the post-focal region the energy in the fundamental again begins to reduce.

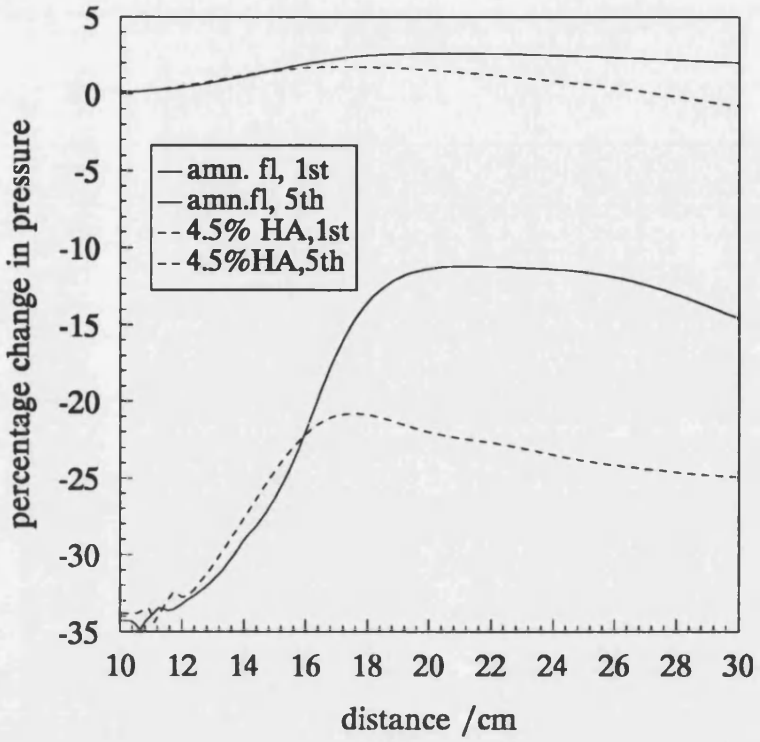

Figure 7.30. The effect of a 10% reduction in the nonlinearity parameter on the axial variation of the fundamental and fifth harmonic; theory.

The situation is clearer to see with the 4.5% Human Albumin solution. Harmonic generation and attenuation results in a more significant loss of energy from the fundamental. It is only after 28 cm that the energy in the fundamental is lower for the lower nonlinearity parameter simulations.

The situation for the fifth harmonic is again similar to the results obtained with a reduction in source pressure, the magnitude of the effects are not however so pronounced. In the Fubini solution the pressure amplitude of a harmonics is less influenced by the nonlinearity parameter than the source pressure.

It should be stressed that neither the Fay nor the Fubini solutions cannot give a complete understanding of the processes taking place as they are not fully applicable

in the region $1.5 < \sigma < 3$, which is the case for the simulations and experiments discussed here. They do however give an order of magnitude estimate of the behaviour of harmonic propagation in such situations.

Figure 7.31 illustrates the effect of increasing the attenuation coefficient by 10%. In amniotic fluid the magnitude of the fundamental is hardly altered, due to its initially low attenuation. In the 4.5% Human Albumin solution one can see a general reduction in fundamental amplitude with distance of a few percent.

The behaviour of the fifth harmonic is similar for the two fluids, the differences being in the magnitude of the change and the presence of a trough in the focal region for the lower loss fluid. The magnitude of the change for amniotic fluid is a few percent close to the transducer rising to approximately 10% at about 30 cm. In the 4.5% Human Albumin solution the percentage change is roughly doubled. The decrease in the value of the pressure for both harmonics and both fluids is expected. The exact variation however is a complex process that involves the extent to which nonlinear propagation is occurring. For example increasing the attenuation coefficient could increase the pressure of a harmonic by reducing the effect of nonlinear propagation and therefore loss of energy from the harmonic.

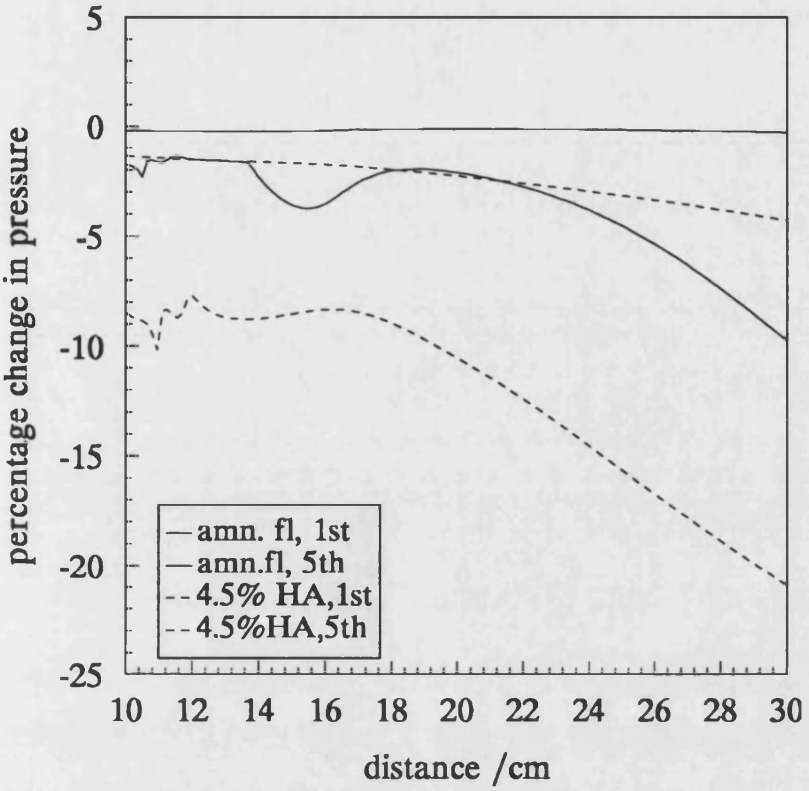

Figure 7.31. The effect of a 10% increase in the attenuation on the axial variation of the fundamental and fifth harmonics; theory.

Figure 7.32 illustrates the effect of reducing the transducer radius from 19 mm to 18.5 mm, for the case of amniotic fluid and a source pressure of 0.137 MPa. With this graph the axial variation of harmonic pressure amplitude is plotted rather than the percentage difference as it is more meaningful. As can be seen a reduction in transducer radius has a number of effects. The diffractive field of the fundamental is altered, with the minima appearing closer to the transducer, the pressure in the focal region is reduced and the pressure variation in the post-focal region is not so rapid. The effects for the fifth harmonic are much smaller, the main observation being that the pressure at its focus is reduced.

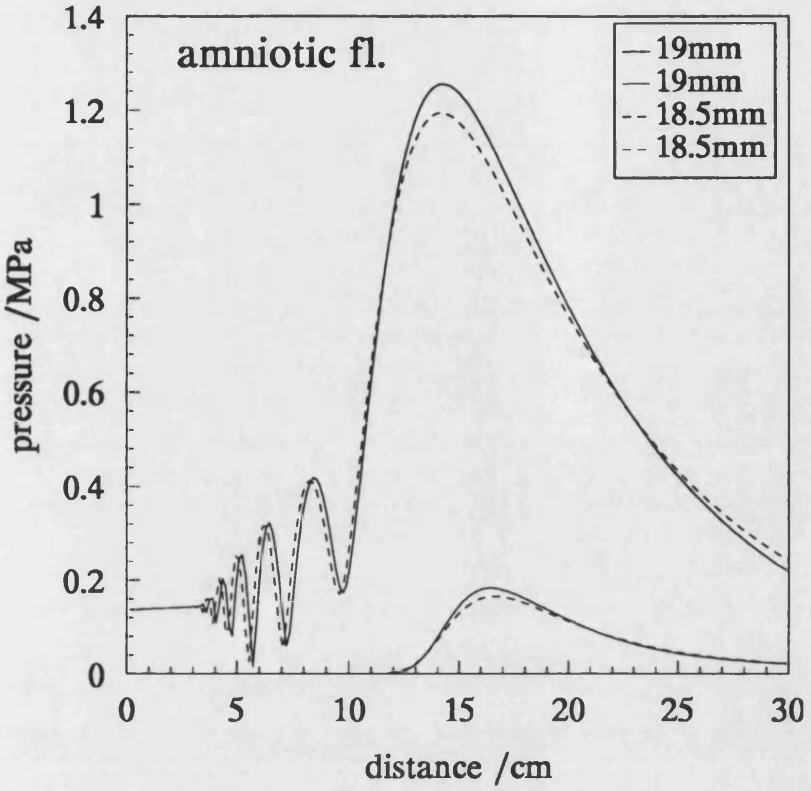

Figure 7.32. The effect, on the axial field of the fundamental and fifth harmonics, of a 0.5 mm decrease in transducer radius; theory.

The purpose of considering changes in the input parameters to the model was to investigate how these parameters may have influenced the agreement between experiment and theory considered earlier. From the above discussion it seems that an accurate knowledge of the source pressure is probably the most important factor, especially for determining the pressure of the higher harmonics. The nonlinearity parameter has also been shown to be significant. The attenuation coefficient has less influence on these results. This is however not a general observation. The source pressures and focusing gains used in the simulations and experiments were such that, due to the low attenuations in the fluids, nonlinear effects dominated. If lower source pressures and gains were employed then changes in the harmonic levels due to changes in attenuation would become much more significant. In addition, if the

attenuation coefficient was higher (for example similar to soft tissue) then even with the source conditions used here the relative importance of attenuation and nonlinear effects would be evident.

8.0 SUMMARY AND CONCLUSIONS

8.1 General

The finite amplitude distortion of acoustic pulses from medical transducers, after passing through body tissues, has been demonstrated previously (Starritt *et al* 1985, 1986). However as the measurement of acoustic fields *in-vivo* is not at present possible, an alternative approach is to try to mathematically model these fields. At present the results of mathematical models, used for predicting nonlinear acoustic fields, have only been verified in water (Baker *et al* 1987, 1988) . The aim of this thesis was to study the nonlinear propagation of ultrasound through biological fluids in order to extend the range of conditions under which the numerical model had been verified, and hence facilitate the modelling of fields *in-vivo*.

This thesis has presented experimental and theoretical results for the axial nonlinear pressure distributions in three biological fluids, amniotic fluid, 4.5% Human Albumin and urine at both room temperature and physiological temperature. The acoustic fields were generated with a 2.25 MHz (38 mm diameter) single element circular transducer with focusing achieved by the addition of a perspex lens: the focusing gain being approximately 12.0 in water. The experimental results presented in Chapter 7 (figures 7.1 to 7.8) illustrate that for all three fluids nonlinear distortion of the waveform is achievable for source pressures below 0.25 MPa. Indeed the level of

second harmonic, in the region of the focus and beyond, reaches levels of 6 dB below the fundamental, indicating that mature shocks have formed.

The model used, to theoretically predict the above acoustic fields, is a numerical solution (Aanonsen *et al* 1984) to the KZK equation (Kuznetsov 1971) and takes account of attenuation, diffraction and nonlinear propagation. A comparison of the experimental and theoretical results (Chapter 7, figures 7.23 to 7.28) show that very good agreement is obtainable. In general the results demonstrate that models based on the KZK equation can be used to determine nonlinear pressure fields in biological fluids (and possibly any homogeneous medium) for circular transducers operating at medical frequencies and pressures.

In order to perform the calculations the model required input parameters relating to the source and medium of propagation. In Chapter 6 broadband (5 MHz to 25 MHz) results were presented for the frequency dependence of attenuation in amniotic fluid, 4.5% and 20% Human Albumin solutions and urine at room temperature and physiological temperature. These results provide unique data for the literature on acoustic properties in biological fluids. They also reinforce conclusions drawn by other workers on the relative effects of water and protein concentration on the subsequent attenuation properties of a material. In addition it is noted that curve fitting procedures previously employed to obtain a functional relationship between frequency and attenuation may result in systematic errors.

Another medium parameter considered was the nonlinearity parameter (B/A). The results presented in appendix A illustrate the difficulty in making accurate measurements of this quantity. The two main problems associated with the method used were hydrophone calibration uncertainty at the fundamental and second harmonic and the avoidance of diffraction effects resulting from the use of a finite size source and receiver. It was found that (B/A) could only measured with an accuracy of +/- 15%.

The results presented in Chapter 7 also demonstrated that an accurate knowledge of the source parameters is important in predicting pressure distributions. In particular it was shown that (figures 7.13 to 7.22) nonplanar phase variations across the source have subtle effects on the structure of the ultrasonic diffractive field: a gaussian phase distribution across the source can modify the overall gain of the transducer.

8.2 Enhanced attenuation

As a result of this work it is now possible to estimate the enhanced attenuation (see Chapter 3) that will occur in the fluids measured in Chapter 7. Simulations were performed for a 3.5 MHz (19 mm diameter) single element transducer with a gain of 6.0 and source pressures of 0.03 MPa and 0.2 MPa. Figure 8.1 tabulates the simulated results for the enhanced attenuation in the region of the focus.

Medium	Enhanced attenuation (dB cm^{-1})	Linear attenuation (dB cm^{-1})	Total attenuation (dB cm^{-1})
Water	0.29 (x17)	0.017	0.3
Amniotic fluid	0.23 (x6)	0.042	0.27
4.5% Human Albumin solution	0.16 (x1.2)	0.14	0.3
20% Human Albumin solution	0.02 (x0.02)	0.85	0.87

Figure 8.1 Tabulated values of the predicted enhancement of attenuation in the region of the transducer focus.

These results illustrate that there is a dramatic increase in the enhancement of attenuation as one goes from 20% Human Albumin solution to low loss fluids such as water and amniotic fluid. These results were obtained using reasonable values of source pressure and focusing gain; higher pressures and gains will undoubtedly increase the value of the total attenuation, especially in low loss fluids. For example the results presented in Chapter 3, for a source pressure of 0.39 MPa and a focusing gain of 6.5, produced a total attenuation of 1 dB cm^{-1} in the region of the transducer focus. Similar results are obtained in simulations with amniotic fluid and urine.

The simulations, discussed above, may have significance in obstetric scanning. At present there is some debate as to whether enhanced streaming can cause perturbation of cell adhesion in first trimester scanning. In obstetric scanning, if one assumes a source pressure of 0.5 MPa (a reasonable estimate) and an overlying tissue thickness of 2 cm then the pressure of the wave entering the amniotic fluid path could be as high as 0.3 MPa (assuming an attenuation coefficient of 0.5 $dBcm^{-1}MHz^{-1}$

at 3.5 MHz for the overlying tissue). Hence with the inclusion of focusing it is likely that acoustic pulses will become highly distorted during passage through the fluid path. It should be noted that the above argument assumes no loss of energy or wavefront disruption due to scattering.

It should also be stressed that given the very short pulse lengths and dwell times, used in clinical applications, the above effects are likely not to produce prolonged temperature rises or streaming effects. An area of more concern is the increased use of Doppler techniques, for example in foetal heart rate monitoring; which use much longer pulses.

In addition to the discussion above, the ability to predict parameters such as enhanced attenuation has usefulness in other areas:

(i) One of the problems encountered with models that predict temperature rises is the lack of input data, in particular the attenuation coefficient of the medium or media of propagation. Added to this there is also the question as to whether such parameters can be treated as constants. As demonstrated in this thesis, the value of the attenuation coefficient is dependent on the degree of nonlinear distortion present in the acoustic beam. More accurate models for calculating temperature elevation can be produced by taking account of nonlinear effects on the subsequent energy loss from the acoustic beam.

(ii) It is common practice to estimate *in situ* exposure by measuring the maximum pressure, from an ultrasound scanner, in water and then de-rating this value with an average attenuation coefficient for tissue (often 0.5 dB cm^{-1} MHz^{-1}). This method however assumes negligible attenuation of the sound beam in water. As has been demonstrated there can be an appreciable amount of nonlinear distortion, resulting in loss of energy, in water based measurements. The method is also dependent on whether one measures the peak positive or peak negative pressure of the nonlinearly distorted acoustic pulse. An alternative method is to consider intensity or PSI. The results presented have shown that this quantity can be modelled accurately including the loss of energy due to nonlinear propagation. Hence intensity and source pressure measurements in water can be corrected for losses due to nonlinear propagation using the results of numerical modelling. These values can then be correctly de-rated using attenuation coefficients for tissue.

Some theoretically determined values of the loss resulting from a 5 MHz transducer with a diameter of 6.5 mm and a focusing gain of 4.45 are presented as a function of source pressures in figure 8.2. By way of example consider a source pressure of 0.65 MPa from figure 8.2. The loss in intensity, in the focal region, due to nonlinear effects is 3.1 dB. The PSI in this region (5.29 MPa MPa s) is corrected with this loss to give a value (7.56 MPa MPa s) resulting from linear propagation. This new value can then be de-rated with a chosen attenuation in tissue.

Source pressure (MPa)	PSI at focus (10^{12} Pa^2 s)	loss (dB)
1.0	6.4	-6.0
0.85	6.0	-4.9
0.75	5.7	-4.0
0.65	5.3	-3.1
0.57	4.9	-2.2
0.49	4.5	-1.3
0.43	4.0	-0.7
0.4	3.6	-0.3

Figure 8.2 Theoretical values for the loss due to nonlinear propagation for a 5 MHz, 13 mm diameter transducer with a focusing gain of 4.45 operated at various source pressures.

On this basis it should be possible to produce a set of tabulated values, through numerical modelling (assuming a simplified source geometry), for common commercial scanner settings, which could be available for general use in estimating *in situ* exposure more accurately.

8.3 Future work

Given that a versatile experimental rig has been constructed, there is a wide variety of work that can be undertaken in characterising the frequency dependence of attenuation and nonlinear pressure distributions for other biological fluids:

(i) The frequency dependence of attenuation with protein concentration in the Human Albumin solutions provides an interesting possibility for making standard solutions to cover a whole range of attenuation coefficients (the 20% Human

Albumin solution has an attenuation coefficient similar to that at the lower end of the range for soft tissue) and frequency dependencies.

In addition, the importance of these quantities in producing various degrees of nonlinear distortion, can be investigated both experimentally and theoretically to validate the mathematical model over a wider range.

(ii) The inclusion of scattering centres (for example graphite, as employed in commercial phantoms) in the Human Albumin solutions would also provide for more realistic tissue mimics and allow the effects of absorption and scattering to be separated and understood in a rigorous manner.

(iii) There is also the possibility of mimicking important clinical situations, for example obstetric scanning. A simple arrangement which incorporates real tissue (or a suitable substitute) in front off and/or behind an amniotic fluid path could provide better estimates of the measured pressure distributions and temperature rises that may occur *in vivo*.

(iv) More work is required in the accurate determination of the nonlinearity parameter, B/A. Diffraction corrections can be minimised by the use of large area receivers, but unless calibration information is improved measurements will still have an appreciable uncertainty.

Theoretically there is also scope for future work in adapting and improving mathematical models:

(i) Probably the most important consideration absent from the present model is that of the scattering of the ultrasound wave in an inhomogeneous medium, such as soft tissue. Models based on the KZK equation cannot, at present, incorporate this in a rigorous manner and much work still needs to be done in this area.

(ii) The usefulness of the model in determining derived parameters, such as the enhanced attenuation has been demonstrated. This work can be extended to consider theoretical determination of temperature rises given that calculation of intensities is possible, either by adapting the existing model or applying its results to present models based on the bio-heat equation.

(iii) Knowledge of the pressure distribution in the whole ultrasonic field allows for the possibility of using this information as a starting point in a hydrodynamic model to predict enhanced streaming resulting from enhanced attenuation.

In addition the significant degree of nonlinear distortion, particularly in amniotic fluid and urine, provides further impetus to investigate the use of nonlinearly generated harmonics for improving the resolution of ultrasonic images in certain clinical areas.

APPENDIX A: MEASUREMENT OF B/A

A1.1 General

In Chapter 1 reference was made to a number of the input parameters required to theoretically predict the experimentally measured nonlinear pressure distributions. One of these was the nonlinearity parameter *B/A*. In Chapter 7 it was shown that using a value of *B/A* for water gave good agreement, between experiment and theory, for the axial nonlinear pressure distributions in the biological fluids under investigation. It was also argued that this was a reasonable assumption to make. The literature on the measurement of *B/A* for biological fluids indicated that the value of this parameter ranged from 5 to 6, representing a maximum difference of 20% from that of water.

Measurements of B/A for the fluids studied in this thesis were also attempted. The method employed is commonly described as the finite amplitude method and follows that used by Law *et al* (1981). In this appendix the method used will be outlined and discussed. Following this, a description of the experimental measurements of B/A for the fluids considered in this thesis will be given. Finally the results obtained will be discussed in relation to their accuracy and the problems associated with the measurement.

A1.2 Finite amplitude method

A1.2.1 Theory

The finite amplitude method of determining B/A involves measurement the source pressure and the growth of the second harmonic as a function of the propagation distance from the source. If measurements are made in the near-field of the source, where diffraction effects are negligible, plane wave analysis can be applied. Using the Fubini solution for plane wave propagation (Alder & Heidmann 1962, Law *et al* 1981) the second harmonic can be expressed as:

$$\left(\frac{P_2(z)}{zP_1^2(0)}\right)_{zP_1(0)} = \left(\frac{B}{A}+2\right)\left(\frac{\pi f}{2\rho_o c^3}\right) \qquad \text{A1.1}$$

where z is the axial distance from the source, $P_2(z)$ is the magnitude of the second harmonic, $P_1(0)$ is the source pressure and f is the fundamental frequency of propagation. Using equation A1.1 B/A can be determined by plotting measured values of $P_2(z)$, expressed in the form of the term on the left hand side of equation A1.1, against the propagation distance z and extrapolating back to $z=0$. The intercept is equal to the right hand side of equation A1.1 and given that values for the sound velocity, density and frequency of propagation are known a value for B/A can be calculated. Apart from the assumption of plane wave propagation the above method is strictly only applicable for lossless media, as attenuation of the fundamental or second harmonic have not been taken into account. However Law *et al* (1981)

suggest that for small source pressures and close to the source the above expression is also valid for attenuating media.

The effect of including attenuation has been studied by Cobb (1983). The approach taken is based on a perturbation solution, obtained by Ingenito & Williams (1971), and is described below. Ingenito and Williams (1971) derived an expression for the second harmonic velocity potential based on cylindrical coordinates. The geometry associated with their situation is illustrated in Figure A1.1. A piston source emits a perfectly collimated beam at the fundamental frequency. The distance between the plane at which the second harmonic is generated and the observation plane is given by *s*.

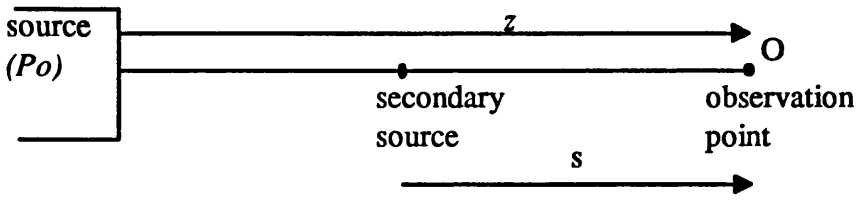

Figure A1.1 Schematic illustrating the geometry used to determine an expression for the second harmonic at point O.

The expression obtained for the second harmonic velocity potential, ϕ_2, is given by:

$$\phi_2(r,z) = \left(\frac{k^2\beta}{4c_o}\right)\int_0^z e^{iks}\left[\phi_1\left(r, z-\frac{s}{2}\right)\right]^2 ds, \qquad \text{A1.2}$$

where ϕ_1 is the velocity potential for the fundamental. Cobb (1983) extended the above expression to include the effects of attenuation of the fundamental and second harmonic. The introduction of attenuation was done in an *ad hoc* manner based on

the assumption that only waves travelling in the z direction would be attenuated given that the beam was perfectly collimated. Cobb's expression is given below:

$$\phi_2(r,z) = \left(\frac{k^2\beta}{4c}\right)\int_0^z e^{iks}e^{-\alpha_2 s}\left[\phi_1\left(r, z-\frac{s}{2}\right)\right]^2 e^{-2\alpha_1(z-s)}ds, \qquad \text{A1.3}$$

where $e^{-\alpha_2 s}$ accounts for the attenuation of the second harmonic from the generation plane to the observation plane and $e^{(-2\alpha_1(z-s))}$ accounts for the attenuation of the fundamental from the source to the generation plane. Using standard relationships between the pressure and the velocity potential, the pressure of the second harmonic was then expressed as:

$$P_2 = \left(\frac{B}{A}+2\right)\left(\frac{\pi f}{2\rho_o c^3}\right)P_1^2(0)\left(\frac{e^{-2\alpha_1 z}-e^{-\alpha_2 z}}{\alpha_2-2\alpha_1}\right). \qquad \text{A1.4}$$

Note that the constant, in front of the integral, in equation A1.3 has been expressed in terms of the medium nonlinearity parameter in equation A1.4.

The attenuation of the second harmonic can be expressed in general form by the expression:

$$\alpha_2 = \alpha_1 h, \qquad \text{A1.5}$$

where $h = 2^m$ and m takes values from 1 to 2. For m=1 we have a linear frequency dependence of attenuation, for m=2 we have a squared law dependence and for values in between correspond to the dependence normally associated with biological fluids. Substituting this into equation A1.4 we obtain:

$$P_2 = \left(\frac{B}{A}+2\right)\left(\frac{\pi f}{2\rho_o c^3}\right)P_1^2(0)\left(\frac{e^{-2\alpha_1 z}-e^{-h\alpha_1 z}}{\alpha_1(h-2)}\right), \qquad (h \neq 2)\ . \qquad \text{A1.6}$$

In order to check the validity of Law's assumption on attenuation, equation A1.5 was evaluated for a range of values of the attenuation coefficient and its frequency dependence. Figure A1.2 illustrates the results for an attenuation coefficient of 0.03 dB cm^{-1} MHz^{-1} and a frequency dependence of 1.4, similar to the 4.5% Human Albumin solution. Values for the density (1000 kg m^{-3}), sound velocity (1500 m s^{-1}) and nonlinearity parameter (5.0) were taken to be the same as water for convenience. Note that in Figure A1.2 the logarithm of equation A1.1 has been plotted, so allowing extrapolation to the intercept using a straight line fit. Regression of the data and calculation of the intercept gives a value of 4.96 for B/A. This confirms the observation made by Law that extrapolation back to z=0, for attenuating media, (with attenuation coefficients in the region given above) is valid in the determination of B/A.

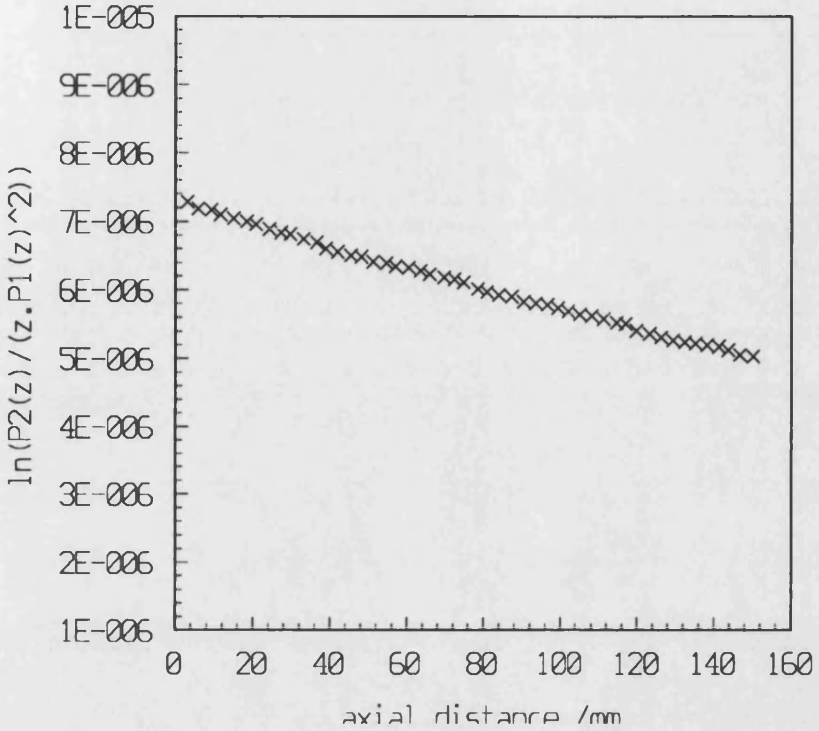

Figure A1.2 Theoretically simulated data for the variation of the second harmonic using equation A1.1, the acoustic parameters relate to 4.5% Human Albumin solution, B/A was input as 5.0.

A1.2.2 Experiment

Measurement of the nonlinearity parameter was made with a similar arrangement to that used for measuring the axial nonlinear pressure distribution, described in Chapter 5. The 2.25 MHz transducer, with no lens attached, was used as the sound source and the 0.5 mm bilaminar PVdF hydrophone was used to measure the growth of the second harmonic with distance. It was necessary to use this calibrated hydrophone as the absolute pressure of the second harmonic and source pressure were required to calculate the nonlinearity parameter. A smaller polyurethane bellows was used for

fluid containment in order to get closer to the transducer and avoid diffraction effects due to edge wave interference.

The measurements were made from 30 mm to 45 mm from the source with a pulse of approximately eight cycles. The source pressure was determined both with a power balance and the 0.5 mm PVdF hydrophone and set to be 0.26 MPa. The fifth cycle in the pulse was used to analyse the fundamental and second harmonic components in the waveform. Below are presented some results for the determination of B/A in amniotic fluid and 4.5% Human Albumin solution.

A1.2.3 Results

Figure A1.3 illustrates the axial variation of the second harmonic with propagation distance, the graph is plotted in accordance to equation A1.1. The x-axis represents the axial distance from the source and the y-axis represents the magnitude of the logarithm of the second harmonic divided by the source pressure and axial distance of the measurement point. The two sets of data show the results for amniotic fluid and 4.5% Human Albumin solution at room temperature. As can be seen the variation in the second harmonic, with axial distance, is in accordance with that expected from other workers (Law *et al* 1981). Also illustrated in Figure A1.3 are the lines of best fit for the two sets of results. Determination of the intercept *(I)* was used to calculate the value of B/A and gave results of:

B/A=4.5 for Amniotic fluid;

B/A=5.7 for 4.5% Human Albumin solution.

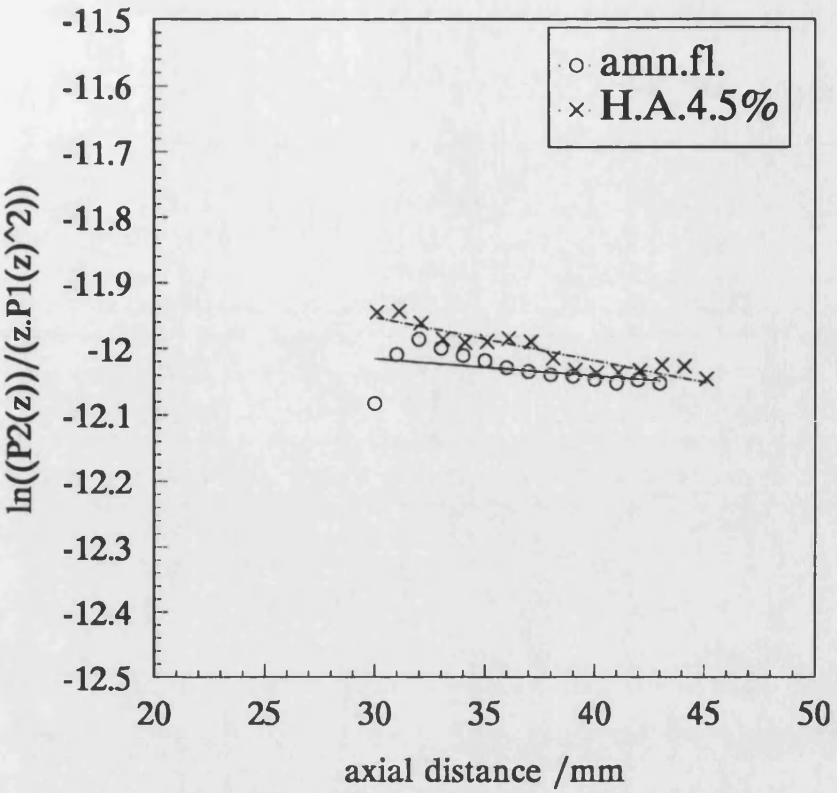

Figure A1.3 Plot of the second harmonic versus axial distance, in accordance with equation A1.1, illustrating the determination of the nonlinearity parameter.

As can be seen the two results yield values of B/A that are roughly (within 15% of the value quoted for water) in accordance with those expected for the two fluids. However the accuracy of these measurements needs to be considered.

(a) The standard error of the regression lines is relatively small (+/- 0.02), this represents a less than 1% change in the intercept. However if the upper and lower bound values for the intercept are used in equation A1.1 then the overall change in the value of B/A is approximately 3%. This represents one aspect of the finite amplitude method of determination of B/A: the results are very sensitive to the value of the intercept due to the exponential nature of the relationship in equation A1.2. A 1% change in the value of the intercept can lead to a 10% change in the value of B/A.

(b) This highlights a problem with the experimental arrangement used to measure B/A. Due to the physical limitations associated with having a fluid tight but variable length chamber, the minimum distance to the source was 30 mm. Measurements made closer to the source would have given a more accurate estimation of the value of the intercept.

(c) Probably the most significant error associated with the finite amplitude method is in the calibration of the hydrophone at the fundamental and second harmonic frequencies. The error, quoted in the NPL calibration document at each frequency is approximately 7%. Taking into account that the results are dependent on the square of the source pressure the uncertainty in this quantity becomes approximately 14%. Combining the uncertainties at the two frequencies one obtains upper and lower limit values for B/A in 4.5% Human Albumin solution, for example, of 6.4 and 5.0. It should however be noted that part of the quoted hydrophone sensitivity error will be due to systematic errors in the calibration procedure that are similar at both frequencies. The effect of this will be to reduce the overall uncertainty and may well result in the total uncertainty being smaller for the measured vales of B/A.

Given the limitations of the calibration for the source pressure and second harmonic and the limitations of the experimental method employed it seems justified to use the B/A for water in the analysis in Chapter 7.

ACKNOWLEDGEMENTS

I am indebted to the supervision and help of Dr Victor Humphrey and to the help of Dr Andrew Baker, Dr Francis Duck and Dr Hazel Starritt. Many thanks to Barry Ward, Paul Chinnery, Sue Zhang, Fawaz Abu-Sitta, Mark Cahill and Claire Doody for useful discussions and in particular to Mair Jones for also proof reading this thesis. Thanks go to members of the School of Physics for providing an amiable working atmosphere in particular Colin Cooper, Cathy Dyer, Brian Gay and Les Steele.

I would also like to acknowledge the support of the Science and Engineering Research council for providing a studentship, the Royal Society for providing a grant for the bilaminar hydrophone, Oddstock Hospital, Salisbury for providing the amniotic fluid and the Medical Physics department at the Royal United Hospital for providing a pleasant working environment.

I am also very pleased to thank Bob and Dave for many many amusing distractions, Gray for having a baby and so avoiding distracting me, Caroline and Beanz for Thomas St, Awal and Kash for Bath Tandoori, John for going off on one, Izzy for nothing in particular, Al for tunes, Kev for the hammock and Pand for being bohemian.

Finally I am very grateful for the support and encouragement from my mother, father, Dhiru and Shekhar and especially to Shraddha for being there.

References

Aanonsen, S.I., Barkve, T. Tjotta, J.N. & Tjotta, S.(1984) Distortion and harmonic generation in the nearfield of a finite amplitude sound beam. J.Acoust.Soc.Amer.**75**, 749-768.

AIUM/NEMA (American Institute of Ultrasound in Medicine/ National Electrical Manufacturers Association) (1983) Safety standard for diagnostic ultrasound equipment, UL1-1981. J.Ultrasound.Med. 2 (supplement).

AIUM (1988) Bioeffects considered for the safety of diagnostic ultrasound. American Institute for Ultrasound in Medicine bioeffects committee. J.Ultrasound.Med. 7.

Alder,L. & Hiedmann, E.A., (1962) Determination of nonlinear parameter B/A for water and m-Xylene.J.Acoust.Soc.Amer.**34**(4), 410-412.

Apfel, R.E. (1983) The effective nonlinearity parameter for immiscible liquid mixtures.J.Acoust.Soc.Amer.**74**,1866-1868.

Apfel, R.E. (1986) Prediction of tissue composition from ultrasonic measurements and mixture rules. J.Acoust.Soc.Amer, **79**,148-152.

Bacon, D.R. (1982) Characteristics of a Pvdf membrane hydrophone for use in the range 1-100 MHz. IEEE Trans.Sonics. & Ultrasonics, SU-29, 18-25.

Bacon, D.R., & Carstensen, E.L. (1990) Increased heating by diagnostic ultrasound due to nonlinear propogation. J.Acoust.Soc.Amer.**88**(1),26-33.

Baker, A.C., Anastasiadis, K. & Humphrey, V.F. (1987) Nonlinear propagation in focussed fields: Experiment and theory. Proc.Ultrasonics.Int 87, Butterworths. p184-189.

Baker, A.C., Anastasiadis, K. & Humphrey, V.F. (1988) The nonlinear pressure field of a plane circular piston: Theory and Experiment.J.Acoust.Soc.Amer. **84**, p1483-1487.

Baker, A.C. & Humphrey, V.F. (1989) Nonlinear propagation in pulsed ultrasonic fields.

Bamber,J.C., Hill, C.R., Fry, M.J., & Dunn, F. (1977) Ultrasonic attenuation and backscattering by mammalian organs as a function of time after excision. Ultrasound.Med.Biol.**3**, 15-20.

Bamber,J.C.(1979) Ultrasonic characterisation of structure and pathology in human soft tissues. PhD Thesis, University of London.
Bass, R. (1958) Diffraction effects in the ultrasonic field of a psiton source. J.Acoust.Soc.Amer. **30**, 602-605.

Beissner, K. (1981) Exact expression for the diffraction loss of a circular piston source. Acoustica.**49**,212-217.

Beissner, K. (1985) Maximum hydrophone size in ultrasound field measuremnts. Acoustica. **59**, 61-66.

Beyer,R.T. (1960). Parameter of nonlinearity in fluids.J.Acoust.Soc.Amer.**32**, 719-721.

Beyer,R.T. (1974) 'Nonlinear acoustics' American department of the Navy (Naval sea systems command)

Blackstock, D.T. (1966) Connection between Fay and Fubini solutions for plane sound waves of finite amplitude, JAcout.Soc.Amer. **39**, 1019-1026.

Blackstock, D.T. (1964) On plane spherical and cylindrical sound waves of finite amplitude in lossless fluids.J.Acoust.Soc.Amer. **36**, p217.

Blackstock, D.T. (1962) Propagation of plane sound waves of finite amplitude in non-dissipative fluids. J.Acoust.Soc.Amer. **34**, 9-30.

Beakbane (1994) Beakbane Ltd. PO Box 10, Stourport Rd, Kidderminster, Worcestershire, England. DY11 7QT.

Carstensen, E.L., Li, K. & Schwan, H.P.(1953) Determination of the acoustic properties of blood and its components.J.Acoust.Soc.Amer..**25**,286-289.

Carstensen, E.L. & Schwan, H.P. (1959) Absorption of sound arising from the presence of intact calls in blood.J.Acoust.Soc.Amer.**31**,185-189.

Carstensen, E.L. & Schwan, H.P. (1959b) Acoustic properties of haemoglobin solutions. J.Acout.Soc.Amer. **31**, 305-310.

Carstensen, E.L., Law, W.K., McKay, N.D. & Muir, T.G. (1980) Demonstration of nonlinear acoustical effects at biomedical frequncies and intensities. Ultrasound.Med.Biol.**6**,359-368.

Carstensen, E.L., McKay, N.D., Dalecki, D. & Muir T.G. (1982) Absorption of finite amplitude ultrasound in tissues.Acoustica.**51**,116-123.

Choi, P.K., Bae, J.R. & Takagi, K.(1990) Ultrasonic spectroscopy in bovine serum albumin solutions.J.Acoust.Soc.Amer.**87**,874-881.

Christopher, P.T. & Parker, K.J. (1991) New approaches to nonlinear diffractive field propagation.J.Acoust.Soc.Amer.**90**(1),488-499.
Cobb, W.N. (1983) Finite amplitude method for the determination of the acoustic nonlinearity parameter B/A. J.Acoust.Soc.Amer. **73**(5) 1525-1531.

Dickinson, J.A.. & Shah, D.M. (1972) The effects of hyperthermia (42°C) on the biochemistry and growth of a malignant cell line. Europ.J.Cancer, **8**, 561-571

Duck, F.A. (1990) Physical properties of tissue: a comprehensive reference book. Acedemic press ltd.

Duck, F.A., Perkins, M.A. (1988) Amplitude dependent losses in ultrasound exposure measurement, IEEE.Trans.Ultrson.Ferroelec.Freq.Contr,**35**,232-241.

Dunn, F. (1962) Temperature and amplitude dependence of acoustic absorption in tissue.J.Acoust.Soc.Amer.**34**(10), 1545-1547.

Dunn, F. & Breyer, J.E. (1962) Generation and detection of Ultra-High-Frequency sound in liquids. J.Acoust.Soc.Amer. **34**, N°6 775-778.

Dunn, F. & O'Brien W.D. (1976) Ultrasonic Biophysics. Hutchinson & Ross Inc.

Dunn, F. (1976) Ultrasonic attenuation, absorption and velocity in tissues and organs. Proceedings of seminar on ultrasonic tissue characterisation held at NBS, Gaithersberg, MD, May 1975. National Bureau of standards special publications 453, 21-28.

Dunn, F. (1986) Attenuation and speed of ultrasound in lung: dependence upon frequency and inflation. J.Acoust.Soc.Amer. **80**, 1248-1250.

Dussik, K.T., Fritch, D.J., Kyiazidou, M. & Sear, R.S. (1958) Measurements of articular tissue with ultrasound. Am.J.Phys.Med. **37**, 160-165.

Earnshaw, S. (1860) On the mathematical theory of sound. Trans.Roy.Soc.150 p133.

Eggars,F. & Funck,Th.(1973) Ultrasonic measurements with milliliter liquid samples in the 0.5-100 Mhz range.Rev.Sci.Instrum.,**44**,969-977.

Eggars, F., Funck, Th. & Richmann, K.H. (1981) Ultrasonic absorption measurements with a millimetre short-path pulse cell.J.Phys.E:Sci.Instrum.**14**, p113-116.

Errabolu, R.L., Sehgal, C.M., Bahn, R.C. & Greenleaf, J.F. (1988) Measurement of ultrasonic nonlinear parameter in excised fat tissues. Ultrasound in Med.Biol. **14**, 137-146.

Everbach, E.C., (1989) Tissue composition via measurement of the acoustic nonlinearity parameter, Techn Memo N° .6., Department of Mechanical Engineering, Yale University.
Fay, R.D. (1931) Plane sound waves of finite amplitude. J.Acout.Soc.Amer. **3**, 222-241.

Fox, F.E. & Wallace, W.A. (1954) Absorption of finite amplitude sound waves. J.Acoust.Soc.Amer.**26**(6), 994.

Fubini, E. (1935) Anomalies in the propagation of an acoustic wave of large amplitude. Alta.Freq, **4**, 173-180.

Frizzell,L.A., Carstensen,E.L., & Davis,D.(1979) ultrasonic absorption in liver tissue.J.Acoust.Soc.Amer.**65**, 1309-1312.

Fry, W.J. & Fry,R.B.(1954) Determination of absolute sound levels and acoustic absorption coefficients by thermocouple probes-experiment.J.Acoust.Soc.Amer.**26**, 311-317.

Fry, F.J. & Barger, J.E. (1978) Acoustical properties of the human skull. J.Acoust.Soc.Amer. **63**, 1576-1590.

Greenfield, M.A., Craven, J.D., Huddleston, A. (1981) Measurement of the velocity of ultrasound in human cortical bone in-vivo. Radiology, **138**, 701-710.

Gong, X., Zhu, Z., Shi, T. & Huang, J. (1989) Determination of the acoustic nonlinearity parameter in biological media usinf FAIS and ITD methods. J.Acoust.Soc.Amer, **86**, 1-5.

Goss,S.A., Cobb,J.W., & Frizzell,L.A.(1977) Effect of beam width and thermocouple size on the measurement of ultrasonic absorption using the thermocouple technique. 1977 Ultrasonics Symposium Proc.IEEE Cat.No.77CH 1264-1SU, 206-211.

Goss,S.A.,Johnston,R.L.,& Dunn,F.(1978) Comprehensive compilation of empirical ultrasonic properties of mammalian tissues.J.acoust.Soc.Amer.**64**,423-457.

Goss, S.A., Frizzell, L.A., & Dunn, F. (1979) Ultrasonic absorption and attenuation in mammalian tissue. Ultrasound.Med.Biol. **5**, 181-186.

Goss,S.A.,Johnston,R.L.,& Dunn,F.(1980) Compilation of empirical ultrasonic properties of mammalian tissues.II.J.acoust.soc.Amer.**68**,93-108.

Hamilton, M.F., Tjotta, J.N. & Tjotta, S.(1985) Nonlinear effects in the farfield of a directive sound source.J.Acoust.Soc.Amer.**78**, 202-216.

Hart, T.S. & Hamilton, M.F. (1988) Nonlinear effects in focused sound fields. J.Acoust.Soc.Amer.**84**, 1488-1496.

Hill, C.R. (1986) Physical principles of medical ultrasonics. Ellis Horwood Limited. John Wiley & Sons.

Humphrey, V.F. & Berktay, H.O. (1985) The transmission coefficient of a panel measured with a parametric source. J.Sound.Vib. **101**(1), 85-106.

Humphrey, V.F., Burgess, M. & Sampson, N. (1986) Harmonic generation due to nonlinear propagation in a focused ultrasonic field. Ultrasound in Medicine Conference. Proc.Inst.Acoust. **8**, 47-54.

Hutchins, D.A., Mair, H.D., Puhach, P.A. & Osei, A.J.(1986) Continuous wave pressure fields of ultrasonic transducers.J.Acoust.Soc.Amer.**80**(1),1-12

Hynynen, K. (1987) Demonstration of enhanced temperature elavation due to nonlinear propagation of focussed ultrasound in dog's thigh in-vivo. Ultrasound in Med. & Biol. **13**, N°2 85-91.

IEC 1102 (1991) Measurement and characterisation of ultrasonic fields using hydrophones in the frequency range 0.5 MHz to 15 MHz. IOC publications, Linford wood, Milton Keynes MK14 6LE.

Ingenito, F. & Williams, A.O. (1971) Calculation of second harmonic generation in a piston beam.J.Acoust.Soc.Amer.**49**(1) p.319.

Huntingdon, H.B., Emslie, A.G. & Hughes, V.W. (1948) J.Franklin Inst., **245**, 1-23

Kaye & Laby (1986) Tables of Physical and Chemical constants. Longman Scientific & Technical.

Kensulat (1994) Private communication. Kensulat plc, Sovereign Park, Coronation Rd, London NW10 &QP.

Kremkau,F.W., Barnes,R.W. & McGraw,C.P. (1981) Ultrasonic attenuation and propagation speed in normal human brain.J.Acoust.Soc.Amer.**70**,29-38.

Kremkau, F.W. & Carstensen, E.L. (1973) Macromolecular interaction in the absorption of ultrasound in fixed erythrocytes. J.Acoust.Soc.Amer. **5**, 1448-1451.

King, L.V. (1934) Can.J.Research **11**, 135

Kinsler, E.R. & Frey, A.R. (1962) Fundamentals of acoustics. John Wiley and Sons Inc., New York.

Korpel, A. (1980) Frequency approach to nonlinear dispersive waves. J.Acoust.Soc.Amer, **67**, 1954-1958.

Kossoff, G., Fry, E.K. & Jellins, J. (1973) Average velocity of ultrasound in the human female breast. J.Acout.Soc.Amer. **53**, 1730-1736.

Kuznetsov, V.P.(1971) Equations of nonlinear acoustics. Sov.Phys.Acoust.**16**, 467-470.

Lang, J., Zana, R., Gairard, B., Dale, G. & Gros, Ch.M. (1978) Ultrasonic absorption in the human breast cyst liquids. Ultrasound in Med. & Biol. **4**, 125-130.

Law, W.K., Frizzell, L.A., & Dunn, F. (1985) Determination of the nonlinearity parameter of biological media.Ultrasound.Med.Biol.,**11**(2), 307-318.

Lommel, E. (1886). In: Gray, A., Mathews, G.B. & MacRobert, T.M. Atreatise on Bessel functions (MacMillan, London, 1931)

Lucas, B.G. & Muir, T.G. (1982) Field of a focusing source. J.Acoust.Soc.Amer.**72**(4), 1289-1296.

Lucas, B.G. & Muir, T.G. (1983) Field of a finite amplitude focusing source. J.Acout.Soc.Amer. **74**, 1522-1528.

Ludwig,G.D.(1950) The velocity of sound through tissues and the acoustic impedence of tissues.J.Acoust.Soc.Amer.**22**,862-866.

Madsen, E.L., Goodsitt, M.M. & Zagzebski, J.A. (1981) Continuous waves generated by focused radiators. J.Acout.Soc.Amer. **70**, 1508-1517.

Mair, H.D., Hutchins, D.A., Puhach, P.A. (1987) Intensity fields of continuous wave axisymmetric transducers J.Acout.Soc.Amer.**81**(2) 328-334

Marcus, P.W. & Carstensen, E.L. (1975). Problems with absorption measurements of inhomogeneous solids.J.Acoust.Soc.Amer.**58**,1334-1335.

Mols, C.R. & Breddels, P.A. (1982) Ultrasound velocity in muscle. J.Acoust.Soc.Amer. **71**, 455-461.

Muir,T.G. & Carstensen, E.L.(1980) Prediction of nonlinear acoustic effects at biomedical frequencies and intensities.Ultrasound.Med.Biol.**6**,345-357.

Narayana, P.A., Ophir, J. & Maklad, N.F. (1984) The attenuation of ultrasound in biological fluids. J.Acoust.Soc.Amer. **76**, 1-4.

Nassiri, D.K. & Hill, C.R. (1986) The differential and total bulk acoustic scattering cross sections of some human and animal tissues.J.Acoust.Soc.Amer. **79**,2034-2047.

O'Brien, W.D. (1977) The relationship between collagen and ultrasonic attenuation and velocity in tissue. Ultrasonics International, 194-205.

NCRP(1983) Biological effects of ultrasound: mechanisms and clinical implications. National Council on Radiation Protection and Measurement, Report N°74, Bethesda, M.D.

NPL (1994) Certificate of Calibration for a Pvdf ultrasonic hydrophone. GEC-Marconi, type Y-34-3598, serial N° ER175.
O'Brien, W.D., Erdman, J.W. & Hebner, T.B.(1988) Ultrasonic propagation properties (@ 100 Mhz) in excessively fatty rat liver.J.Acoust.Soc.Amer.**83**, 1159-1166.

O'Donnell, M. & Miller, J.G. (1979) Mechanisms of ultrasonic attenuation on soft tissue: Ultrasonic tissue characterisation.II.(ed.Linzer,M.), NBS spec.Publ.525, Washington,D.C.,37-40.

O'Neil, H.T. (1949) Theory of focusing radiators. J.Acoust.Soc.Amer. **21**,516-526.

Papoulis, A. (1981) Systems and transforms with applications in optics. R.E.Krieger, 346-347.

Papadakis,E.P., Fowler, K.A., & Lynnworth, L.(1973). Ultrasonic attenuation by spectrum analysis of pulses in buffer rods: Methods and diffraction corrections.J.Acoust.Soc.Amer.**53**,1336-1343.

Parker,K.J. (1983) Ultrasonic attenuation and absorption in liver tissue. Ultrasound.Med.Biol.**9**,363-369.

Pauly,H. & Schwan,H.P.(1971) Mechanism of absorption of ultrasound in liver tissue.J.Acoust.Soc.Amer.**50**,692-699.

Pellam,J.R. & Galt,J.K.(1946) Ultrasonic propagation in liquids: I.Applications of pulse techniques to velocity and absorption measurements at 15 megacycles. J.chem.Phys.**14**,608-614.

Perkins, M.A. (1989) A versatile force balance for ultrasound power measurement. Phys.Med.Biol, Vol **34** N° 11 1645-1651.

Pinkerton, J.M.M. (1947) A pulse method for the measurement of ultrasonic absorption in liquids:results for water. Nature, **160**, 128-129.

Povall, J.M., Aindow, J.D., Chivers, R.C., & Driscoll, A.M. (1984) Speed of ultrasound in amniotic fluid. Acoust.Lett. **7**, 181-186.

Preston, R.C. (1988) The ultrasound beam calibrator. IEEE Trans.Ultrason.Ferroelec.Freq.Contr. **35**, 122-139.

Pretson, R.C., Bacon, D.R., Livett, A.J. & Ragendran, K. (1983) Pvdf membrane hydrophone performance properties and their relevance to the measurement of the acoustic output of medical ultrasonic equipment. J.Phys.E:Sci.Instrum. **16**, 786-796.

Rajogopalan, B., Greenleaf, J.F., Thomas, P.J., Johnson, S.A. & Bahn, R.C. (1979) Variation of acoustic speed with temperature in various excised human tissues studied by ultrasound computerised tomography. Linzer: Ultrasonic tissue characterisation II, 227-233.

Schwan, H.P. & Carstensen, E.L. (1952) Ultrasonic aids diathermy experiments. Electronics, July' 52, 216.

Sehgal, C.M., Bahn, R.C. & Greenleaf, J.F. (1984) Measurement of the acoustic nonlinearity parameter B/A in human tissues by the thermodynamic method. J.Acoust.Soc.Amer **76**(4) 1023-1029

Sehgal, C.M., Brown, G.M., Bahn, R.C. & Greenleaf, J.F.(1986) Measurement and use of acoustic nonlinearity and sound speed to estimate composition of excised livers.Ultrasound.Med.Biol.**12**,865-874.

Seki, H. Granato, A. & Truell, R. (1956) Diffraction effects in the ultrasonic field of a piston source and their importance in the accurate measurement of attenuation.J.Acoust.Soc.Amer.**28**, p.230-238.

Starritt, H.C. (1990) Streaming induced by high amplitude acoustic pulses and its implications. PhD thesie. University of Bath.

Starritt, H.C., Perkins, M.A., Duck, F.A. & Humphrey, V.F. (1985) Evidence for ultrasound finite-amplitude distortion in muscle using medical equipment. J.Acoust.Soc.Amer. **77**, 302-306.

Starritt, H.C., Duck, D.A. & Hawkins, A.J. (1986) The development of harmonic distortion in pulsed finite amplitude ultrasound passing through liver, Phys.Med.Biol. **31**, 1401-1409.

Stokes, G,C. (1845) Trans.Camb.Phil.Soc.**8**, 287

Sun Yongchen, Dong Yanwu & Zhao Hengyuan. (1985) Study of the acoustic nonlinearity parameter in highly attenuating biological media. IEEE Ultrasonics.symp .proc. 891-894.

Sun Yongchen, Dong Yanwu, Tong Jie & Tang Zhensheng (1986) Ultrasonic propagation parameters in human tissue. IEEE Ultrasonics.Synp.Proc, 905-908.

Trivett, D.H. & Van Buren, A.L. (1981) Propagation of plane, cylindrical and spherical finite amplitude waves.J.Acoust.Soc.Amer.**69**, 943-949.

Tjotta, J. & Tjotta, S. (1980) An analytical model for the nearfield of a baffled oistin transducer. J.Acout.Soc.Amer. **68**,334-339.

Tjotta, J. & Tjotta, S. (1981) Nonlinear equations of acoustics, with application to parametric arrays. J.Acoust.Soc.Amer. **69**, 1644-1652.
Ward, B. (1995) Private communication

WFUMB (1991) Issues and recommendations regarding thermal mechanisms for biological effects of ultrasound. WFUMB symposium on safety and standardisation in medical ultrasound.
Williams, A.O. (1951) The piston source at high frequencies. J.Acoust.Soc.Amer. **23**, 1-6.

Yoon, H.S. & Katz, J.L. (1979) Ultrasonic properties and microtexture of human cortical bone. Linzer Ultrasonic tissue characterisation II 189-196

Zabolotskaya, E.A. & Khokhlov, R.V. (1969) Quasi-plane waves in the nonlinear acoustics of confined beams. Sov.Phys.Acoust. **15** 35-40

Zana, R. & Lang, J. (1974) Interaction of ultrasound with amniotic fluid. Ultrasound.Med.Biol.Vol **1** 253-258.

Zemanek, J.(1970) Beam behaviour within the nearfield of a vibrating piston. J.Acoust.Soc.Amer.**49**(1),181-191.

Zeqiri (1985) In: Physics in medical ultrasound. Ed. Evans, D.H. The institute of physical sciences in medicine.

Zeqiri, B.(1992) Errors in attenuation measurements due to nonlinear propagation effects.J.Acoust.Soc.Amer.**91**(5),2585-2593.

Zeqiri, B. (1995) Private communication.

PUBLICATIONS:

TITLE: ENHANCED ABSORPTION DUE TO NONLINEAR PROPAGATION IN DIAGNOSTIC ULTRASOUND

AUTHORS: P.K.Verma, V.F.Humphrey & H.C.Starritt

SOURCE: 13th International Symposium on Nonlinear Acoustics, Bergen, Norway (July 1993)

PAGES: 297-302

ENHANCED ABSORPTION DUE TO NONLINEAR PROPAGATION IN DIAGNOSTIC ULTRASOUND

P.K. VERMA, V.F. HUMPHREY
School of Physics, University of Bath, Bath BA2 7AY, UK.

and

H.C. STARRITT
Royal United Hospital, Combe Park, Bath BA1 3NG, UK.

ABSTRACT

Experimental work has demonstrated that nonlinear propagation results in both enhanced streaming and enhanced absorption in the nearfield of focussed diagnostic transducers[1]. This situation has been investigated theoretically using a finite difference model based on the KZK equation. This has enabled the pressure squared integral (P.S.I.) to be calculated on axis for a diagnostic transducer in water. The transducer had a nominal radius of 9.5mm, a moderate gain and was driven at 3.5 MHz with the source pressure ranging from 0.03 MPa to 0.39 MPa. The axial variation of P.S.I. shows significant departures from those expected on the basis of linear propagation, with a significant reduction beyond the focus for high drive levels. The attenuation in a region just beyond the focal plane is 0.96 dB cm^{-1} at the highest drive level. For a linear wave the attenuation would be 0.027 dB cm^{-1}. The enhancement of energy loss by a factor of 36 indicates that on axis 97% of the total absorption is due to the generation and attenuation of harmonics. The results are shown to be in reasonably good agreement with those obtained experimentally.

1. Introduction

The enhanced streaming observed in pulsed diagnostic fields[1] has been attributed to the influence of nonlinear propagation and the enhanced absorption resulting from the attenuation of harmonics. The aim of this work is to investigate the use of a finite difference model to predict this enhanced absorption and compare the results obtained with those observed experimentally.

2. Theory

The model used in these calculations is based on a finite difference solution[2] of the KZK parabolic approximation to the nonlinear wave equation. It accounts for the attenuation and diffraction of all the harmonics, nonlinearity and focussing. Baker *et al*[3] have shown that theoretical predictions of the harmonic pressure distributions agree well with experimental measurements for medical ultrasound transducers with circular geometries.

In order to determine the enhanced absorption, due to nonlinear propagation and harmonic attenuation, the model has been adapted to calculate the pressure squared integral (P.S.I.), a quantity closely related to intensity. Intensity is defined as I=p.v, where p is the acoustic pressure and v is the particle velocity, with both I and v being vector quantities. For an infinite plane progressive wave the pressure and particle velocity are in phase and the intensity at any point in the field then becomes proportional to p^2. Propagation from a piston source, however, produces a diffractive field where the pressure and particle velocity cannot be assumed to be in phase. However for ranges significantly greater than the transducer radius the difference is small and quasi-plane wave propagation results. In addition if one is only concerned with on-axis variations then the radial components of particle velocity are zero and only the axial component remains. Given quasi-plane wave propagation the intensity, on axis, can be assumed to be proportional to p^2. The validity of this assumption has been studied by Mair *et al*[4].

For a plane wave, the time average intensity is given by

$$I = \frac{1}{(\rho_o c)}\frac{1}{\tau}\int_0^{\tau} P^2(t)dt \qquad eq.(1)$$

where τ is the fundamental period of the wave, c is the velocity of sound, ρ_o is the fluid density and P(t) is the complex acoustic pressure. For a distorted sine wave P(t) may be written as a summation over its harmonic components

$$P(t) = \sum_{(n=1)}^{\infty} p_n e^{(n\omega t)} e^{(i\phi_n t)} \qquad eq.(2)$$

where p_n and ϕ_n are the amplitude and phase of the n^{th} harmonic respectively. In this case (eq.1) the intensity can be shown to reduce to

$$I = \frac{1}{(\rho_o c)}\frac{1}{\tau}\Sigma_n p_n^2 \tau. \qquad eq.(3)$$

So by summing the squares of the harmonic component amplitudes, the intensity, on axis, can be inferred. The integral part of eq.(1) is known as the pressure squared integral (P.S.I.).

3. Experimental determination of the enhanced absorption

The theoretical predictions of this paper are compared with the existing determinations of enhanced absorption made by Starritt[5]. These experimental measurements of P.S.I. were made on the field of a 9.5mm radius circular transducer with a focussing gain of 6.5 driven at 3.5 MHz. The field was measured with a 0.5mm diameter bilaminar p.v.d.f. membrane hydrophone in water. The P.S.I. was determined by digitizing the detected waveform and calculating the time integral of the square of the instantaneous pressure. In order to determine the enhanced absorption the P.S.I. was calculated for two drive levels, one (beam 'A') when propagation was nonlinear and the other (beam 'B') when the propagation was essentially linear. Case 'A' corresponded to a source pressure of 0.39 MPa and case 'B' to a source pressure of 0.03 MPa. Comparing the ratio of the P.S.I.s for the two cases compensated for diffraction and linear attenuation. Hence changes in the P.S.I. ratio with distance gave a measure of the extra attenuation occurring due to nonlinear propagation.

4. Simulations

In order to make a quantitative comparison the initial conditions in the simulations were chosen to model the experimental measurements. Initially the axial pressure distribution was obtained for the low drive case (linear beam 'B') and was compared with the experimental pressure distribution to determine whether the source parameters were defining the ultrasonic field accurately. A reasonable agreement was obtained by using a focal gain of 6.5 and a transducer radius of 9.5mm.

Figs. 1 and 2 illustrate the axial variation of the first three harmonics for the nonlinear (beam 'A') and linear cases (beam 'B'). The figure illustrates that the low drive case is indeed approximated to a linear beam with the second harmonic 20dB down on the fundamental in the region of the focus. By comparison the high drive case is highly shocked with the second harmonic 5.7dB below the fundamental near the focus.

5. Results and Discussion

In order to predict the enhanced absorption theoretically, the calculation of P.S.I. was incorporated into the model for points on axis. Fig. 3 illustrates the axial variation of P.S.I. for the two drive cases ('A' and 'B'). It should be noted that the theoretical graphs are normalised to the P.S.I. at the transducer face. As can be seen in a region from 6cm to 17cm the normalised P.S.I. for the high drive case (beam 'A') is lower than the linear case. This implies that the axial intensity in the nonlinear beam is lower, due to the enhanced absorption resulting from harmonic generation and absorption. The extent to which the energy is transferred to the harmonics can be seen from fig. 4. This illustrates the axial variation of the partial P.S.I. for the nonlinear beam. Curve 1 is the contribution, to the total P.S.I., from only the fundamental frequency, and curve 2 is the contribution summed over the first ten harmonics. A comparison of fig. 3 and fig. 4 reveals that, near the last axial maximum, about 10% of the axial intensity is contained within the 11^{th} and higher harmonics. Fig. 4 also indicates that the maximum intensity does not coincide with the position of the last axial maximum of the fundamental. The reason for this is that the harmonics, generated by nonlinear propagation, are not as strongly diffracted as the fundamental and so focus beyond the maximum of the fundamental.

Enhanced absorption, due to nonlinear propagation, can be calculated by comparing the P.S.I. in the high drive case to the low drive case. Fig. 5 illustrates the ratio of beam 'A' P.S.I. to beam 'B' P.S.I. on axis. Fig. 6 is a graph of the experimentally observed P.S.I. ratio for the two beams. As can be seen the general behaviour of the curves in both figures are similar. It should be noted that both results have been normalised to the source P.S.I. The behaviour of the P.S.I. ratio can be explained by considering three different regions in fig. 5.

The first region extends from the transducer up to 6cm. This represents the nearfield of the ultrasonic field. Here the P.S.I. ratio is unity except for some sharp rises. In this region nonlinear effects have not had time to build up, due to the rapid oscillations in the field of the fundamental, so almost all the energy is confined to the first harmonic in both cases. The sharp rises within this region correspond with the minima in the field of the

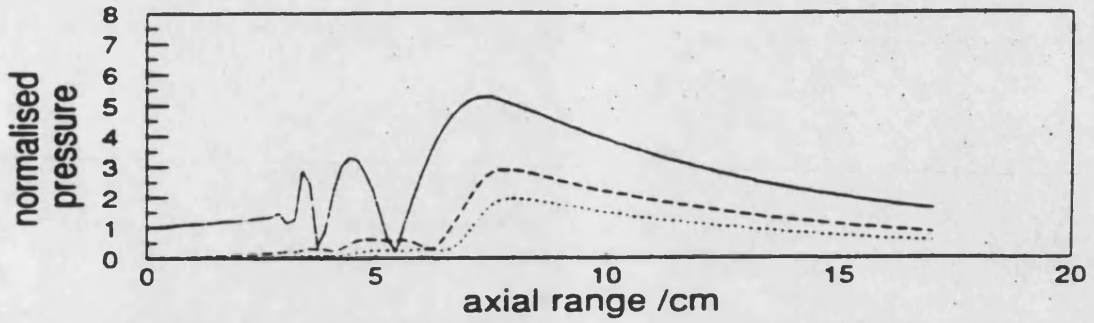

Fig. 1. Axial variation of harmonic pressure amplitudes for beam 'A'; 1st (—), 2nd (- - -) and 3rd (···) harmonic.

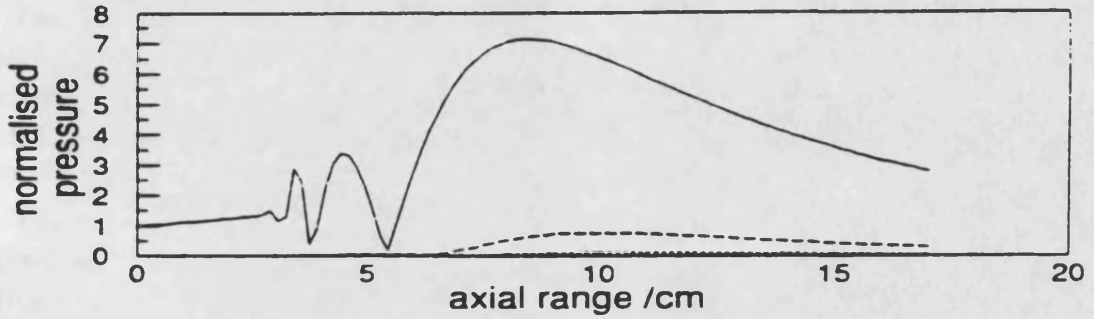

Fig. 2. Axial variation of harmonic pressure amplitudes for beam 'B'; 1st (—), 2nd (- - -) and 3rd (···) harmonic.

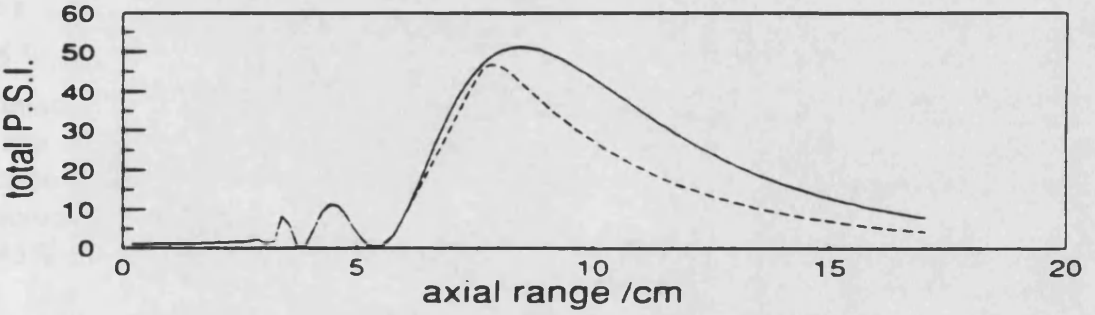

Fig. 3. Normalised axial variation of total P.S.I. for the two beams; beam 'B' (—) and beam 'A' (- - -).

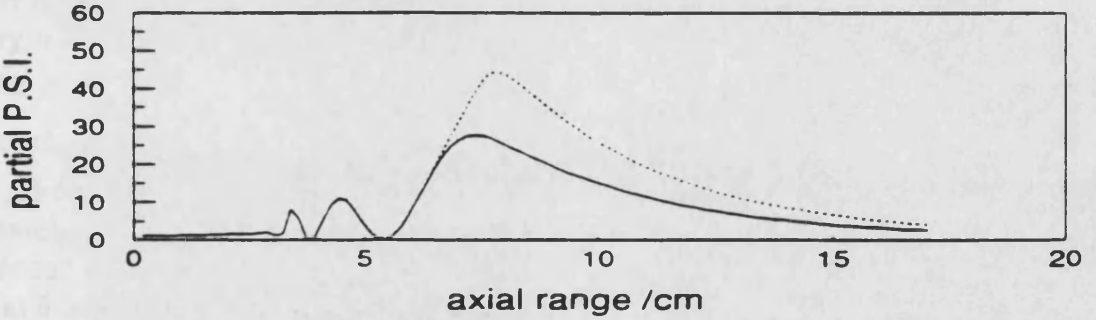

Fig. 4. Axial variation of partial P.S.I. for beam 'A'; P.S.I. of 1st harmonic (—) and P.S.I. summed over first 10 harmonics (- - -).

fundamental. At these places a small amount of second harmonic is present in the nonlinear beam while there is no second harmonic is the linear beam. The result is that the P.S.I. ratio rises to a large value.

The second region extends from 6cm to 10cm. Here the P.S.I. ratio falls below unity implying that more energy is present in the linear beam. The physical reason for this is as follows. In the region of the focus energy is transferred to the harmonics in the nonlinear beam. The attenuation of the harmonics is proportional to frequency squared and therefore energy is lost from the wave at a faster rate than would be expected from an undistorted waveform. There is also a peak present near 8cm, implying that the axial intensity in the nonlinear beam is building up over a short region. This peak is due to the focussing of the harmonics described above.

The third region extends from 10cm to 17cm. This is the post focal region where the harmonics are governed by attenuation and nonlinear propagation, diffraction effects being less important. In this region the rate of loss due to nonlinear effects decreases and the P.S.I. ratio reaches a plateau. By this point the fundamental has lost a significant proportion of its amplitude as a result or nonlinear effects.

The enhanced absorption in the post focal region (8cm to 10cm) can be calculated from the gradient of fig. 5. If the attenuation is assumed to depend on a single attenuation coefficient α_T, then the intensity can be expressed as

$$I_x = I_o e^{-2\alpha_T x}. \qquad eq.(4)$$

Over a 1cm region, this yields a value for α_T of 0.96 dB cm^{-1}. For a linear wave the attenuation at 3.5 MHz gives α_o as 0.027 dB cm^{-1}. This corresponds to an enhancement of energy loss by a factor of 36. The experimental results indicate an enhanced absorption of 1.1 dB cm^{-1}. The two results show reasonably good agreement. Furthermore the enhanced absorption indicates that, on axis, 97% of the total absorption is due to generation and attenuation of harmonics. Fig. 5 also illustrates that after sufficient propagation the nonlinear wave has lost 45% of its intensity on axis while the experimentally observed loss is higher at about 60%. This difference may be due to the limited frequency response of the receiving system.

Work in this area is still in progress with experiments having been performed using a 5MHz diagnostic transducer with a focal gain of approximately 6.0. Both experiment and theory indicate an enhanced absorption of 1.75 dB cm^{-1} in the post focal region, approximately 34 times the normal linear attenuation.

6. Conclusions

These calculations indicate that models based on the KZK equation can be used to accurately predict enhanced attenuation. The values observed in the post focal region of diagnostic transducers can reach values of 0.96 dB cm^{-1} in water at 3.5 MHz and 1.75 dB cm^{-1} at 5 MHz, i.e. typically 35 times the linear attenuation coefficient.

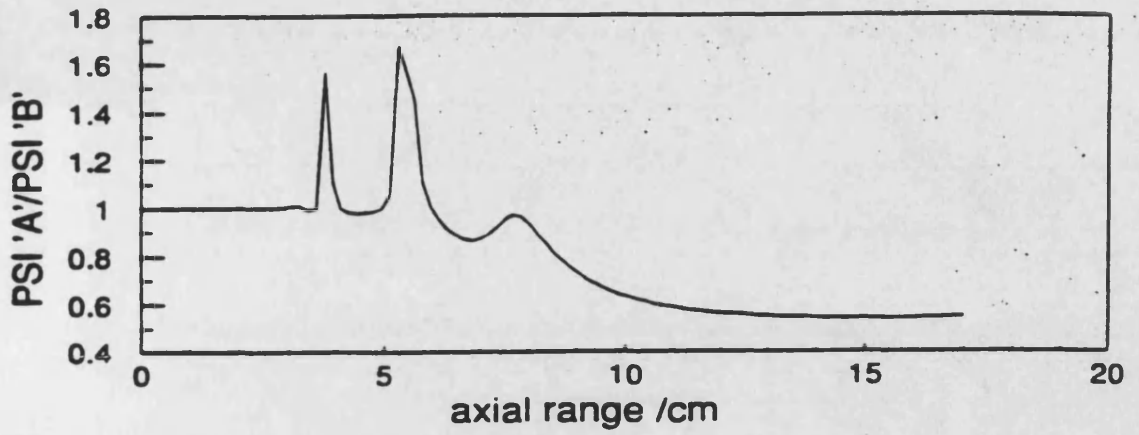

Fig. 5. Axial variation of PSI ratio (theory) of beam 'A' to beam 'B' (normalised).

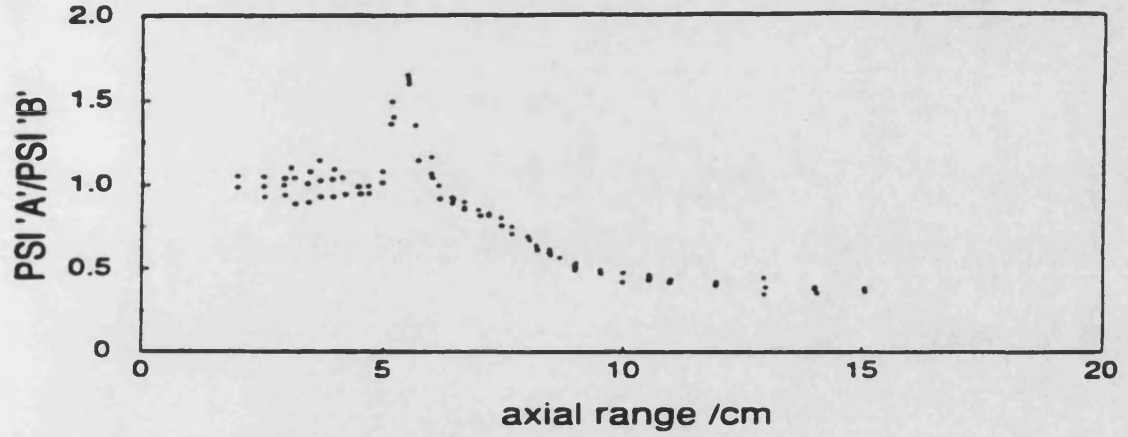

Fig. 6. Axial variation of PSI ratio (experiment) of beam 'A' to beam 'B'.

7. References

1. H. C. Starritt, F. A. Duck and V. F. Humphrey, *Ultrasound in Med. & Biol.* **15** (1989) p363-373.

2. S.I. Aanonsen, T. Barkve, J Naze Tjøtta and S Tjøtta, *J. Acoust. Soc. Am.* (1984) p749-768.

3. A. C. Baker, K. Anastasiadis and V. F. Humphrey, *Proceedings of Ultrasonics International 87* (Butterworths, 1987), p184-189.

4. H. D. Mair, D.A. Hutchins, and P.A. Puhach, *J. Acoust. Soc. Amer.* **81** (1987) p328-334.

5. H. C. Starritt, *Streaming Induced by High Amplitude Acoustic Pulses and its Implications*. (Ph.D. Thesis, University of Bath, 1990).

ENHANCED ABSORPTION DUE TO NONLINEAR PROPAGATION IN DIAGNOSTIC ULTRASOUND

P.K. VERMA, V.F. HUMPHREY
School of Physics, University of Bath, Bath BA2 7AY, UK.

and

H.C. STARRITT
Royal United Hospital, Combe Park, Bath BA1 3NG, UK.

ABSTRACT

Experimental work has demonstrated that nonlinear propagation results in both enhanced streaming and enhanced absorption in the nearfield of focussed diagnostic transducers[1]. This situation has been investigated theoretically using a finite difference model based on the KZK equation. This has enabled the pressure squared integral (P.S.I.) to be calculated on axis for a diagnostic transducer in water. The transducer had a nominal radius of 9.5mm, a moderate gain and was driven at 3.5 MHz with the source pressure ranging from 0.03 MPa to 0.39 MPa. The axial variation of P.S.I. shows significant departures from those expected on the basis of linear propagation, with a significant reduction beyond the focus for high drive levels. The attenuation in a region just beyond the focal plane is 0.96 dB cm^{-1} at the highest drive level. For a linear wave the attenuation would be 0.027 dB cm^{-1}. The enhancement of energy loss by a factor of 36 indicates that on axis 97% of the total absorption is due to the generation and attenuation of harmonics. The results are shown to be in reasonably good agreement with those obtained experimentally.

1. Introduction

The enhanced streaming observed in pulsed diagnostic fields[1] has been attributed to the influence of nonlinear propagation and the enhanced absorption resulting from the attenuation of harmonics. The aim of this work is to investigate the use of a finite difference model to predict this enhanced absorption and compare the results obtained with those observed experimentally.

2. Theory

The model used in these calculations is based on a finite difference solution[2] of the KZK parabolic approximation to the nonlinear wave equation. It accounts for the attenuation and diffraction of all the harmonics, nonlinearity and focussing. Baker *et al*[3] have shown that theoretical predictions of the harmonic pressure distributions agree well with experimental measurements for medical ultrasound transducers with circular geometries.

In order to determine the enhanced absorption, due to nonlinear propagation and harmonic attenuation, the model has been adapted to calculate the pressure squared integral (P.S.I.), a quantity closely related to intensity. Intensity is defined as **I**=p.**v**, where p is the acoustic pressure and **v** is the particle velocity, with both **I** and **v** being vector quantities. For an infinite plane progressive wave the pressure and particle velocity are in phase and the intensity at any point in the field then becomes proportional to p^2. Propagation from a piston source, however, produces a diffractive field where the pressure and particle velocity cannot be assumed to be in phase. However for ranges significantly greater than the transducer radius the difference is small and quasi-plane wave propagation results. In addition if one is only concerned with on-axis variations then the radial components of particle velocity are zero and only the axial component remains. Given quasi-plane wave propagation the intensity, on axis, can be assumed to be proportional to p^2. The validity of this assumption has been studied by Mair *et al*[4].

For a plane wave, the time average intensity is given by

$$I = \frac{1}{(\rho_o c)} \frac{1}{\tau} \int_0^{\tau} P^2(t) dt \qquad eq.(1)$$

where τ is the fundamental period of the wave, c is the velocity of sound, ρ_o is the fluid density and P(t) is the complex acoustic pressure. For a distorted sine wave P(t) may be written as a summation over its harmonic components

$$P(t) = \sum_{(n=1)}^{\infty} p_n e^{(in\omega t)} e^{(i\phi_n t)} \qquad eq.(2)$$

where p_n and ϕ_n are the amplitude and phase of the n^{th} harmonic respectively. In this case (eq.1) the intensity can be shown to reduce to

$$I = \frac{1}{(\rho_o c)} \frac{1}{\tau} \Sigma_n p_n^2 \tau. \qquad eq.(3)$$

So by summing the squares of the harmonic component amplitudes, the intensity, on axis, can be inferred. The integral part of eq.(1) is known as the pressure squared integral (P.S.I.).

3. Experimental determination of the enhanced absorption

The theoretical predictions of this paper are compared with the existing determinations of enhanced absorption made by Starritt[5]. These experimental measurements of P.S.I. were made on the field of a 9.5mm radius circular transducer with a focussing gain of 6.5 driven at 3.5 MHz. The field was measured with a 0.5mm diameter bilaminar p.v.d.f. membrane hydrophone in water. The P.S.I. was determined by digitizing the detected waveform and calculating the time integral of the square of the instantaneous pressure. In order to determine the enhanced absorption the P.S.I. was calculated for two drive levels, one (beam 'A') when propagation was nonlinear and the other (beam 'B') when the propagation was essentially linear. Case 'A' corresponded to a source pressure of 0.39 MPa and case 'B' to a source pressure of 0.03 MPa. Comparing the ratio of the P.S.I.s for the two cases compensated for diffraction and linear attenuation. Hence changes in the P.S.I. ratio with distance gave a measure of the extra attenuation occurring due to nonlinear propagation.

4. Simulations

In order to make a quantitative comparison the initial conditions in the simulations were chosen to model the experimental measurements. Initially the axial pressure distribution was obtained for the low drive case (linear beam 'B') and was compared with the experimental pressure distribution to determine whether the source parameters were defining the ultrasonic field accurately. A reasonable agreement was obtained by using a focal gain of 6.5 and a transducer radius of 9.5mm.

Figs. 1 and 2 illustrate the axial variation of the first three harmonics for the nonlinear (beam 'A') and linear cases (beam 'B'). The figure illustrates that the low drive case is indeed approximated to a linear beam with the second harmonic 20dB down on the fundamental in the region of the focus. By comparison the high drive case is highly shocked with the second harmonic 5.7dB below the fundamental near the focus.

5. Results and Discussion

In order to predict the enhanced absorption theoretically, the calculation of P.S.I. was incorporated into the model for points on axis. Fig. 3 illustrates the axial variation of P.S.I. for the two drive cases ('A' and 'B'). It should be noted that the theoretical graphs are normalised to the P.S.I. at the transducer face. As can be seen in a region from 6cm to 17cm the normalised P.S.I. for the high drive case (beam 'A') is lower than the linear case. This implies that the axial intensity in the nonlinear beam is lower, due to the enhanced absorption resulting from harmonic generation and absorption. The extent to which the energy is transferred to the harmonics can be seen from fig. 4. This illustrates the axial variation of the partial P.S.I. for the nonlinear beam. Curve 1 is the contribution, to the total P.S.I., from only the fundamental frequency, and curve 2 is the contribution summed over the first ten harmonics. A comparison of fig. 3 and fig. 4 reveals that, near the last axial maximum, about 10% of the axial intensity is contained within the 11^{th} and higher harmonics. Fig. 4 also indicates that the maximum intensity does not coincide with the position of the last axial maximum of the fundamental. The reason for this is that the harmonics, generated by nonlinear propagation, are not as strongly diffracted as the fundamental and so focus beyond the maximum of the fundamental.

Enhanced absorption, due to nonlinear propagation, can be calculated by comparing the P.S.I. in the high drive case to the low drive case. Fig. 5 illustrates the ratio of beam 'A' P.S.I. to beam 'B' P.S.I. on axis. Fig. 6 is a graph of the experimentally observed P.S.I. ratio for the two beams. As can be seen the general behaviour of the curves in both figures are similar. It should be noted that both results have been normalised to the source P.S.I. The behaviour of the P.S.I. ratio can be explained by considering three different regions in fig. 5.

The first region extends from the transducer up to 6cm. This represents the nearfield of the ultrasonic field. Here the P.S.I. ratio is unity except for some sharp rises. In this region nonlinear effects have not had time to build up, due to the rapid oscillations in the field of the fundamental, so almost all the energy is confined to the first harmonic in both cases. The sharp rises within this region correspond with the minima in the field of the

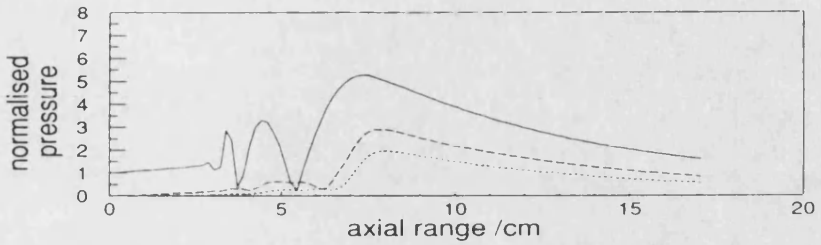

Fig. 1. Axial variation of harmonic pressure amplitudes for beam 'A'; 1st (—), 2nd (- - -) and 3rd (···) harmonic.

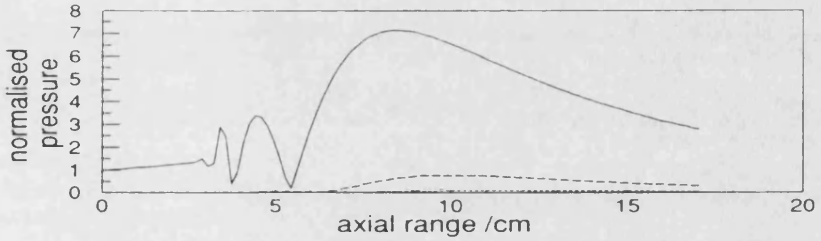

Fig. 2. Axial variation of harmonic pressure amplitudes for beam 'B'; 1st (—), 2nd (- - -) and 3rd (···) harmonic.

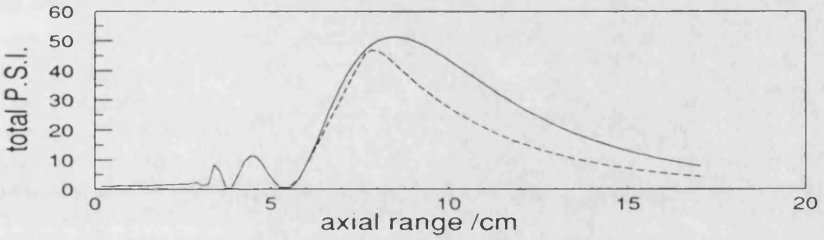

Fig. 3. Normalised axial variation of total P.S.I. for the two beams; beam 'B' (—) and beam 'A' (- - -).

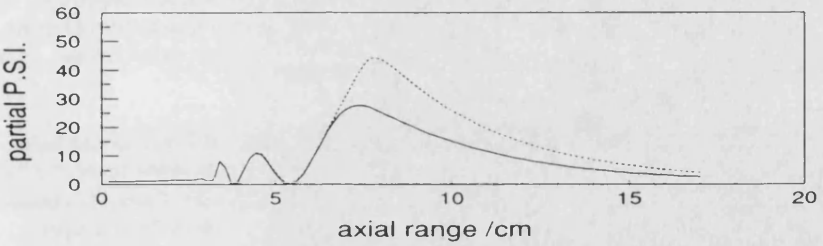

Fig. 4. Axial variation of partial P.S.I. for beam 'A'; P.S.I. of 1st harmonic (—) and P.S.I. summed over first 10 harmonics (- - -).

fundamental. At these places a small amount of second harmonic is present in the nonlinear beam while there is no second harmonic is the linear beam. The result is that the P.S.I. ratio rises to a large value.

The second region extends from 6cm to 10cm. Here the P.S.I. ratio falls below unity implying that more energy is present in the linear beam. The physical reason for this is as follows. In the region of the focus energy is transferred to the harmonics in the nonlinear beam. The attenuation of the harmonics is proportional to frequency squared and therefore energy is lost from the wave at a faster rate than would be expected from an undistorted waveform. There is also a peak present near 8cm, implying that the axial intensity in the nonlinear beam is building up over a short region. This peak is due to the focussing of the harmonics described above.

The third region extends from 10cm to 17cm. This is the post focal region where the harmonics are governed by attenuation and nonlinear propagation, diffraction effects being less important. In this region the rate of loss due to nonlinear effects decreases and the P.S.I. ratio reaches a plateau. By this point the fundamental has lost a significant proportion of its amplitude as a result or nonlinear effects.

The enhanced absorption in the post focal region (8cm to 10cm) can be calculated from the gradient of fig. 5. If the attenuation is assumed to depend on a single attenuation coefficient α_T, then the intensity can be expressed as

$$I_x = I_o e^{-2\alpha_T x}. \qquad eq.(4)$$

Over a 1cm region, this yields a value for α_T of 0.96 dB cm^{-1}. For a linear wave the attenuation at 3.5 MHz gives α_o as 0.027 dB cm^{-1}. This corresponds to an enhancement of energy loss by a factor of 36. The experimental results indicate an enhanced absorption of 1.1 dB cm^{-1}. The two results show reasonably good agreement. Furthermore the enhanced absorption indicates that, on axis, 97% of the total absorption is due to generation and attenuation of harmonics. Fig. 5 also illustrates that after sufficient propagation the nonlinear wave has lost 45% of its intensity on axis while the experimentally observed loss is higher at about 60%. This difference may be due to the limited frequency response of the receiving system.

Work in this area is still in progress with experiments having been performed using a 5MHz diagnostic transducer with a focal gain of approximately 6.0. Both experiment and theory indicate an enhanced absorption of 1.75 dB cm^{-1} in the post focal region, approximately 34 times the normal linear attenuation.

6. Conclusions

These calculations indicate that models based on the KZK equation can be used to accurately predict enhanced attenuation. The values observed in the post focal region of diagnostic transducers can reach values of 0.96 dB cm^{-1} in water at 3.5 MHz and 1.75 dB cm^{-1} at 5 MHz, i.e. typically 35 times the linear attenuation coefficient.

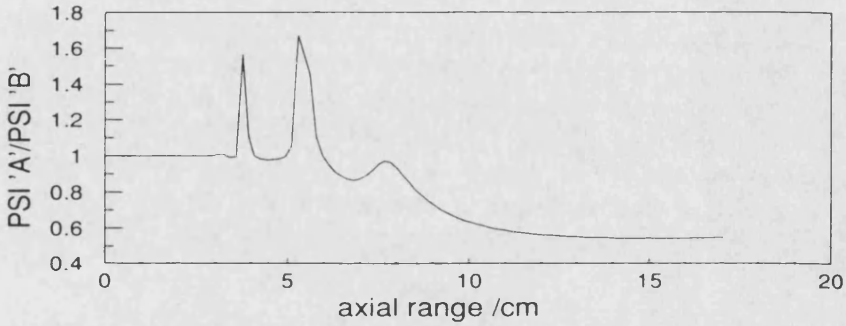

Fig. 5. Axial variation of PSI ratio (theory) of beam 'A' to beam 'B' (normalised).

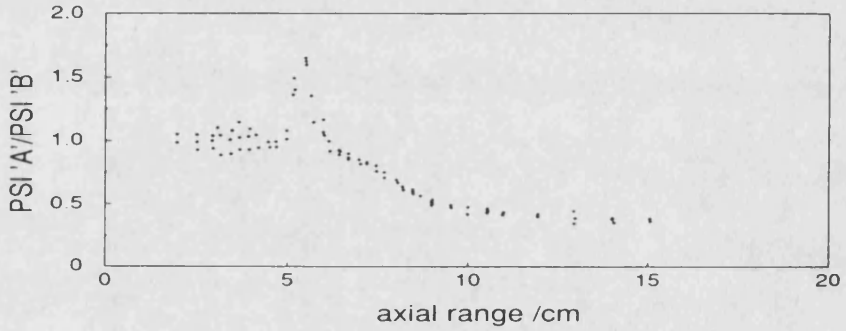

Fig. 6. Axial variation of PSI ratio (experiment) of beam 'A' to beam 'B'.

7. References

1. H. C. Starritt, F. A. Duck and V. F. Humphrey, *Ultrasound in Med. & Biol.* **15** (1989) p363-373.

2. S.I. Aanonsen, T. Barkve, J Naze Tjøtta and S Tjøtta, *J. Acoust. Soc. Am.* (1984) p749-768.

3. A. C. Baker, K. Anastasiadis and V. F. Humphrey, *Proceedings of Ultrasonics International 87* (Butterworths, 1987), p184-189.

4. H. D. Mair, D.A. Hutchins, and P.A.Puhach, *J. Acoust. Soc. Amer.* **81** (1987) p328-334.

5. H. C. Starritt, *Streaming Induced by High Amplitude Acoustic Pulses and its Implications.* (Ph.D. Thesis, University of Bath, 1990).